January 2015

A Real Time Radio Spectrum Scanning Technique Based On The Bayesian Model And Its Comparison With The Frequentist Technique

Sriram Subramaniam

A REAL TIME RADIO SPECTRUM SCANNING TECHNIQUE BASED ON THE BAYESIAN MODEL AND ITS COMPARISON WITH THE FREQUENTIST TECHNIQUE

by

Sriram Subramaniam
Bachelor of Engineering, Visvesvaraya Technological University, 2011

A Thesis

Submitted to the Graduate Faculty

of the

University of North Dakota

in partial fulfillment of the requirements

for the degree of

Master of Science

Grand Forks, North Dakota
December
2015

This thesis, submitted by Sriram Subramaniam in partial fulfillment of the requirements for the Degree of Master of Science from the University of North Dakota, has been read by the Faculty Advisory Committee under whom the work has been done and is hereby approved.

Naima Kaabouch, Ph.D., Chairperson

Saleh Faruque, Ph.D.

Wen-Chen Hu, Ph.D.

This thesis meets the standards for appearance, conforms to the style and format requirements of the Graduate School of the University of North Dakota, and is hereby approved.

Wayne Swisher,
Dean of the Graduate School

October 1, 2015
Date

PERMISSION

Title	A Real Time Radio Spectrum Scanning Technique Based on the Bayesian Model and its comparison with the Frequentist Technique
Department	Electrical Engineering
Degree	Master of Science

In presenting this thesis in partial fulfillment of the requirements for a graduate degree from the University of North Dakota, I agree that the library of this University shall make it freely available for inspection. I further agree that permission for extensive copying for scholarly purposes may be granted by the professor who supervised my thesis work or, in his absence, by the chairperson of the department or the dean of the Graduate School. It is understood that any copying or publication or other use of this thesis or part thereof for financial gain shall not be allowed without my written permission. It is also understood that due recognition shall be given to me and to the University of North Dakota in any scholarly use which may be made of any material in my thesis.

Sriram Subramaniam
September 2015

TABLE OF CONTENTS

LIST OF FIGURES

LIST OF TABLES

ACKNOWLEDGEMENTS

First of all, I would like to thank my parents for encouraging and supporting me throughout the journey of my master's program.

I am very grateful to my advisor Dr.Naima Kaabouch for her continued guidance and support. Her advising has always been of great value and it is that which has made me achieve a lot in my master's journey. I would also like to express my gratitude to Dr.Saleh Faruque and Dr.Wen-Chen Hu whose course teachings have been very useful to me in my research work. I also thank Dr. Ganesh Rao who guided me in the building of my fundamentals in the field of digital communication.

I am also thankful to my mentor Hector Reyes and my colleagues Madhur Shetty, Debabrata Ghosh, Anupam Mukherjee and to every other person who gave me valuable advice and contributed to making this journey a successful one.

Above all, I am grateful to the almighty lord who has blessed me with all these opportunities and has walked the path with me in turning this opportunity into a successful one.

Lastly, I would like to acknowledge the support of NSF grant #1443861 and EPSCoRINSF grant #EPS-0184442.

ABSTRACT

The proliferation of mobile devices led to an exponential demand for wireless radio spectrum resources. The current fixed spectrum assignment has caused some portions of the radio spectrum to be heavily used whereas others to be scarcely used. This has resulted in underutilization of spectrum resources, and, hence has demanded the need for solutions to address the spectrum scarcity problem. Cognitive radio was proposed as one of the solutions. One of the techniques involved in cognitive radio is the dynamic spectrum access technique. This technique requires the identification of free channels in order to allow secondary users to exploit the spectrum resources. The process of identification of free channels is known as radio spectrum scanning, which is performed by sensing a particular channel in the radio spectrum to determine the presence or absence of a signal. In most of existing studies, the frequentist technique using energy detection with fixed threshold was used to scan the radio spectrum. However, this method comes with a major drawbacks. First, energy detection is unable to distinguish between signals and noise and suffer for high false detection rates. Second, energy detection has high false alarm probability. Finally, frequentist techniques are subject to uncertainty and do not provide real time monitoring/sensing. Therefore, the goal of this thesis is to develop a more efficient scanning technique that deals with uncertainty and scans the radio spectrum in real time and determines its occupancy levels.

An enhanced spectrum scanning approach is developed using an efficient spectrum sensing technique: an uncertainty handling Bayesian model along with a Bayesian inferential approach. Two Bayesian models are developed: 1) a simplified model, and 2) an improved model to incorporate the Bayesian inferential approach to estimate the spectrum occupancy level.

The performance evaluation of the proposed technique has been done using simulations as well as real experiments. For this purpose, two metrics were used: probability of detection and probability of false alarm. Furthermore, the efficiency of the proposed technique was compared to the efficiency of the frequentist technique, which uses only a spectrum sensing technique to identify the occupancy of the spectrum channels. As expected significant improvements in the spectrum occupancy measurements have been observed with the proposed Bayesian inference method.

Chapter 1

INTRODUCTION

1.1. Spectrum Scarcity Problem

With the exponential increase of portable device utilization and ever-growing demand for greater wireless data transmission rates, an increasing demand for spectrum channels has been observed over the last decade. Conventionally, licensed spectrum channels are assigned for comparatively long time spans to license holders who may not continuously use them, creating an under-utilized spectrum. This inefficient use of spectrum resources has motivated researchers to look for advanced, innovative technologies that enable more efficient spectrum resource use [1.1]. Figure 1 depicts the under-utilization of the spectrum wherein certain parts of the spectrum are sparsely used and certain portions are heavily used. The figure also indicates a spectrum utilization of less than 6%.

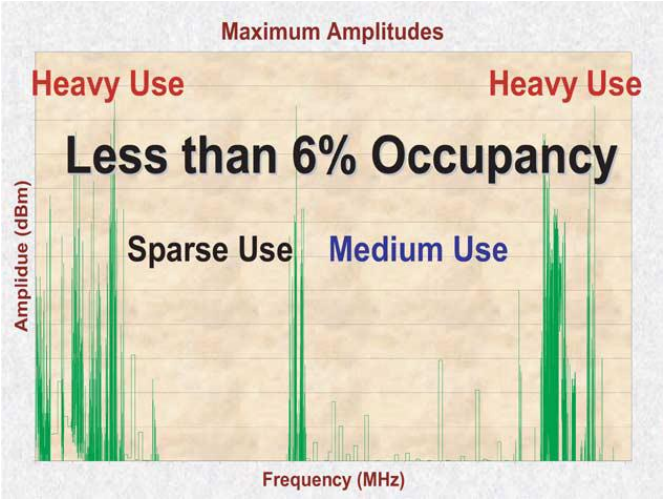

Figure 1. Spectrum utilization [1.2]

This inefficient usage necessitated the development of dynamic spectrum access techniques. Dynamic spectrum access techniques allow secondary users or unlicensed users of the radio spectrum to access the licensed portion of the spectrum on a temporary basis. This approach is can increase the efficiency of the utilization of the radio resources as well as solve the problem of spectrum scarcity by re-utilizing the licensed portions of the spectrum. Dynamic spectrum access techniques enable cognitive radios to operate in the best available channel which ensures an interference free operation between the primary and the secondary users. The process of identifying the holes or white space in the radio spectrum to decide on the best available channel is achieved by scanning the radio spectrum. Figure 2 illustrates the usage of a licensed spectrum. In this figure different channels are occupied for varying durations thereby creating white spaces or holes during the channel's inactivity period. These white spaces open up opportunities for the secondary user to use the licensed part of the spectrum.

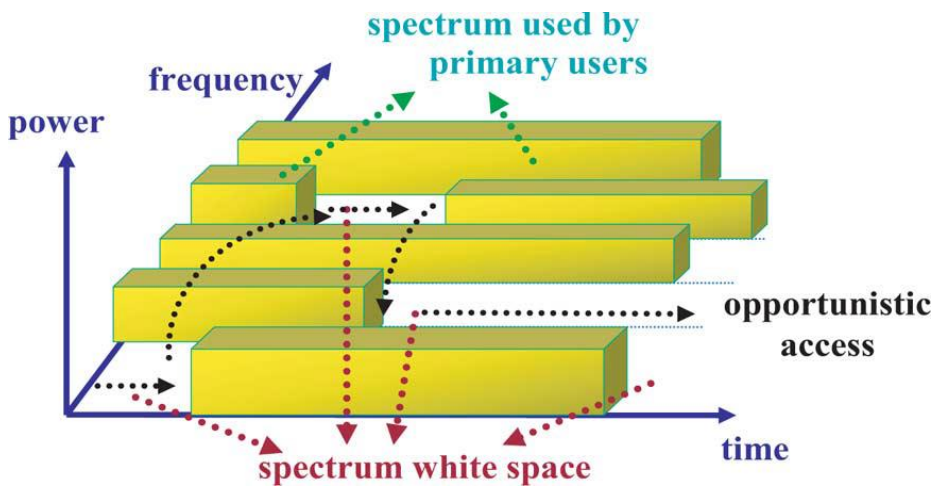

Figure 2. Illustration of licensed spectrum [1.2]

1.2. Cognitive Radio

The concept of cognitive radio was introduced as a solution to address the scarcity

problem of the radio spectrum. It was conceived originally by Mitola in [1.3], is that the cognitive radio executes a set of processes in a sequential order such as observing the radio spectrum, deciding the presence of the signal, and taking an action to adjust the operating parameters of the cognitive radio. This sequence of processes is known as the "Cognitive Cycle". An illustration of the cognitive cycle as described in [1.4] is shown in Figure 3, wherein each ellipse represents a process in the cognitive cycle. In the "Observing" phase, the cognitive radio performs spectrum sensing to check for the presence of a signal. Based on this result, decisions are made in the "Deciding" process and then the "Taking Action" process takes an action dependent on the decision made previously.

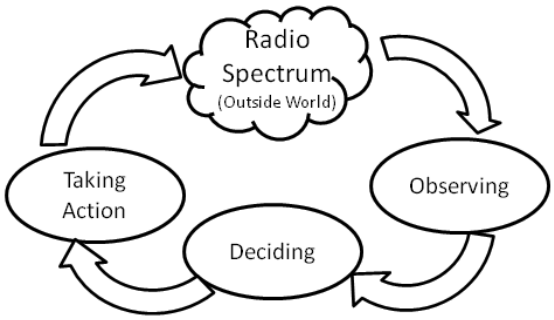

Figure 3. Cognitive Cycle (modified from [1.4])

Cognitive radio is the component that detects the transmissions of the primary users who own the license to use specific portions of the radio spectrum. It is designed to be context aware of the environment it operates. This awareness functionality is supported by spectrum sensing and channel estimation. Spectrum sensing is the process of obtaining awareness about the spectrum usage and existence of primary users in a determined area [1.5] and is one of the key processes in radio spectrum scanning.

1.3. Uncertainty in Cognitive Radios

In cognitive radio networks, the observation phase is a critical part of the cognitive cycle. In this phase the spectrum sensing is performed to obtain measurements which are used in the decision making phase to make decisions based on the observations made. Multipath fading, shadowing, and other varying channel conditions [1.6] are random thus they affect the complete cognitive cycle process. Since the observations made are uncertain this would impact the system by taking wrong or incorrect decisions based on these uncertain observations. This wrong decision would in turn influence in a wrong action being taken by the cognitive radio. Therefore an uncertainty propagation is noticed from the observation phase to the action taken thereby affecting the performance of the cognitive radio. Mitigating this uncertainty would enhance the performance of the cognitive radio by observing the spectrum correctly, making the right decisions and taking the needed actions correctly. Spectrum sensing decisions are influenced by various parameters such as noise, fading by multipath effect, shadowing from obstacles in the channel and other sources of interferences.

In order to handle the uncertainty in cognition cycles, a model that considers uncertainty in all stages of the cognition cycle should be developed in which the handling uncertainty solution is used in the cognition cycle to provide reliable decisions, leading to intelligent actions by the cognitive radio system. Current spectrum sensing models do not have the right decision-making protocols when elements of uncertainty are present or parameters are missing due to channel condition changes [1.7]. Mathematical models have been proposed to address uncertainties such as the one proposed by R.Tandra et al in [1.8] addressing the noise uncertainty and fading by the proposition of a signal-to-noise ratio wall that quantified the sensing decision.

Therefore an efficient spectrum sensing technique and an uncertainty handling technique or model can aid in achieving more accurate and precise occupancy results.

1.4. Goal and Objectives of this Thesis

The goal of this thesis is to develop a model for sensing and scanning the radio spectrum and dealing with uncertainty in cognitive radio systems. To achieve this goal, the following objectives are pursued:

1) Develop an efficient spectrum sensing technique
2) Build a simplified Bayesian model to perform Bayesian inference and compare it with the Frequentist inference
3) Improve the simplified Bayesian model to perform uncertainty handling

This thesis will be organized as followed. In the second chapter, a study of the different types of uncertainties will be performed followed with the development of a simplified and an improved Bayesian model. The third chapter will consist of a literature study of the various noise estimation techniques followed by the implementation of one of the studied techniques. The fourth chapter shall provide an overview into the current spectrum sensing techniques and also describe the development of an efficient spectrum sensing technique. The fifth chapter shall discuss about the Bayesian and the Frequentist inferential techniques and the results of the radio spectrum scanning experiments performed.

Chapter 2

BAYESIAN MODELLING

2.1. Uncertainty and its Handling Techniques

Uncertainty is classified as aleatoric or epistemic as illustrated in Figure 4 [2.1]. The reason for the occurrence of aleatoric uncertainties is purely because of the natural and unpredictable variation in the performance of the system. This type of uncertainty is referred to as irreducible uncertainty as no knowledge can aid in the reduction of the aleatoric uncertainty. In simple terms it refers to the notion of randomness as it is directly influenced by the inherent random effects of the system. A classical example of this uncertainty is the coin-flip experiment where the outcome of this experiment has a stochastic component that cannot be reduced or eliminated with the addition of any further information. Therefore with the best efforts, a model can only provide probabilities of occurrence for the two outcomes but not a definite answer [2.2].

On the other hand, epistemic uncertainty arises primarily due to lack of knowledge of the behavior of the system, which on availability of further knowledge overcomes in conceptually resolving the uncertainty. Unlike the aleatoric uncertainty, the epistemic uncertainty can be reduced with the availability of further knowledge and therefore refers to the reducible part of the total uncertainty. An example of this type of uncertainty is a medical doctor’s true diagnosis of a patient.

A situation of uncertainty prevails until medical tests are performed to diagnose the patient. Gathering more information such as knowledge from the medical test reports aids in the detection of the disease and thereby reducing the uncertainty involved.

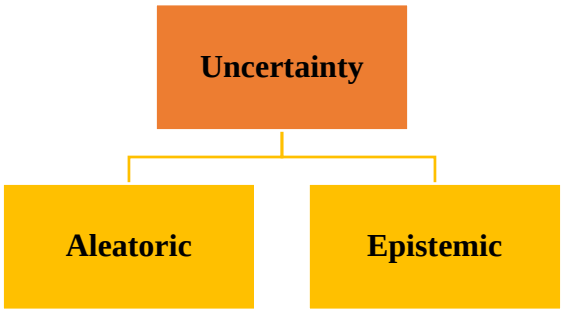

Figure 4. Classification of Uncertainty

Epistemic uncertainty is also known by a few other names such as reducible uncertainty, subjective uncertainty, model form uncertainty, state of knowledge, type B uncertainty and *de dicto* [2.3]. As shown in Figure 5, this uncertainty is further classified in two types:

- Model Uncertainty
- Phenomenological Uncertainty
- Behavioral Uncertainty

Model Uncertainty is attributed to the accuracy of the mathematical model that describes the actual physical system under consideration. Since the model design depends on the designer, this type of uncertainty is also due to lack of knowledge. Every model is a representation of reality and therefore a perfect model is not true although a model can be better than another. Uncertainties in a model arises from approximation, numerical, and programming errors. For a system that is well defined, a nearly accurate model can be designed. In such scenarios, deficiencies could arise due to errors rather than uncertainties.

Numerical errors arise due to finite precision arithmetic which can be reduced by higher precision computers and software, whereas, programming errors arise due to bugs, defects and design errors caused by the programmer.

Phenomenological Uncertainty arises during the design or development of the model, wherein certain phenomenon, principle of working or any other execution conditions are unknown.

Behavioral Uncertainty arises from the actions of an individual or an organization. Selection over a choice of components by an engineer (design uncertainty), deciding upon the variables in a model independent of the engineer, of which the engineer does not have knowledge (requirement uncertainty), future actions and decisions of individuals or other organizations (volitional uncertainty) and any other human errors that occur during the development of a system or project.

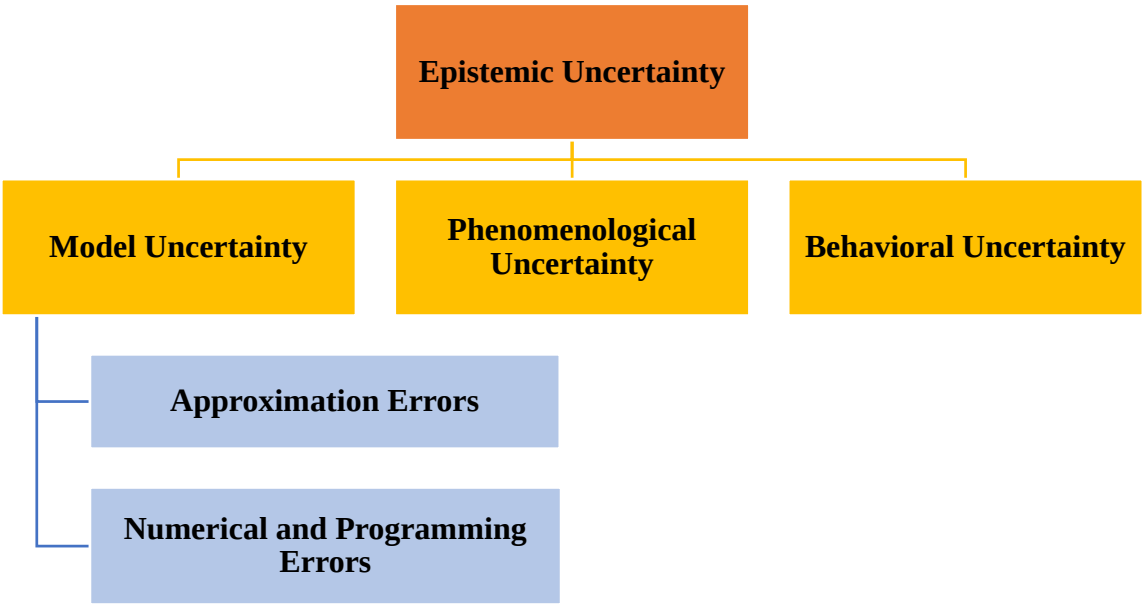

Figure 5. Classification of Epistemic Uncertainty

Uncertainty handling reduces the number of errors in the system and makes the system more reliable and stable. Since the epistemic uncertainty is the reducible uncertainty, few uncertainty handling methods have been proposed. They are classified into four categories 1) Probabilistic Theory, 2) Fuzzy Set Theory, 3) Evidence Theory, and 4) Possibility Theory, as shown in Figure 6. Probabilistic theory is a popular mathematical approach applied in the estimation of various measure of uncertainty and aims at analyzing random phenomena based on stochastic process and random variables [2.4]. Fuzzy set theory and possibility theory deal with mitigation of uncertainty and incomplete information, whereas the evidence theory based-methods serve as alternate approaches to the probabilistic theory.

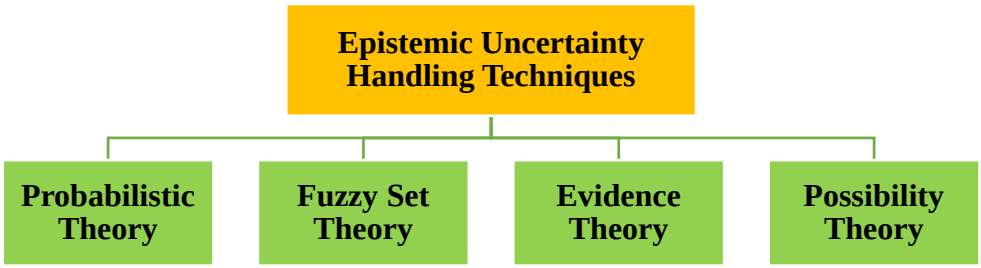

Figure 6. Epistemic Uncertainty Handling Techniques

Figure 7 shows the classification of probabilistic methods. These methods deal with both aleatory and epistemic uncertainty through experiments and provides a degree of belief which replaces the knowledge about the system state. The degree of belief is usually attached to all the events associated with a system and is expressed in the form of probabilities. Probabilities relating statements to a state of knowledge are expressed as $P(A|B)$ which changes with the aviablabitly of new evidence and is expressed as $P(A|B,C)$ [2.5]. Certain refining techniques have been proposed such as graphical models, Bayesian networks [2.6], Markov networks [2.7], and factor graphs [2.8].

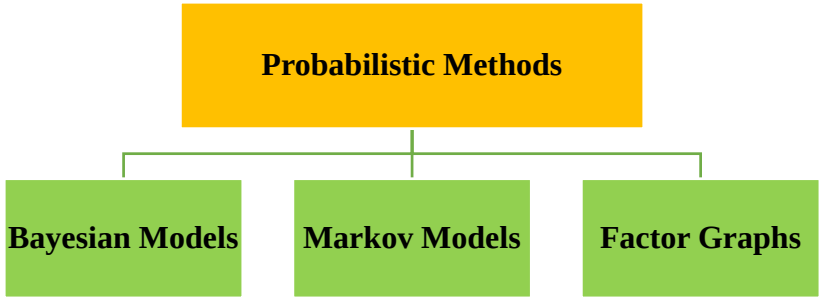

Figure 7. Classification of probabilistic methods

2.2. Bayes' Rule and Bayesian Networks

Bayes' Rule was initially discovered by Thomas Bayes. The Bayes' Rule describes the conditional probability of an event i.e. the probability of an event which is based on certain conditions that are related to the event. For two given events x and y, if the occurrence of event x is conditioned on the occurrence of event y then the proabability of event x given y for $P(y) \neq 0$ is defined as,

$$P(x|y) \equiv \frac{P(x,y)}{P(y)} \tag{1}$$

where $P(x,y)$ is known as the joint distribution of x and y [2.9]. In the case of conditional independence where event x and event y are independent of each other, $P(x) \neq 0$ and $P(y) \neq 0$, then mathematically it is expressed as,

$$P(x,y) = P(x)P(y) \tag{2}$$

Bayesian Networks, also known as belief networks or Bayes networks, is a graphical model that encodes probabilistic relationships among intervening variables of a model that influence one another via a directed acyclic graph (DAG). Since the model encodes dependencies among all variables, it is capable of handling different scenarios where certain data might be unavailable. A graph consists of vertices and edges wherein a

vertex is a node and an edge is a link between the vertices. When all the edges are directed (have an arrow in a single direction), then the graph is called a directed graph. A DAG is a special form of a directed graph such that traversing a path of vertices from one node to another along the direction of each edge, no path will revisit a vertex [2.9]. The nodes or the variables can be binary or discrete propositions or continuous quantities which can be observable or hidden. Causal relations can also take upon various functional forms such as linear or non-linear, deterministic or probabilistic, generative or inhibitory [2.10]. Two variables can possess a correlation irrespective of their connection being direct or indirect. If the two variables are connected indirectly then their correlation is mediated by one or more different variables.

Figure 8, illustrates the relationships in a DAG, consisting of seven nodes each representing a random variable, of which some of them are dependent on other variables and some are independent. From this, our understanding of a DAG becomes clear signifying that each vertex has an edge directed towards another vertex and the traversal over this path of edges does not revisit any vertex. The relationship between vertices is of a parent-child where the vertex from which the edge originates is the parent and the vertex where the edge is directed towards is the child. This is a causal relationship indicating the dependency of the child on the parent. Absence of a link, indicates conditional independence between the nodes [2.11]. Extracting the details of the parent-child relationship from Figure 8, we have four parent vertices and four child vertices and one vertex being a parent and a child. The relationship for each vertex is as follows:

$$Vertex\ x_1: \qquad Parent\{x_4, x_5\}$$

$Vertex\ x_2$: $Parent\{x_1\}$

$Vertex\ x_3$: $Parent\{x_5\}$

$Vertex\ x_4$: $Child\{x_1\}$

$Vertex\ x_5$: $Child\{x_1, x_2, x_3\}$ $Parent\{x_6, x_7\}$

$Vertex\ x_6$: $Child\{x_5\}$

$Vertex\ x_7$: $Child\{x_3, x_5\}$

With the definition of the model, the qualitative component of the Bayesian network is accomplished. The quantitative component is accomplished by characterizing the variables with probability distributions. Bayesian networks deal with joint probability distributions and conditional probability distributions, thereby allowing it to be used as a factorization tool. Applying the Bayes' Rule repeatedly on the model illustrated in Figure 8, we get,

$$P(x_1, x_2, x_3, x_4, x_5, x_6, x_7)$$

$$= P(x_7|x_6, x_5, x_4, x_3, x_2, x_1)P(x_6, x_5, x_4, x_3, x_2, x_1)$$

$$= P(x_7|x_5, x_3)P(x_6|x_5, x_4, x_3, x_2, x_1)P(x_5, x_4, x_3, x_2, x_1)$$

$$= P(x_7|x_5, x_3)P(x_6|x_5)P(x_5|x_4, x_3, x_2, x_1)P(x_4, x_3, x_2, x_1)$$

$$= P(x_7|x_5, x_3)P(x_6|x_5)P(x_5|x_3, x_2, x_1)P(x_4|x_3, x_2, x_1)P(x_3, x_2, x_1)$$

$$= P(x_7|x_5, x_3)P(x_6|x_5)P(x_5|x_3, x_2, x_1)P(x_4|x_1)P(x_3)P(x_2)P(x_1)$$

In a generalized form we can write,

$$P(x_1, \dots, x_n) = P(x_1|x_2, \dots, x_n)P(x_2, \dots, x_n)$$

$$P(x_1, \dots, x_n) = P(x_1|x_2, \dots, x_n)P(x_2|x_3, \dots, x_n)P(x_3, \dots, x_n)$$

$$P(x_1, \dots, x_n) = P(x_n) \prod_{i=1}^{n-1} P(x_i | x_{i+1}, \dots, x_n) \tag{3}$$

Therefore, Bayes' Rule allows for the representation of causal dependencies between various contextual events [2.12] [2.13] and also aids in the computation of probabilities in the case of no direct information available about the event under analysis.

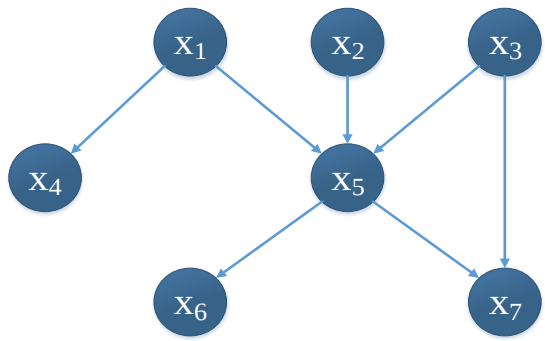

Figure 8. Relationships in a DAG and a Bayesian Network example

2.3. Bayesian Model for Scanning the Radio Spectrum

A Bayesian model, as described previously, is a graphical model encoding the probabilistic relationship among its intervening variables that influence each other via a directed acyclic graph**.** With the design of a Bayesian model, one can infer the probabilities of the intervening variables using the Bayes' rule and this process of inference is known as Bayesian Inference.

2.3.1. Simplified Bayesian Model

We first developed a preliminary Bayesian model that includes purely deterministic and measured variables, as shown in Figure 9. The black ellipses are deterministic variables of which the cognitive radio has knowledge about. The cognitive radio is aware about the time, frequency and location details at any given instant. The light blue shaded ellipses are

measured variables which are influenced by deterministic variables or measured variables. The usage level is a measured variable that is influenced by the time, frequency, and location. It is basically the past/previous usage level of the channel under consideration. The spectrum sensing decision is considered as a deterministic variable whose value is known as the binary result of the spectrum sensing process. The spectrum occupancy level is a measured variable which represents the final calculated spectrum occupancy level inferred using the past value (usage level) and the currently observed value (spectrum sensing decision). With the application of Bayesian inference, one can infer the probability of the variable spectrum occupancy level.

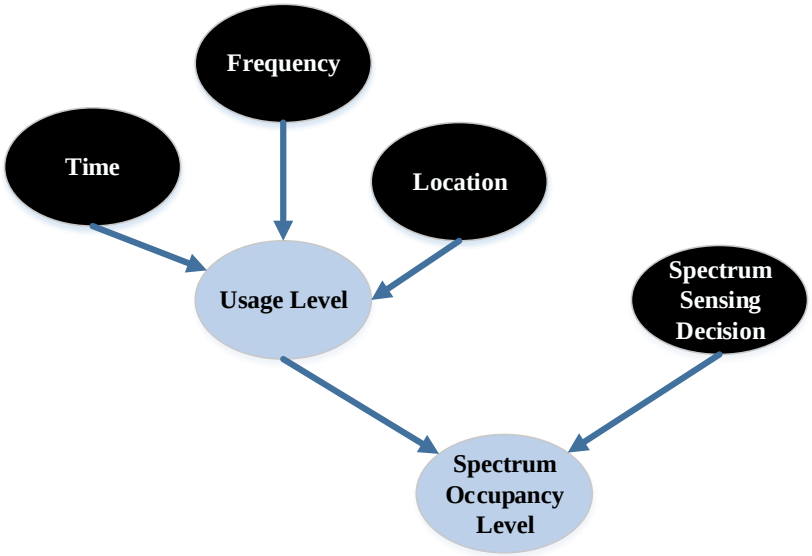

Figure 9. Simplified Bayesian Model to perform Bayesian Inference

2.3.2. Improved Bayesian Model

The model of Figure 9 does not take into consideration the uncertainty of sensing techniques. These techniques are characterized by probabilities of detection and false alarm. In this section we describe an improved model to take into consideration these

probabilities, and, hence deal with uncertainty. Figure 10 shows this improved Bayesian model. The new model, besides consisting of deterministic and measured variables also includes random variables. The variables in the black ellipses are deterministic variables of which the cognitive radio has knowledge about as they are parameters whose values are certain. On the other hand, the variables in the white ellipses, are random variables whose values are uncertain and subject to changes at any given instant of time. The variables in the light blue shade ellipses are those that can be measured. Time, frequency, and location are all deterministic variables whose values are known by the cognitive radio. As mentioned previously, the usage level represents the past/previous usage level of a given channel. The received power is a random variable, whose value is changing randomly. This power is affected by several factors, including the noise in the system, interference, and propagation losses. The SNR is a measured variable that is influenced by the received power which in turn influences the probability of detection and false alarm of the sensing technique used. These probabilities are deterministic as their values are known for a given value of SNR. The spectrum occupancy level is another measured variable which is of interest as it provides the current occupancy level of the channel under consideration.

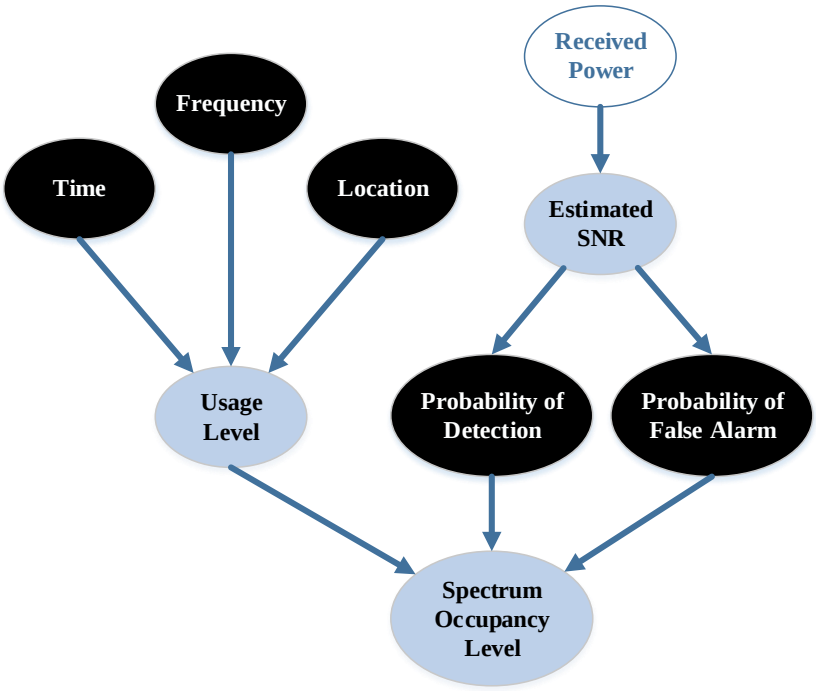

Figure 10. Improved Bayesian Model to perform Bayesian Inference

With the improved Bayesian model and the application of Bayesian inference, one can infer the probability of the measured variable, spectrum occupancy level. The detection and false alarm probabilities for each of the spectrum sensing technique was experimentally determined for a given value of SNR and are used in the Bayesian inferential process to infer the spectrum occupancy level.

Chapter 3

NOISE ESTIMATION

3.1 Background

In the field of cognitive radio, signal-to-noise ratio is a very important variable that affects the probabilities of detection and false alarm. Being able to estimate this variable can help in the process of spectrum sensing to identify the available channel and in decision-making phase to estimate the usage level of different channels of the radio spectrum. The received samples are a combination of the signal and noise. However, there is no method or tool to measure the power of the signal or the power of the noise; it can be only estimated. Several signal-to-noise ratio estimation techniques have been proposed to estimate the signal-to-noise. The following section describes the state-of-the art of these techniques in an additive white Gaussian noise channel.

3.2 State-of-the-Art: Classification of Signal-to-Noise Ratio (SNR) Estimators

Figure 11 describes the classification of the SNR estimation techniques. They are broadly classified into two main categories: 1) data aided and 2) non-data aided. Data aided estimation techniques require the knowledge of the characteristics of the transmitted data sequences. On the other hand non-data aided estimation techniques do not need any knowledge of the transmitted data sequences characteristics. Techniques of this category use approaches, such as extracting and analyzing the inherent properties of the received

signal to estimate the noise and signal powers. Data aided estimation techniques category is further divided into two types: transmitted and received data aided estimators. The transmitted data aided estimators, denoted as TxDA, requires the knowledge of the transmitted data sequence whereas the receiver data aided estimators, denoted as RxDA, use an estimate of the transmitted data sequence from the receiver decisions. Examples of techniques are those described by Pauluzzi et al. [3.1]. These techniques are studied by performing simulations using modulated signals such as BPSK signals in the case of real AWGN and 8-PSK signals in the case of complex AWGN. The authors used only simulations to investigate the performance of the estimators surveyed.

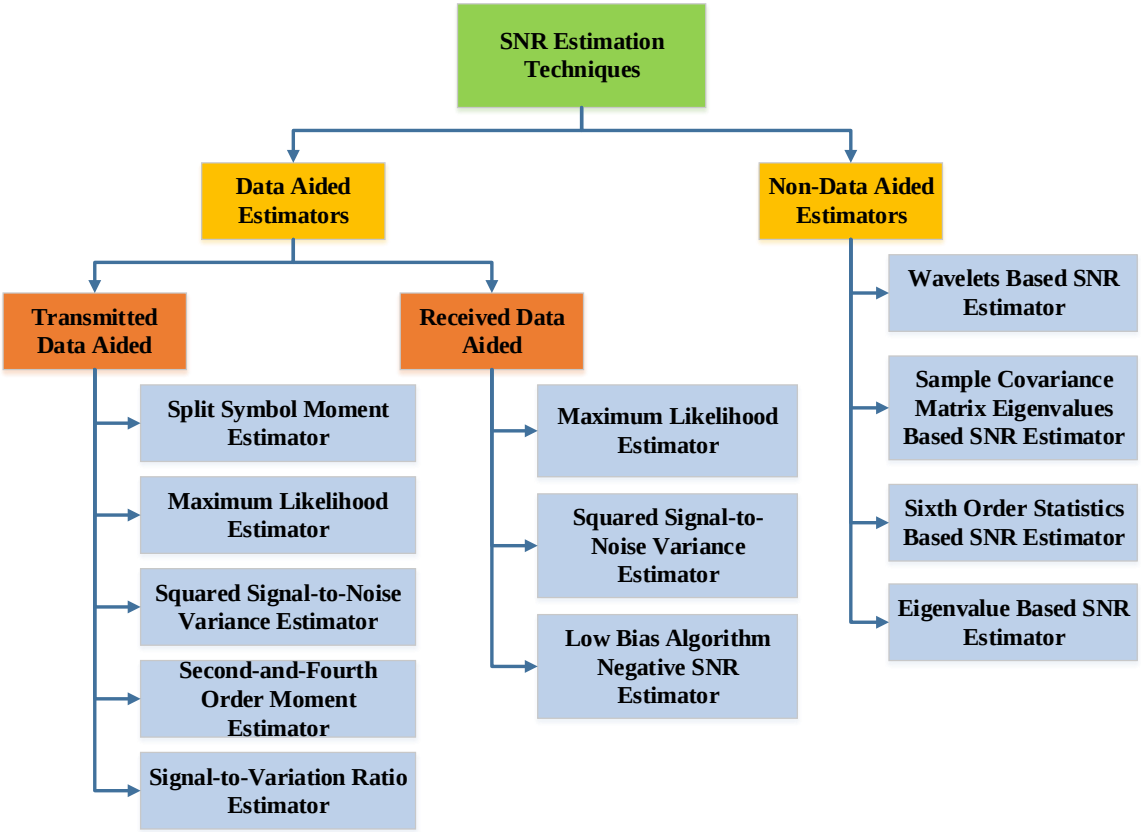

Figure 11. Classification of SNR Estimators

3.2.1 Data Aided Estimators

Examples of data aided estimation techniques include:

- Split-Symbol Moments estimator
- Maximum-Likelihood estimator
- Squared Signal-to-Noise Variance (SNV) Estimator
- Second-Order and Fourth-Order Moments Estimator
- Signal-to-Variation Ratio (SVR) Estimator
- Low Bias Algorithm Negative Signal-to-Ratio Estimator

a) Split-Symbol Moments Estimator

Split-symbol moments estimator was initially developed for a Binary Phase Shift Keying modulated signal in a real wide-band AWGN channel [3.2]. This estimator, denoted as $SSME_0$, was further improvised for implementation in band-limited channels ($SSME_1$) by Shah and Hinedi in [3.3] and narrow-band channels ($SSME_2$) by Shah and Holmes in [3.4]. The signal-to-noise ratio in this method is estimated by determining the solutions S and N to the system of linear equations [3.1]:

$$m_p = c_{11}S + c_{12}N \tag{1}$$

$$m_{ss} = c_{21}S + c_{22}N \tag{2}$$

Where m_p and m_{ss} are computed as functions of the samples obtained at the receiver. The coefficients c_{ij} are functions of the transmitter and receiver filter coefficients and are determined by computing the expected values of m_p and m_{ss} . In a further approach, the authors of [3.1] examined a variant of the $SSME_1$ by replacing m_p and m_{ss} with m_q and m_{sq} . This approach was denoted as $SSME_2$ and was applied for narrow-band channels. Similar to $SSME_0$ the signal-to-noise ratio was estimated by determining the solution of S and N to the system of quadratic equations given by:

$$m_q = d_{11}S^2 + d_{12}SN + d_{13}N^2 \quad (3)$$

$$m_{sq} = d_{21}S^2 + d_{22}SN + d_{23}N^2 \quad (4)$$

Where m_q and m_{sq} are functions of the samples obtained at the receiver and d_{ij} are functions of the transmitter and receiver coefficients. Similar to c_{ij}, d_{ij} can also be computed by using the expected values of m_q and m_{sq}. This estimator was only applied to BPSK-modulated signal in a real AWGN channel. Due to the complexity to extend it to higher degrees of modulation, this estimator was not studied for complex forms.

b) Maximum-Likelihood (ML) Estimator

The ML estimation theory [3.5] was introduced by Kerr [3.6] and Gagliardi et al.[3.7]. This estimator was derived by Gagliardi and Thomas for a BPSK-modulated signal in a real AWGN channel, but was further applied to M-ary PSK signals in complex AWGN by the authors of [3.1]. The samples of the complex received signal expressed in terms of real and imaginary parts is given by,

$$r_k = r_{I_k} + jr_{Q_k} = \sqrt{S}\left(m_{I_k} + jm_{Q_k}\right) + \sqrt{N}(z_{I_k} + jz_{Q_k}) \quad (5)$$

Where, r_k is the transmitted signal, r_{I_k} is the in-phase component of the transmitted signal, jr_{Q_k} is the complex quadrature component, m_{I_k} and m_{Q_k} are the in-phase and quadrature components of the information bearing signal, z_{I_k} and z_{Q_k} are the in-phase and quadrature components of the complex, sampled, zero-mean AWGN of unit variance, S is a signal power scale factor, and N is a noise power scale factor. The in-phase and quadrature components of the noise having a zero mean and variance $N/2$ are assumed to be independent of each other. Furthermore the signal and noise components are assumed to

be independent of each other and hence their joint probability density functions for $K = N_{sym}N_{ss}$ received samples is given by,

$$f\left(r_I, r_Q \middle| S, N, i\right) = \prod_{k=0}^{K-1} f\left(r_{I_k}, r_{Q_k} \middle| S, N, i\right)$$

$$= (\pi N)^{-K} \exp\left[\frac{-1}{N}\left(\sum_{k=0}^{K-1}\left(r_{I_k} - \sqrt{S}m_{I_k}^{i}\right)^2 + \sum_{k=0}^{K-1}\left(r_{Q_k} - \sqrt{S}m_{Q_k}^{i}\right)^2\right)\right] \qquad (6)$$

Where ${m_{I_k}}^{(i)}$ and ${m_{Q_k}}^{(i)}$ are the in-phase and quadrature components of the sampled and pulse-shaped information signal, i denotes the ith sequence of the $M^{N_{sym}}$ possibly transmitted message sequences, K is the total number of received samples, r_{I_k} is the in-phase component of the transmitted signal, r_{Q_k} is the quadrature component, S is a signal power scale factor and N is a noise power scale factor. The likelihood function is given by,

$$\Gamma(S, N, i) = \ln f\left(r_I, r_Q \middle| S, N, i\right)$$

$$= -K\ln(\pi N) - \frac{1}{N}\left[\left(\sum_{k=0}^{K-1}\left(r_{I_k} - \sqrt{S}m_{I_k}^{i}\right)^2 + \sum_{k=0}^{K-1}\left(r_{Q_k} - \sqrt{S}m_{Q_k}^{i}\right)^2\right)\right] \qquad (7)$$

Where $\Gamma(S, N, i)$ denotes the likelihood function, ${m_{I_k}}^{(i)}$ and ${m_{Q_k}}^{(i)}$ are the in-phase and quadrature components of the sampled and pulse-shaped information signal, i denotes the ith sequence of the $M^{N_{sym}}$ possibly transmitted message sequences, K is the total number of received samples, r_{I_k} is the in-phase component of the transmitted signal, r_{Q_k} is the quadrature component, S is a signal power scale factor and N is a noise power scale factor. The maximum likelihood estimate of the SNR, $\hat{\rho}_{ML}$ is calculated based on the property that the maximum likelihood estimate of the ratio of two parameters is the ratio of their individual maximum likelihood estimates [3.7]. Therefore the maximum likelihood estimate of the SNR is given by,

$$\hat{\rho}_{ML} = \frac{\hat{S}_{ML}}{\hat{N}_{ML}} \tag{8}$$

Where $\hat{\rho}_{ML}$ is the SNR estimate, $\hat{S}_{ML}$, the signal power and $\hat{N}_{ML}$, the noise power are calculated as the solution of the system of equations,

$$\frac{\partial(\Gamma(S,N,i)}{\partial S} = 0 \tag{9}$$

$$\frac{\partial(\Gamma(S,N,i)}{\partial N} = 0 \tag{10}$$

The respective solutions for $\hat{S}_{ML}$ and $\hat{N}_{ML}$ are given by,

$$\hat{S}_{ML} = \left[\left(\frac{1}{K}\right)\sum_{k=0}^{K-1}(r_{I_k}m_{I_k}^{i} + r_{Q_k}m_{Q_k}^{i}) \Big/ \left(\frac{1}{K}\right)\sum_{k=0}^{K-1}({m_{I_k}^{i}}^{2} + {m_{Q_k}^{i}}^{2})\right]^2 \tag{11}$$

$$\hat{N}_{ML} = \left(\frac{1}{K}\right)\sum_{k=0}^{K-1}({r_{I_k}}^{2} + {r_{Q_k}}^{2}) - \hat{S}\frac{1}{K}\sum_{k=0}^{K-1}({m_{I_k}^{i}}^{2} + {m_{Q_k}^{i}}^{2}) \tag{12}$$

Where ${m_{I_k}}^{(i)}$ and ${m_{Q_k}}^{(i)}$ are the in-phase and quadrature components of the sampled and pulse-shaped information signal, i denotes the ith sequence of the $M^{N_{sym}}$ possibly transmitted message sequences, K is the total number of received samples, r_{I_k} is the in-phase component of the transmitted signal, r_{Q_k} is the quadrature component. The authors of [3.1] extended the above works, further to the case of complex signals and the SNR is given by,

$$\hat{\rho}_{ML\ RxDA,complex}$$

$$= {N_{ss}}^2\left[\frac{1}{K}\sum_{k=0}^{K-1}Re\{r_k^* m_k^i\}\right]^2 \Bigg/ \left(\left(\frac{1}{K}\right)\sum_{k=0}^{K-1}|r_k|^2 - N_{ss}\left[\frac{1}{K}\sum_{k=0}^{K-1}Re\{r_k^* m_k^i\}\right]^2\right) \tag{13}$$

Where Re{.} denotes the real part of a complex quantity, K is the total number of symbols, N_{ss} is the number of samples per symbol, ${m_{I_k}}^{(i)}$ is the in-phase component of the sampled

and pulse-shaped information signal, i denotes the ith sequence of the $M^{N_{sym}}$ possibly transmitted message sequences, K is the total number of received samples and r_k is the transmitted signal. In order to obtain the above for a real channel the complex quantities are replaced by their corresponding real quantities. Thomas in [3.8] proved that the estimator has a bias that can be reduced by multiplying the denominator by $K/(K-3)$.

$$\hat{\rho}'_{ML\,RxDA,\ real} = N_{ss}{}^2 \left[\frac{1}{K}\sum_{k=0}^{K-1} r_k m_k^i\right]^2 \Bigg/ \left(\left(\frac{1}{K-3}\right)\sum_{k=0}^{K-1} r_k{}^2 - \frac{N_{ss}}{K(K-3)}\left[\sum_{k=0}^{K-1} r_k m_k{}^{(i)}\right]^2\right) \quad (14)$$

Where K is the total number of symbols, N_{ss} is the number of samples per symbol, $m_{I_k}{}^{(i)}$ is the in-phase component of the sampled and pulse-shaped information signal, i denotes the ith sequence of the $M^{N_{sym}}$ possibly transmitted message sequences, K is the total number of received samples and r_k is the transmitted signal. The authors of [1] also obtained a complex channel reduced bias estimator as given below,

$$\hat{\rho}'_{ML\,RxDA,\ complex} = N_{ss}{}^2 \left[\frac{1}{K}\sum_{k=0}^{K-1} Re\{r_k^* m_k^i\}\right]^2 \Bigg/ \left(\left(\frac{1}{K-\frac{3}{2}}\right)\left\{\sum_{k=0}^{K-1} |r_k|^2 - \frac{N_{ss}}{K}\left[\sum_{k=0}^{K-1} Re\{r_k^* m_k^i\}\right]^2\right\}\right) \quad (15)$$

Where K is the total number of symbols, N_{ss} is the number of samples per symbol, $m_{I_k}{}^{(i)}$ is the in-phase component of the sampled and pulse-shaped information signal, i denotes the ith sequence of the $M^{N_{sym}}$ possibly transmitted message sequences, K is the total number of received samples and r_k is the transmitted signal.

c) Squared Signal-to-Noise Variance (SNV) Estimator

The squared signal-to-noise variance estimator is based upon the first absolute moment and the second moment of the sampled output of the matched filter. This technique was initially formulated by Gilchriest et al. [3.9] for BPSK signals in real AWGN channel. The SNV RxDA estimator as given in [3.9] is expressed in terms of the sampled output of the matched filter as

$$\hat{\rho}_{SNV\ RxDA,\ real} = \left[\frac{1}{N_{sym}}\sum_{n=0}^{N_{sym}-1}|y_n|\right]^2 \Bigg/ \left(\left(\frac{1}{N_{sym}-1}\right)\sum_{n=0}^{N_{sym}-1} {y_n}^2 - \frac{1}{N_{sym}(N_{sym}-1)}\left[\sum_{n=0}^{N_{sym}-1}|y_n|\right]^2\right) \quad (16)$$

Where N_{sym} is the number of M-ary source symbols and y_n is the received signal sample. The SNV SNR estimator is considered as a special case of the ML estimator, as the ML estimator operates on N_{SS} samples per symbol at the input to the matched filter and the SNV SNR estimator operates on the optimally sampled output of the matched filter with $N_{ss} = 1$. Furthermore, it can be seen that the factor $1/(N_{sym} - 1)$ in the denominator can be replaced by $1/(N_{sym} - 3)$ to attain a reduced bias form of the estimator for real channels. The TxDA form of this estimator is obtained by replacing the estimated symbols a_n^i, with the transmitted symbols a_n.

$$\hat{\rho}'_{SNV\ TxDA,\ real} = \left[\frac{1}{N_{sym}}\sum_{n=0}^{N_{sym}-1} y_n a_n\right]^2 \Bigg/ \left(\left(\frac{1}{N_{sym}-3}\right)\sum_{n=0}^{N_{sym}-1} {y_n}^2 - \frac{1}{N_{sym}(N_{sym}-3)}\left[\sum_{n=0}^{N_{sym}-1} y_n a_n\right]^2\right) \quad (17)$$

Where N_{sym} is the number of M-ary source symbols, y_n is the received signal sample and a_n is the transmitted symbol. The complex channel, reduced bias estimator may be expressed as an adaptation of equation 15 a**s** shown below,

$$\hat{\rho}'_{SNV\ RxDA,\ complex}$$

$$= \left[\frac{1}{N_{sym}} \sum_{n=0}^{N_{sym}-1} Re\{y_n^* a_n^i\}\right]^2 \Bigg/ \left(\frac{1}{N_{sym} - \frac{3}{2}}\right)\left(\sum_{n=0}^{N_{sym}-1} |y_n^2| - \left(\frac{1}{N_{sym}}\right)\left[\sum_{n=0}^{N_{sym}-1} Re\{y_n^* a_n^i\}\right]^2\right) \quad (18)$$

Where Re{.} denotes the real component, N_{sym} is the number of M-ary source symbols, y_n is the received signal sample and a_n^i is the ith transmitted symbol. The TxDA version of the above can be obtained by replacing the receiver estimates a_n^i with the transmitted symbols a_n.

d) Second-Order and Fourth-Order Moments Estimator

Benedict et al. [3.10] applied the second and fourth order moments to estimate the carrier strength and noise strength in real AWGN channels separately. Matzner [3.11] provided a detailed derivation of an SNR estimator that yielded expressions similar to [3.10]. The authors of [3.1] derive the expressions provided in [3.11] for complex channels and then provide the modified form for application to real channels.

The second moment of y_n is given by

$$M_2 = E\{y_n y_n^*\} = SE\{|a_n|^2\} + \sqrt{SN}E\{a_n w_n^*\} + NE\{|w_n|^2\} + \sqrt{SN}E\{w_n a_n^*\} \quad (19)$$

Where $E\{.\}$ denotes the expectation operator, M_2 is the second moment, S is the signal power scale factor, a_n is the transmitted symbol, N is the noise power scale factor and w_n is the AWGN. The fourth moment of y_n is given by

$$
\begin{aligned}
M_4 = \; & E\{(y_n y_n^*)^2\} \\
& = S^2 E\{|a_n|^4\} \\
& + 2S\sqrt{SN}.(E\{|a_n|^2 a_n w_n^*\} + E\{|a_n|^2 a_n^* w_n\}) \\
& + SN.(E\{(a_n w_n^*)^2\} + 4E\{|a_n|^2 |w_n|^2\} + E\{(a_n^* w_n)^2\}) \\
& + 2N\sqrt{SN}(E\{|w_n^2| a_n w_n^*\} + E\{|w_n^2| a_n^* w_n\}) + N^2 E\{|w_n|^4\}
\end{aligned} \tag{20}
$$

Where $E\{.\}$ denotes the expectation operator, M_4 is the fourth moment, S is the signal power scale factor, a_n is the transmitted symbol, N is the noise power scale factor and w_n is the AWGN. Assuming the noise and signal are zero mean and independent and also the in-phase and quadrature components of the noise are independent the above two equations reduce to:

$$M_2 = S + N \tag{21}$$

$$M_4 = k_a S^2 + 4SN + k_w N^2 \tag{22}$$

Where M_2 is the second moment, M_4 is the fourth moment, S is the signal power scale factor, a_n is the transmitted symbol, N is the noise power scale factor, $k_a = E\{|a_n|^4\}/E\{|a_n|^2\}^2$ is the kurtosis of signal and $k_w = E\{|w_n|^4\}/E\{|w_n|^2\}^2$ is the kurtosis of noise. $\hat{S}$ and $\widehat{N}$ being the solutions of S and N respectively are given by,

$$\hat{S} = \frac{M_2(k_w - 2) \pm \sqrt{(4 - k_a k_w)M_2^2 + M_4(k_a + k_w - 4)}}{k_a + k_w - 4} \tag{23}$$

$$\widehat{N} = M_2 - \hat{S} \tag{24}$$

Where M_2 is the second moment, M_4 is the fourth moment, S is the signal power scale factor, a_n is the transmitted symbol, N is the noise power scale factor, k_a is the kurtosis of signal, k_w is the kurtosis of noise and $\hat{S}$ and $\widehat{N}$ are the solutions of S and N respectively. Calculating the ratio of $\hat{S}$ to $\widehat{N}$, we obtain the M_2M_4 estimator for a complex channel with

$k_a = 1$ and $k_w = 2$ for M-ary PSK signal and complex noise respectively. The expression is given by,

$$\hat{\rho}_{M_2M_4,complex} = \frac{\sqrt{2M_2^2 - M_4}}{M_2 - \sqrt{2M_2^2 - M_4}} \tag{25}$$

Where M_2 and M_4 are the second and fourth moments. Assuming y_n is real, M_2 is same as above but $M_4 = E\{y_n^4\}$ is given by

$$M_4 = k_a S^2 + 6SN + k_w N^2 \tag{26}$$

Where M_4 is the fourth moment, S is the signal power scale factor, N is the noise power scale factor, k_a is the kurtosis of signal and k_w is the kurtosis of noise. Solving for $\hat{S}$ using M_2 and M_4 we get,

$$\hat{S} = \frac{M_2(k_w - 3) \pm \sqrt{(9 - k_a k_w)M_2^2 + M_4(k_a + k_w - 6)}}{k_a + k_w - 6} \tag{27}$$

Where M_2 is the second moment, k_a is the kurtosis of signal and k_w is the kurtosis of noise. The final estimator expression for real channels assuming a BPSK signal with real noise where $k_a = 1$ and $k_w = 3$, is given by,

$$\hat{\rho}_{M_2M_4,real} = \frac{(\frac{1}{2})\sqrt{6M_2^2 - 2M_4}}{M_2 - (\frac{1}{2})\sqrt{6M_2^2 - 2M_4}} \tag{28}$$

Where M_2 and M_4 are the second and fourth moments. In both the cases, the negative root of $\hat{S}$ is chosen so that the final SNR is positive. This estimator is not a data-aided estimator as it relies completely on the second and fourth order moments of the received signal and also does not take into consideration the receiver decisions.

e) Signal-to-Variation Ratio (SVR) Estimator

A moment based estimator, initially developed for monitoring the channel quality in multipath fading channels, can also be applied to measure the quality of an AWGN channel. Described by Brandão et *al*. in [3.12], this estimator was designed to operate only on M-ary PSK modulated signal. The authors of [3.1] have sketched the derivation for complex channels and further modified it for real channels. The SVR estimator is expressed as a function of the parameter,

$$\beta = \frac{E\{y_n y_n^* y_{n-1} y_{n-1}^*\}}{E\{(y_n y_n^*)^2\} - E\{y_n y_n^* y_{n-1} y_{n-1}^*\}} \tag{29}$$

Where y_n is the received sampled signal. Substituting $E\{(y_n y_n^*)^2\} = M_4$ from the previous section of second and fourth order moments based estimator and simplification of the term $E\{y_n y_n^* y_{n-1} y_{n-1}^*\} = S^2 + 2SN + N^2$, yields,

$$\beta = \frac{\rho^2 + 2\rho + 1}{(k_a - 1)\rho^2 + 2\rho + (k_w - 1)} \tag{30}$$

Where ρ is the SNR, k_a is the kurtosis of signal and k_w is the kurtosis of noise. Solving for ρ, and substituting $k_a = 1$ and $k_w = 2$ for M-ary PSK signal in a complex AWGN channel we get,

$$\hat{\rho}_{SVR,complex}$$

$$= \frac{(\beta - 1) \pm (\sqrt{(\beta - 1)^2 - [1 - \beta(k_a - 1)][1 - \beta(k_w - 1)]}}{1 - \beta(k_a - 1)}$$

$$= \beta - 1 + \sqrt{\beta(\beta - 1)} \tag{31}$$

Where β is the SVR function parameter. For real signals,

$$\beta = \frac{E\{y_n^2 y_{n-1}^2\}}{E\{y_n^4\} - E\{y_n^2 y_{n-1}^2\}} \tag{32}$$

Where y_n is the received signal sample. Substituting $\{y_n^4\} = k_a S^2 + 6SN + k_w N^2$, simplifying $E\{y_n^2 y_{n-1}^2\}$ to $S^2 + 2SN + N^2$ and substituting $k_a = 1$ and $k_w = 3$ for a BPSK modulated signal in real AWGN channel yields the expression,

$$\hat{\rho}_{SVR,real} = \frac{(2\beta - 1) \pm \sqrt{(2\beta - 1)^2 - [1 - \beta(k_a - 1)][1 - \beta(k_w - 1)]}}{1 - \beta(k_a - 1)}$$

$$= (2\beta - 1) + \sqrt{2\beta(2\beta - 1)} \tag{33}$$

Where β is the SVR function parameter, k_a is the kurtosis of signal and k_w is the kurtosis of noise.

f) Low Bias Algorithm Negative Signal-to-Ratio Estimator

Most of the previously described estimation techniques perform poorly in the estimation of negative SNR values. In [3.13], the authors developed an algorithm that is based upon the maximum-likelihood principle and has lower estimation bias at lower and negative ranges of SNR. This technique was developed for a BPSK signal assuming a timing and career phase synchronization. The transmitted signals take values between {+A, -A} with equal probabilities and are corrupted by real AWGN samples with variance σ^2. The authors of [3.13] developed an iterative search algorithm that estimated the amplitude satisfying the below equation from the vector of received samples, r_k.

$$A = \frac{1}{N} \sum_{k=1}^{N} r_k th\left(\frac{A r_k}{\sigma^2}\right) \tag{34}$$

where $th(x) = \frac{e^x - e^{-x}}{e^x + e^{-x}}$ and $th(\frac{A r_k}{\sigma^2}) = \begin{cases} +1, & r_k > 0 \\ -1, & r_k < 0 \end{cases}$

Where A is the amplitude of the transmitted signal, r_k is the vector of received samples and σ_z^2 is the variance of noise. The solution to equation 34 is the maximum-likelihood estimate of A which can be expressed as,

$$\hat{A} = \frac{1}{N}\sum_{k=1}^{N}|r_k| \tag{35}$$

Where $\hat{A}$ is the maximum likelihood estimate of A, N is the number of received samples vector and r_k is the received samples vector. The iterative search algorithm performed a set of computations in each and every iteration, resulting in an amplitude which after several iterations resulted in the best estimate of the amplitude. Using this estimated amplitude, the signal-to-noise ratio was computed and given by

$$\rho = \frac{A_m^2}{1 - A_m^2} \tag{36}$$

where A_m is the estimated amplitude and ρ is the estimated signal-to-noise ratio.

3.2.2 Non-Data Aided Estimators

Examples of this category of estimators include:

- Wavelets based SNR estimation
- Sample Covariance Matrix Eigenvalues Based SNR Estimation Technique
- Sixth-order Statistics based Non-Data aided SNR Estimator
- Eigenvalue-based SNR Estimation

a) Wavelets Based SNR Estimation

Paula Quintana-Quiros et al. [3.14] developed an estimation technique based on wavelets concept to perform jamming detection. Matched filters are used in coherent digital receivers to deal with the decoding of digital signals associated with specific timing and waveform characteristics. The waveform of these digital signals is characterized by abrupt transitions and discrete amplitude levels which is exploited by the wavelet theory to measure the SNR. Wavelets have the ability to perform local analysis i.e. to analyze a

portion of a larger signal in time. This technique does not intend to adapt to the modulation scheme of the received signal at this moment although this could be a future work.

Wavelet analysis is the decomposition of a signal into shifted and scaled versions of a mother wavelet, ψ, providing a time-view scale of the signal [3.14] .Wavelet transform is defined as the summation over time of the signal multiplied by the scaled and shifted versions of ψ, producing coefficients that are a function of the wavelet scale and position and also indicate the degree of correlation of the wavelet to the portion of signal under analysis.

Discrete Wavelet Transform (DWT) is implemented using filter banks, comprised by low-pass and high-pass filters, which decompose the analyzed signal into approximations and details. Approximations are high-scale, low frequency components whereas details are low-scale, high frequency components.

Wavelet-based Estimators are of two types:

1. Trend Detector (Figure 12)
2. Self-Similarity Detector (Figure 13)

Trend Detector based estimator seeks to extract the amplitude trend and is based on the principle that noise changes at a higher rate [3.14]. It implements the wavelet analysis to detect the overall trend of the received signal's amplitude, which is corrupted by CWGN. The trend is the slowest part of the signal corresponding to the greatest scale value in wavelet analysis.

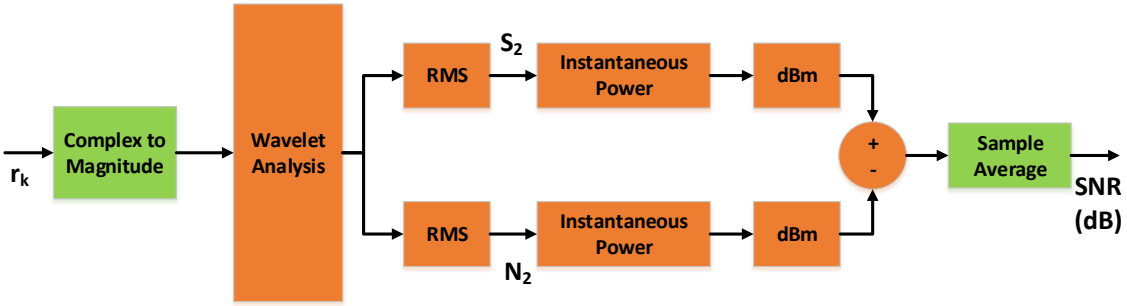

Figure 12. Wavelet-based Estimator 1: Trend Detector

Self-Similarity Detector based estimator performs signal extraction based on the similarity between the signal under consideration and the mother wavelet. The wavelet coefficients are correlation indexes of the signal under analysis and the wavelet. Larger the value of the coefficient of correlation, stronger is the resemblance between the signal and the wavelet.

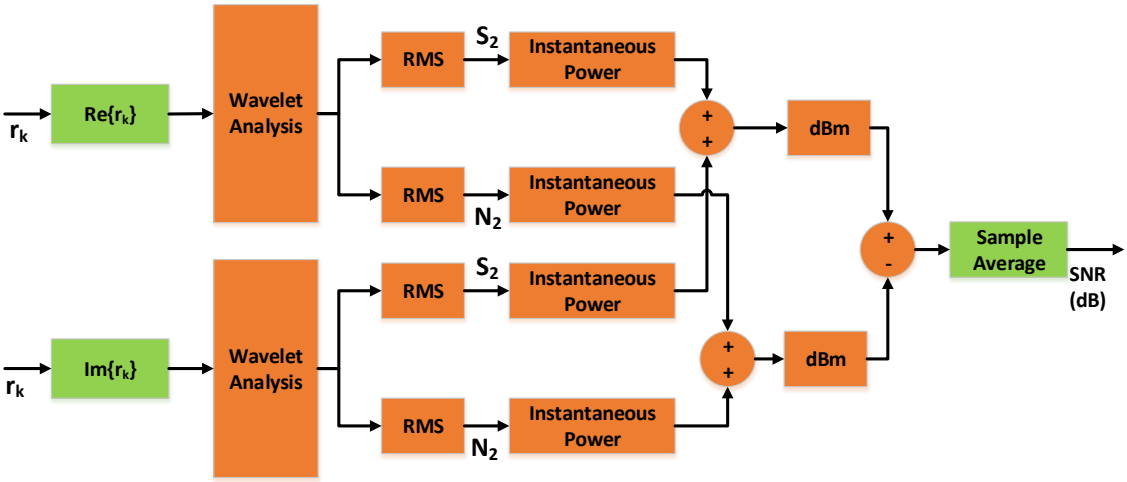

Figure 13. Wavelet-based estimator 2: Self-Similarity Detector

b) Sample Covariance Matrix Eigenvalues Based SNR Estimation Technique

Another recently developed SNR estimation technique is based on the eigenvalues of the sample covariance matrix of the received signal [3.15]. It initially detects the eigenvalues as in [3.16-3.19]. Then the Minimum Descriptive Length criterion is used to

split the signal and noise corresponding eigenvalues. This technique is referred to as a blind estimation technique because the signal and the noise power are unknown and are estimated from the received samples.

The received signal, $\boldsymbol{X}$, is assumed to be either a noise only component, $\boldsymbol{Z}$, or a mixture of both noise component, $\boldsymbol{Z}$, and transmitted signal components, $\boldsymbol{S}$. Under the binary hypothesis it is expressed as,

$$\boldsymbol{X} = \begin{cases} \boldsymbol{Z} & H_0 \\ \boldsymbol{S} + \boldsymbol{Z} & H_1 \end{cases} \tag{37}$$

Where H_0, is the null hypothesis when only noise is received and H_1, is the positive hypothesis when a mixture of signal and noise is received. The received signal is expressed as an N x L matrix as shown below,

$$\boldsymbol{X} = \begin{pmatrix} x_{1,1} & \cdots & x_{1,N} \\ \vdots & \ddots & \vdots \\ x_{L,1} & \cdots & x_{L,N} \end{pmatrix}$$

Where $x_{i,j}$ is the vector of received signal samples. The noise and signal are assumed to be independent and the noise is assumed to be white Gaussian noise components with mean 0 and variance σ_z^2, therefore rewriting equation 37 as,

$$\boldsymbol{x_i} = \begin{cases} \boldsymbol{z_i} & H_0 \\ \boldsymbol{s_i} + \boldsymbol{z_i} & H_1 \end{cases} \tag{38}$$

Where $x_i = \left[x_{i,1} \dots x_{i,N}\right]^T$ is the received signal component, $s_i = \left[s_{i,1} \dots s_{i,N}\right]^T$ is the transmitted signal component and $z_i = \left[z_{i,1} \dots z_{i,N}\right]^T$ is the noise component $\forall i = 1,2 \dots L$. Given an observation bandwidth, B and a transmitted signal with occupied bandwidth, b; in the sample covariance matrix eigenvalues domain, $M \leq L$, implies that $\left\{\frac{M}{L}\right\}$ fraction of the whole observation bandwidth is occupied by the transmitted signal and the rest

$\left\{L - \left(\frac{M}{L}\right)\right\}$ fraction represents the noise only component. When $N, L \to \infty$, the statistical covariance matrices of the noise, signal and received samples is defined as,

$$\mathbf{R}_z = E\{\boldsymbol{z}(n)\boldsymbol{z}^H(n)\} = \sigma_z^2 \boldsymbol{I}_L \ ; \ -\infty < n < \infty \tag{39}$$

$$\mathbf{R}_s = E\{\boldsymbol{s}(n)\boldsymbol{s}^H(n)\} \tag{40}$$

$$\mathbf{R}_x = E\{\boldsymbol{x}(n)\boldsymbol{x}^H(n)\} \tag{41}$$

Where $\mathbf{R}_z$ is the noise statistical covariance matrix, $\mathbf{R}_{\boldsymbol{s}}$ is the signal statistical covariance matrix, $\mathbf{R}_{\boldsymbol{x}}$ is the noise statistical covariance matrix, $(.)^H$ denotes complex conjugate transpose, σ_z^2 is the noise variance and $\boldsymbol{I}_L$ is the L-order identity matrix. Since the signal and noise are independent,

$$\boldsymbol{R}_x = \boldsymbol{R}_s + \boldsymbol{R}_z = \boldsymbol{R}_s + \sigma_z^2 \boldsymbol{I} \tag{42}$$

Obtaining the eigenvalues, λ_x of $\boldsymbol{R}_x$ and λ_s of $\boldsymbol{R}_s$ in a descending order, we see that,

$$\lambda_{xi} = \lambda_{si} + \sigma_z^2 \quad \forall i = 1, 2 \ldots M$$

$$\lambda_{xi} = \sigma_z^2 \quad \forall i = M+1, M+2 \ldots L$$

Where λ denotes the group of eigenvalues and the statistical covariance matrix eigenvalues are equal to signal components power.

As in [3.16] sample covariance matrices, $\widehat{\boldsymbol{R}}_x$ of the received signal samples can be computed instead of statistical covariance matrix as there exists a finite number of samples. The sample covariance matrix of the received signal is computed as,

$$\widehat{\boldsymbol{R}}_x = \frac{1}{N}\boldsymbol{X}\boldsymbol{X}^H \tag{43}$$

The eigenvalues of the samples covariance matrix deviate from the signal power components and follow Marcenko Pastuer density [3.20] which depends on the value

of L/N. The value of M is estimated using the Minimum Descriptive Length criterion. The estimated value of M is denoted as $\widehat{M}$ and is given by,

$$\widehat{M} = \underset{M}{argmin}\left(-(L-M)N\log\left(\frac{\theta(M)}{\phi(M)}\right) + \frac{1}{2}M(2L-M)\ logN\right); \tag{44}$$

$$0 \leq M \leq L-1$$

Where,

$$\theta(M) = \prod_{i=M+1}^{L} \lambda_i^{\frac{1}{L-M}} \tag{45}$$

$$\phi(M) = \frac{1}{L-M}\sum_{i=M+1}^{L} \lambda_i \tag{46}$$

Where L is the number of eigenvalues, N is the number of samples and λ_i is the set of eigenvalues. After estimating the value of $\widehat{M}$, the signal group of eigenvalues is determined as $\lambda_1 \ldots \lambda_{\widehat{M}}$ and the noise group eigenvalues as $\lambda_{\widehat{M}+1} \ldots \lambda_L$. To compute the noise variance σ_z^2, two values σ_{z1}^2 and σ_{z2}^2 are calculated as follows:

$$\sigma_{z1}^2 = \frac{\lambda_L}{\left(1-\sqrt{c}\right)^2} \tag{47}$$

$$\sigma_{z2}^2 = \frac{\lambda_{\widehat{M}+1}}{\left(1+\sqrt{c}\right)^2} \tag{48}$$

K linearly spaced values in the range $[\sigma_{z1}^2, \sigma_{z2}^2]$ are denoted as π_k, where 1 ≤ k ≤ K. The Marcenko Pastuer density of parameters c, σ_z, is given by,

$$MP(c,\sigma_z) = dF^W(\nu) = \frac{\sqrt{\left(\nu - \sigma_z^2\left(1-\sqrt{c}\right)^2\right)\left(\sigma_z^2\left(1+\sqrt{c}\right)^2 - \nu\right)}}{2\pi\sigma_z^2\nu c}d\nu \tag{49}$$

Where

$$\sigma_z^2\left(1-\sqrt{c}\right)^2 \leq \nu \leq \sigma_z^2\left(1+\sqrt{c}\right)^2$$

Using equation 49 we can determine K Marcenko Pasteur densities of the parameters $\left(1-\hat{\beta}\right)c$ and π_k where $\hat{\beta}=\frac{\hat{M}}{L}$ and the empirical distribution function (edf) of the noise group eigenvalues is given by,

$$edf = F_n(t) = \frac{\text{number of sample values} \leq \text{t}}{\text{n}} \tag{50}$$

Where n is the total number of sample values in the noise eigenvalues. The noise eigenvalues empirical distribution is then compared with the Marcenko Pastuer densities and a goodness of fitting is used to pick the best estimate of π_k in order to estimate the value of σ_z^2. $D(\pi_k)$ is used to denote the goodness of fitting and is given by,

$$D(\pi_k) = \left\| edf - MP\left(\left(1-\hat{\beta}\right)c, \pi_k\right)\right\|_2 \tag{51}$$

The estimate of noise variance, $\widehat{\sigma_z^2}$, is given by,

$$\widehat{\sigma_z^2} = \underset{\pi_k}{argmin}\left(D(\pi_k)\right) \tag{52}$$

The total received power is given by,

$$\widehat{P_t} = \left(\frac{1}{NL}\sum_{j=1}^{L}\sum_{i=1}^{N}\left|x_{i,j}\right|^2\right) \tag{53}$$

Where $x_{i,j}$ is the received signal samples. Therefore the SNR is given by,

$$\hat{\gamma} = \frac{\widehat{P_s}}{\widehat{\sigma_z^2}} = \frac{\widehat{P_t} - \widehat{\sigma_z^2}}{\widehat{\sigma_z^2}} = \left(\frac{1}{NL\widehat{\sigma_z^2}}\sum_{j=1}^{L}\sum_{i=1}^{N}\left|x_{i,j}\right|^2\right) - 1 \tag{54}$$

c) Sixth-order Statistics based Non-Data aided SNR Estimator

The second and fourth-order moment based SNR estimators were studied. The SNR estimator considered here is based on the sixth-order statistics. The second and fourth order estimator perform well with constant modulus constellations as its variance tends to be a

constant with SNR→∞. In the case of non-constant modulus constellations the variance increases as the SNR is squared. This being undesirable a workaround would be to partition the set of observations in subsets corresponding to symbols of equal modulus and then perform estimation [3.21]. Unless the SNR is high this partitioning technique also has lots of errors leading to a low-performance estimator. The 6th-order statistics estimator's advantage is to deal with constellations with two different amplitude levels. From the process of estimating the SNR with the second and fourth order estimators we re-write equation 22 as,

$$M_4 = c_4 S^2 + 4SN + 2N^2 \tag{55}$$

Where S is the signal power scale factor, N is the noise power scale factor, $k_a = c_4$ and $k_w = 2$. In general constellation moments for x_k complex-valued transmitted symbols is given by,

$$c_p = E\{|x_k|^p\} \tag{56}$$

We know that the moments-based estimators are based on the sample moments given by,

$$\widehat{M}_p = \frac{1}{K}\sum_{k=1}^{K}|r_k|^p \tag{57}$$

Using the fact that $E\{|n_k|^{2m} = m!.N^m$ and the even-order moments M_{2n} are seen to admit closed form expression in terms of S, N and c_{2m}, 0 ≤ m ≤ n [3.21]:

$$M_{2n} = \sum_{m=0}^{n}\frac{(n!)^2 c_{2m} S^m N^{n-m}}{(n-m)!\,(m!)^2} \tag{58}$$

Proceeding further we obtain the equations for M_2^3, $M_2 M_4$ and M_6 as,

$$M_2^3 = S^3 + S^2 N + 3SN^2 + N^3 \tag{59}$$

$$M_2M_4 = c_4S^3 + (4 + c_4)S^2N + 6SN^2 + 2N^3 \tag{60}$$

$$M_6 = c_6S^3 + 9c_4S^2N + 18SN^2 + 6N^3 \tag{61}$$

The authors of [3.21] established a linear relationship between the above three variables as,

$$D = M_6 - aM_2^3 - bM_2M_4 \tag{62}$$

Where M_2 is the second order moment, M_4 is the fourth order moment, M_6 is the sixth order moment and M_2M_4 is the second and fourth order moment. Choosing $a = 2(3 - b)$, substituting equation 59, 60 and 61 in equation 62 we see that the terms SN^2 and N^3, get cancelled out and yield,

$$D = [(c_6 - 6) - b(c_4 - 2)]S^3 + (9 - b)(c_4 - 2)S^2N \tag{63}$$

Substituting equation 21 in equation 60 and dividing by M_2^3 on both sides we get,

$$\frac{D}{M_2^3} = (c_6 - 9c_4 + 12)z^3 + (9 - b)(c_4 - 2)z^2 \tag{64}$$

Where z is the normalized SNR given by,

$$z = \frac{S}{S + N} \tag{65}$$

Therefore, with $\widehat{D} = \widehat{M}_6 - 2(3 - b)\widehat{M}_2^3 - b\widehat{M}_2\widehat{M}_4$ an estimate $\hat{z}$ can be obtained by solving for the roots in (0, 1) of

$$-\frac{\widehat{D}}{\widehat{M}_2^3} + (c_6 - 9c_4 + 12)\hat{z}^3 + (9 - b)(c_4 - 2)\hat{z}^2 = 0 \tag{66}$$

The roots are found by tabulating it in terms of $\widehat{D}/\widehat{M}_2^3$ with an iterative rule using,

$$\hat{z}^{n+1} = \sqrt{\frac{\widehat{D}/\widehat{M}_2^3}{(\alpha\hat{z}^n + \beta')}} \tag{67}$$

Where $\alpha = (c_6 - 9c_4 + 12)$ and $\beta' = (9 - b)(c_4 - 2)$; choosing $\hat{z}^0 = 0\ or\ 1$ as the starting point. The authors of [21] observed that for large$|b|$, this estimator approaches the M_2M_4 estimator, whereas for $b = 0$, it was seen that this estimator approached the estimator proposed in [3.22]. Hence based on the constellation used, the value of the free parameter b must be chosen.

d) Eigenvalue-based SNR Estimation

In [3.23], an eigenvalue based spectrum sensing technique in the presence of correlated noise is analyzed. The final spectrum sensing decision is made using the standard-condition-number (SCN)-based decision statistics which is based on the asymptotic random matrix theory (RMT). The author here proposes an SNR estimation technique which is based on the maximum eigenvalue of the covariance matrix of the received signal. The author has also studied the effect of noise correlation on the eigenvalue based spectrum sensing process under both the H_0 (noise only) and H_1 (signal plus noise) hypothesis. Following the work on the eigenvalue based spectrum sensing and the study of noise correlation, the SNR estimation technique under consideration is based on the asymptotic eigenvalue probability distribution function of the covariance matrix of the received signal. The covariance matrix of the received signal is given by,

$$R_Y = \left(\frac{1}{N}\right) YY^H \tag{68}$$

Where Y is the MxN received signal matrix, N is the number of samples and M is the fractional sampling rate at the input of the cognitive receiver. Three cases are considered by the authors 1) Signal plus correlated noise, 2) Correlated noise only and 3) Signal plus white noise. They initially developed a table with different parameters such as SCN, β, SNR(dB) and λ_{max} using the three aforementioned cases. With the study of the eigenvalue

based spectrum sensing technique, they computed the values of the maximum eigenvalues, λ_{max}, for the three different cases and the SCN, which is related to ρ, the correlation coefficient of the noise correlation as

$$SCN = \frac{1+\rho}{1-\rho} \tag{69}$$

The decision of the spectrum sensing is based upon the calculated value of SCN. With the help of the table and the calculated value of $\lambda_{\max}$ of the received signal's covariance matrix, the corresponding value of the SNR can be determined. The value of $\beta = \frac{M}{N}$ is assumed to be known as the operating parameter of the sensing module.

3.2.3 Comparison of SNR Estimators

In the above sections, the different types of SNR estimators have been studied. In order to evaluate the efficiency of the estimators, the performance of the estimators are compared. The best SNR estimator is the one that exhibits least bias or is unbiased and has the smallest variance. The statistical mean square error or MSE is the one that reflects both the bias and variance of the SNR estimate and is given by,

$$MSE\{\hat{\rho}\} = E\{(\hat{\rho} - \rho)^2\} \tag{70}$$

Where, $\hat{\rho}$ is an estimate of the SNR and ρ is the true SNR. The authors of [3.1] performed simulations to compute the sample MSE for each estimator from a number of estimates $\widehat{\rho_i}$ according to

$$MSE\{\hat{\rho}\} = \frac{1}{N_t}\sum_{i=1}^{N_t}(\widehat{\rho_i} - \rho)^2 \tag{71}$$

Where N_t is the number of trials.

Apart from the normalized mean square error, the Cramer-Rao Bound (CRB) is used as a reference to assess the absolute performance of each estimator. In [3.8] Thomas derived the CRB for real channels, based on which the authors of [3.1], extended the derivation to complex channels. For complex AWGN channels the CRB is given by,

$$NMSE\{\hat{\rho}\} \geq \frac{2}{\rho N_{sym}} + \frac{1}{N_{ss} N_{sym}} \tag{72}$$

Whereas for real AWGN channels it is given by,

$$NMSE\{\hat{\rho}\} \geq 2\left(\frac{2}{\rho N_{sym}} + \frac{1}{N_{ss} N_{sym}}\right) \tag{73}$$

Figure 14 compares the performances of the $SSME_1$, $SSME_2$, and the ML SNR Estimators for BPSK modulated signals in real AWGN. From the Figure, it is clearly evident that the ML TxDA performs better when compared to the $SSME_1$ and $SSME_2$. At high levels of SNR the ML RxDA performs well as it avoids enough receiver errors and its performance is indistinguishable from the ML TxDA. The $SSME_1$ and $SSME_2$ do not perform well as compared to the ML TxDA and ML RxDA estimators although $SSME_2$ being a slightly modified approach yields a better performance than the $SSME_1$.

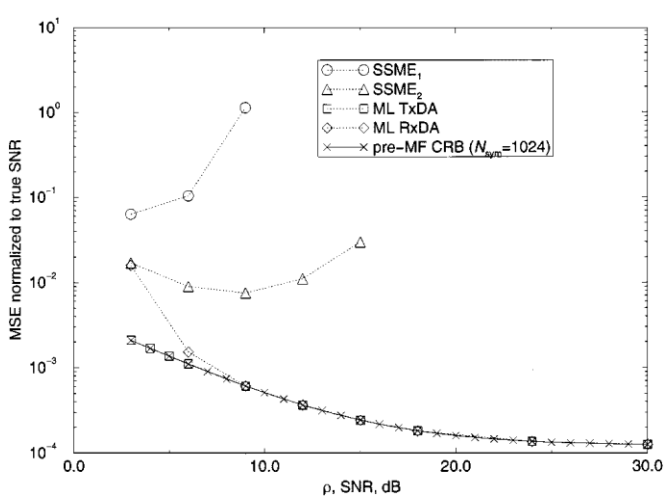

Figure 14. Normalized MSE with BPSK signals in real AWGN (N_{ss}=1 and N_{sym}=64) [3.1]

Figure 15 shows the NMSE comparison of the SVR, M_2M_4 and the SNV estimators. Similar to ML TxDA and ML RxDA in Figure 4, the SNV TxDA and SNV RxDA estimators also exhibit good performance at higher levels of SNR.

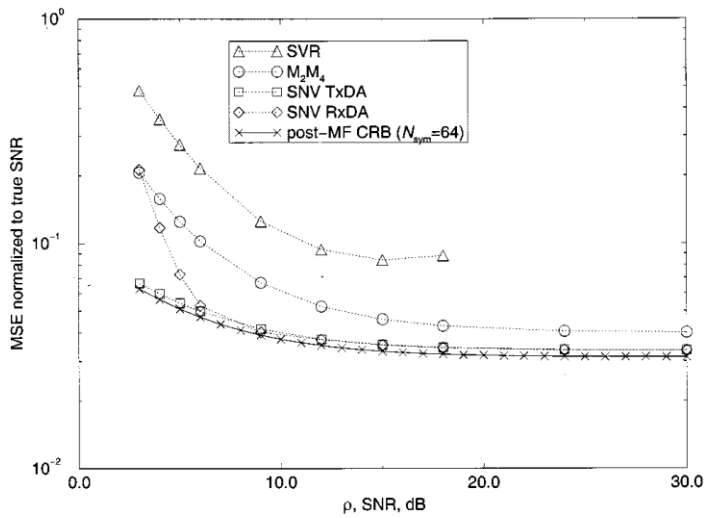

Figure 15. Normalized MSE with BPSK signals in real AWGN (N_{ss}=1 and N_{sym}=64) [3.1]

The authors of [3.13] use the normalized mean square error to compare the performance of their newly proposed SNR estimator to that of some other SNR estimators. The useful range of this estimator extends down to -5 dB and below -3 dB this estimator has an NMSE lower than that of the other techniques. This estimator also has a better performance than the previously discussed SNV RxDA SNR estimator. As observed this estimator has a low bias even at low SNR values and low values of N. Furthermore, with the increase in the value of N, the NMSE and the bias improve significantly when compared to that of the other estimators which exhibit slight improvements. This is shown in Figure 16.

On the other hand, the wavelets based estimator 1 and wavelets based estimator 2 were compared at different sampling frequencies to that of the Moments based estimator and it was observed that the wavelets based estimator 2 with higher sampling frequency

performed well than wavelets bases estimator 1 and was slightly inferior to the moments based estimator at high SNR.

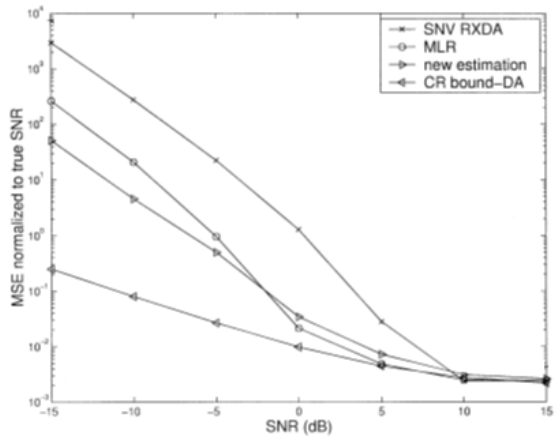

Figure 16. Normalized MSE for various SNR estimators (N=1024) (modified from [13])

Figure 17 illustrates the performance analysis of the sixth-order statistics based estimator for the most optimum value of b and compares that with the M_2M_4 and partition based estimator. The author of [3.21] has performed a Monte Carlo simulation for a 16-APSK constellation similar to the one in the DVB-S2 standard. In comparison to the M_2M_4 estimator, the proposed estimator performs poorly until 5 dB and beyond 5 dB shows performance improvement but tends to be biased for higher SNR.

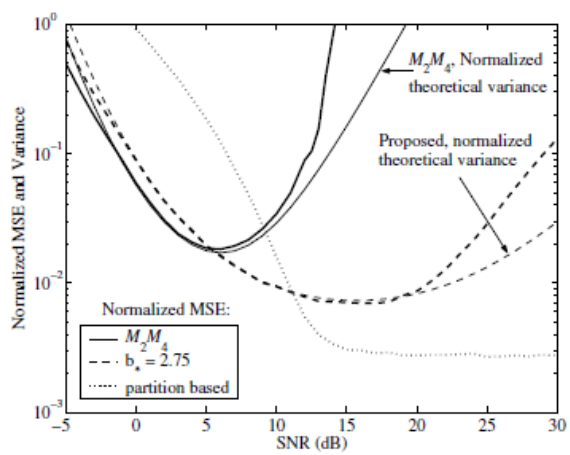

Figure 17. Mean Square Error and Theoretical variance for the SNR estimators, M_2M_4, partition based and 6th order statistics based [3.21]

Figure 18 illustrates the performance of the Eigenvalue based SNR estimator proposed in [3.23]. The results illustrated are for different scenarios of the signal plus the correlated noise and signal plus white noise scenario. Reduction in the SCN decreases the error rate among the correlated noise scenario and still lesser errors are observed in the white noise scenario. The best performance here is exhibited by the white noise scenario having the least NMSE even at -2 dB. Beyond the 3 dB, the NMSE is constant for all the above mentioned cases.

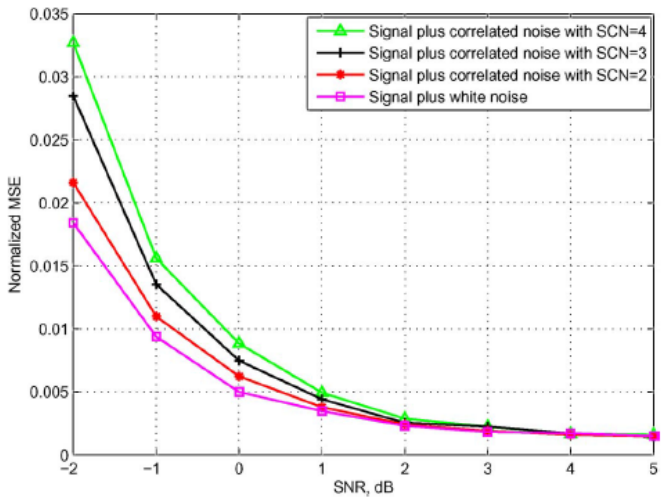

Figure 18. NMSE vs SNR for the technique proposed in [3.23]

In the above sections the different types of SNR estimators that have been developed over the years have been studied. Some of these serve as a fundamental technique for the recent works that are aimed at improving the initial works. Each technique was developed and simulated using different signal conditions in order to assess its overall performance. This performance measurement was done using the normalized mean square error metric. To the best of our knowledge on the study performed above it is seen that the ML TxDA estimator is one of the best estimators. But, this estimator has its own disadvantages like other SNR estimators which requires the knowledge of the transmitted

data sequence. Some other estimators have also been studied that do not make use of the transmitted data sequence. Since the efficiency of the radio spectrum scanning can be improved with estimation of SNR of the received signal samples it is the interest of this thesis to implement an SNR estimation technique that can estimate the SNR based on the received signal samples alone and without any knowledge of the transmitted data sequence.

3.3 Methodology

As previously explained, the Bayesian inference model, to measure in real time the occupancy of the spectrum, depends on several parameters and variables, including SNR. In this section we will describe the methodology used for estimating the SNR, and thus the noise. The technique is based on the eigenvalues of the covariance matrix formed from the received samples. This method was originally proposed by Hamid. M et al [3.15]. In the above section, this SNR estimator was studied and three fundamental variables K (Marchenko-Pastur distribution size), L (number of eigenvalues) and N (number of samples of the received signal) were recognized. The initial works did not involve any analysis of how these variables impacted the results of the SNR estimations. Therefore in our work we implement this SNR estimator and also make a comparative study of these variables and their impact on the estimated SNR.

In this thesis, both simulations and real experiments were performed. The analog signal input to the Universal Software Radio Peripheral (USRP) is digitized with a sampling rate of 1 MHz. The received samples are comprised of both noise component, $\boldsymbol{Z}$, and signal component, $\boldsymbol{S}$. Therefore it is necessary to determine the noise power i.e. noise variance, σ_z^2, in order to estimate the SNR.

N_s number of received signal samples, $x(n)$, from the USRP is obtained and stored in a Python-Numpy array as shown below:

$$[x(0), x(1), x(2), \dots, x(N_s - 1)]$$

A value known as the smoothing factor is chosen and denoted as L. An L x N_s dimension matrix is formed, where each row of the matrix is comprised of L time shifted versions of the received signal samples, $x(n)$, as shown below:

$$\boldsymbol{X} = \begin{pmatrix} x_{1,1} & \cdots & x_{1,N} \\ \vdots & \ddots & \vdots \\ x_{L,1} & \cdots & x_{L,N} \end{pmatrix}$$

Where $x_{i,j}$ is the received signal vector sample, L is the number of eigenvalues and N is the length of the received signal vector. The sample covariance matrix is computed as the product of matrix, X and its Hermitian transpose averaged over N_s samples which is given by,

$$\widehat{\boldsymbol{R}}_x = \frac{1}{N}\boldsymbol{X}\boldsymbol{X}^H \tag{74}$$

The eigenvalues of the resultant L x L matrix is computed, sorted in descending order and stored in an L-element array. The descending order sort is performed as per the Minimum Descriptive Length criterion which implies that the first M eigenvalues represent the transmitted signal component and the rest $L - M$ eigenvalues represent the noise component. The eigenvalues Python-Numpy array is as shown below:

$$[\lambda_1, \lambda_2, \dots, \lambda_M, \lambda_{M+1}, \dots, \lambda_L]$$

The value of M is estimated using the Minimum Descriptive Length criterion as given by,

$$\widehat{M} = \underset{M}{argmin}\left(-(L-M)N\log\left(\frac{\theta(M)}{\phi(M)}\right) + \frac{1}{2}M(2L-M)\ logN\right); \tag{75}$$

$$0 \leq M \leq L - 1$$

where,

$$\theta(M) = \prod_{i=M+1}^{L} \lambda_i^{\frac{1}{L-M}} \tag{76}$$

$$\phi(M) = \frac{1}{L-M} \sum_{i=M+1}^{L} \lambda_i \tag{77}$$

where $\widehat{M}$, is the estimated value of M. After the estimation of M, the array of eigenvalues is split up based on the noise group and transmitted signal group as given below:

$$\lambda_{Signal} = [\lambda_1, \lambda_2, \dots, \lambda_{\widehat{M}}]$$

$$\lambda_{Noise} = [\lambda_{\widehat{M}+1}, \lambda_{\widehat{M}+2}, \dots, \lambda_L]$$

To estimate the noise power, σ_z^2 using the array λ_{Noise}, two values σ_{z1}^2 and σ_{z2}^2 are calculated as follows:

$$\sigma_{z1}^2 = \frac{\lambda_L}{\left(1 - \sqrt{c}\right)^2} \tag{78}$$

$$\sigma_{z2}^2 = \frac{\lambda_{\widehat{M}+1}}{\left(1 + \sqrt{c}\right)^2} \tag{79}$$

where, $c = L/N$. In random matrix theory, the Marchenko-Pastur law provides the probability density function of singular values of large rectangular random matrices, when its dimensions tend to infinity. In this case, the matrix X is the rectangular random matrix whose entries $X_{i,j}$ are independent and identically distributed random variables with mean zero and variance σ^2. A set of K linearly spaced values in the range $[\sigma_{z1}^2, \sigma_{z2}^2]$ are generated and denoted as π_k, where 1 ≤ k ≤ K. The Marchenko-Pastur density of the parameters $\left(1 - \hat{\beta}\right)c$ and π_k where $\hat{\beta} = \frac{\widehat{M}}{L}$ is given by,

$$MP\left((1-\hat{\beta})c, \pi_k\right)$$

$$= \frac{\sqrt{\left(\nu - \left(\pi_k\left(1-\sqrt{(1-\hat{\beta})c}\right)\right)^2\right) * \left(\left(\pi_k\left(1+\sqrt{(1-\hat{\beta})c}\right)\right)^2 - \nu\right)}}{2 * \pi * \pi_k^2 * (1-\hat{\beta})c * \nu} \tag{80}$$

where,

$$\left(\pi_k\left(1-\sqrt{(1-\hat{\beta})c}\right)\right)^2 \leq \nu \leq \left(\pi_k\left(1+\sqrt{(1-\hat{\beta})c}\right)\right)^2$$

The values of the Marchenko-Pastur distribution are computed and stored in an array, MP_d. The empirical distribution function of the noise group eigenvalues, λ_{Noise} is computed by,

$$E_d = F_n(t) = \frac{\text{number of sample values} \leq \text{t}}{\text{n}} = \frac{1}{n}\sum_{i=1}^{n} 1_{\lambda_{Noise}(i) \leq t} \tag{81}$$

where

$$n = L - \widehat{M} + 1$$

and is stored in an array E_d. Both the arrays, MP_d and E_d are compared and a goodness of fitting, $D(\pi_k)$, is used to find the best estimate of π_k, thereby estimating the value of the noise power, σ_z^2. The goodness of fitting is given by,

$$D(\pi_k) = \|E_d - MP_d\|_2 = \sqrt{\sum(E_d - MP_d)^2} \tag{82}$$

From the array of values of $D(\pi_k)$, the index of the minimum value of $D(\pi_k)$ is obtained and the corresponding value of the array π_k for the obtained index is the estimate of noise variance, $\widehat{\sigma_z^2}$, which is given by,

$$\widehat{\sigma_z^2} = \underset{\pi_k}{argmin}\left(D(\pi_k)\right) \tag{83}$$

With the noise power estimated, the signal power can be calculated as the difference between the total received power and the estimated noise power. The total received power is given by,

$$\widehat{P_t} = \left(\frac{1}{N_s L} \sum_{j=1}^{L} \sum_{i=1}^{N_s} \left| x_{i,j} \right|^2 \right) \tag{84}$$

Therefore the SNR, $\hat{\gamma}$, is given by,

$$\hat{\gamma} = \frac{\widehat{P_s}}{\widehat{\sigma_z^2}} = \frac{\widehat{P_t} - \widehat{\sigma_z^2}}{\widehat{\sigma_z^2}} = \left(\frac{1}{N_s L \widehat{\sigma_z^2}} \sum_{j=1}^{L} \sum_{i=1}^{N_s} \left| x_{i,j} \right|^2 \right) - 1 \tag{85}$$

With these mathematical formulations, the process of SNR estimation is programmed in Python. To assess the performance of the SNR estimator, initial experiments were performed by simulating a BPSK signal and fusing it with additive white Gaussian noise with mean 0 and standard deviation, σ_z^2, which was subjected to the SNR estimation technique. This experiment was performed to study how the three independent variables K (Marchenko-Pastur distribution size), L (smoothing factor/number of eigenvalues) and N (number of samples) impacted the accuracy of the estimated SNR value by measuring the normalized mean square error. The values of K, L and N were varied between a range of values and simulations were run repeatedly for a specified number of iterations. The results of these experiments were analyzed and an optimized value for the variables K, L and N were selected for use in real experiments and in the process of scanning the radio spectrum. A flowchart summarizing the estimation technique is as shown in Figure 19. As the first step shows, the received samples are stored in an array and based on the value of the smoothing factor variable L, a received sample' matrix of LxN dimensions is generated. The sample covariance matrix of the newly generated matrix is

computed and its eigenvalues is extracted. From this set of eigenvalues the value of M is estimated which aids in the splitting of noise group and signal group eigenvalues. With the noise group eigenvalues, the Marchenko-Pastur density values and the empirical distribution are computed, from which the noise power is computed. With the availability of the noise power and the total received power, computed from the received signal, the signal power can be calculated as their difference. The ratio of the signal power to the noise power yields the estimated value of the SNR.

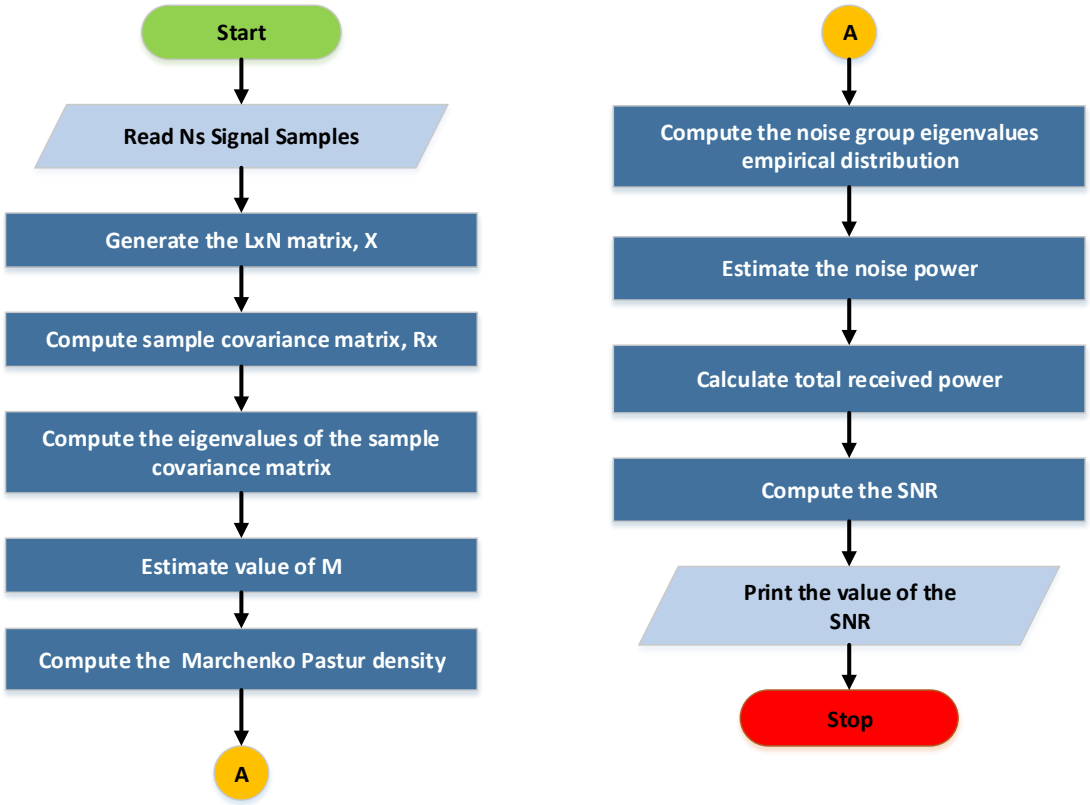

Figure 19. Flowchart of SNR Estimation technique

3.4 Results & Conclusion

From the SNR estimation technique equations, it is observed that N (number of samples), L (smoothing factor), and K (length of Marchenko-Pastur distribution) are the

fundamental variables that affect the efficiency. Therefore, an investigation was performed on how these variables impact the value of the normalized mean square error in the estimation of the SNR. A set of simulation experiments were performed, wherein simulated additive white Gaussian noise was added to a simulated BPSK signal. The values of the three variables N, L, and K were varied in multiple combinations and the resulting values of the normalized mean square error was 3D-plotted in MATLAB against either of the combination of any two variables out of the three keeping the third variable as a constant. It is interesting to note that the 3D-subplots show different colors in different regions of the plot when there is a wide range of variations in the output values. In the current scenario the output value is that of the NMSE and in each subplot if the values of the NMSE is in a wide range, then a color transition is observable from the higher end to the lower end of the values in the output range. All the values of the NMSE have been presented in the semi-log range.

In the first set of results, we shall analyze the changing trend of the normalized mean square error for different values of SNR with respect to the different values of K and L as illustrated in Figure 20 and Figure 21. In these figures**,** K is represented on the x-axis, L on the y-axis and the normalized mean square error (NMSE) on the z-axis. The range of values of K in these experiments is varied from 10 to 50 with a step of 1, whereas L is varied from 10 to 100 with a step of 1. Since the values of K and L have been varied over a range of values, N is kept constant. The value of N in Figure 20 is 1024 whereas that in Figure 21 is 2048. Each 3d-subplot illustrates the variation of the NMSE for a specific value of the SNR. In Figure 20 we see that in each of the subplot, the value of K does not impact the change of the normalized mean square error drastically with the variation of

values from 10 to 50. Few more simulations were performed for higher values of K at the range of 150 and 200, but no change in the value of the normalized mean square error was noticed. With this we understand that the value of K does not impact the error of the estimation and therefore this variable can be fixed to a constant value. Secondly, it was noticed during the experiments that a higher value of K leads a higher processing time in the estimation of the SNR. This is because of the complexity that arises in the for-loop implemented to generate the Marchenko-Pastur distribution values. Since K essentially describes the Marchenko-Pastur distribution size, any increase to the size of the distribution leads in a higher number of for-loops involved in the computation of the distribution values. Therefore in order to choose a fixed value of K, it was ensured that the value was low so that it could produce the same result as that of any higher value of K and at the same time it could also perform the process of SNR estimation consuming the lease amount of time. From this analysis the optimum value of K was set to 10 for real experiments and the spectrum survey.

Proceeding with the analysis of the variable L after the analysis of K, we shall observe how the variable L impacts the value of the NMSE. In Figure 20, in the first three 3D-subplots, wherein the SNR ranges from -5 dB to 5 dB it is seen that the NMSE remains unchanged or is not impacted much with the change in the value of L. From the fourth subplot onwards, wherein the SNR is 10 dB and greater, the range of values of the NMSE show significant variation. In the 3D-subplot with SNR equal to 10 dB the variation of the NMSE is very gradual and this change occurs with the value of L between 30 and 40. With further increase in the value of SNR, in the other subplots too, the same observation is made wherein the value of the NMSE starts to drop with L in the range of 30 to 40, but this

drop turns from a gradual one to a very steep one. The value of L essentially signifies the number of eigenvalues that can be obtained from the sample covariance matrix. It is clearly evident that more the number of eigenvalues available for the estimation process, higher is the accuracy of estimation. Another important observation made during these simulations were that the time taken for estimation of the SNR increased with the value of L. The increase in estimation time with that of the value of L was not highly significant as that of the increase in the value of K where the estimation time increased rapidly. Therefore the value of L that has to be chosen must be a value greater than 40 and one that ensures low error and low processing time. To decide on this value, the timing performance analysis of the estimator had to be studied.

The next variable to analyze is N, which indicates the number of samples that was involved in the SNR estimation process. In Figure 20, the value of N was kept constant at 1024 for the entire simulation. In a similar manner simulations were performed for varying values of K and L, keeping the value of N constant at 2048 and the results of the same is illustrated in Figure 21. From Figure 21, it is seen that the NMSE decreases further on for each value of the SNR as the lower range of the NMSE varies till 10^{-4} when compared to that of Figure 21 where the lower range of the NMSE varies only till 10^{-3}. Similar to L and K, the processing time was seen to be higher with higher value of N. The estimation time increases overall with the increasing number of samples, as it increases the time to acquire N samples and every other computation in the estimation of the SNR has to deal with this N number of samples.

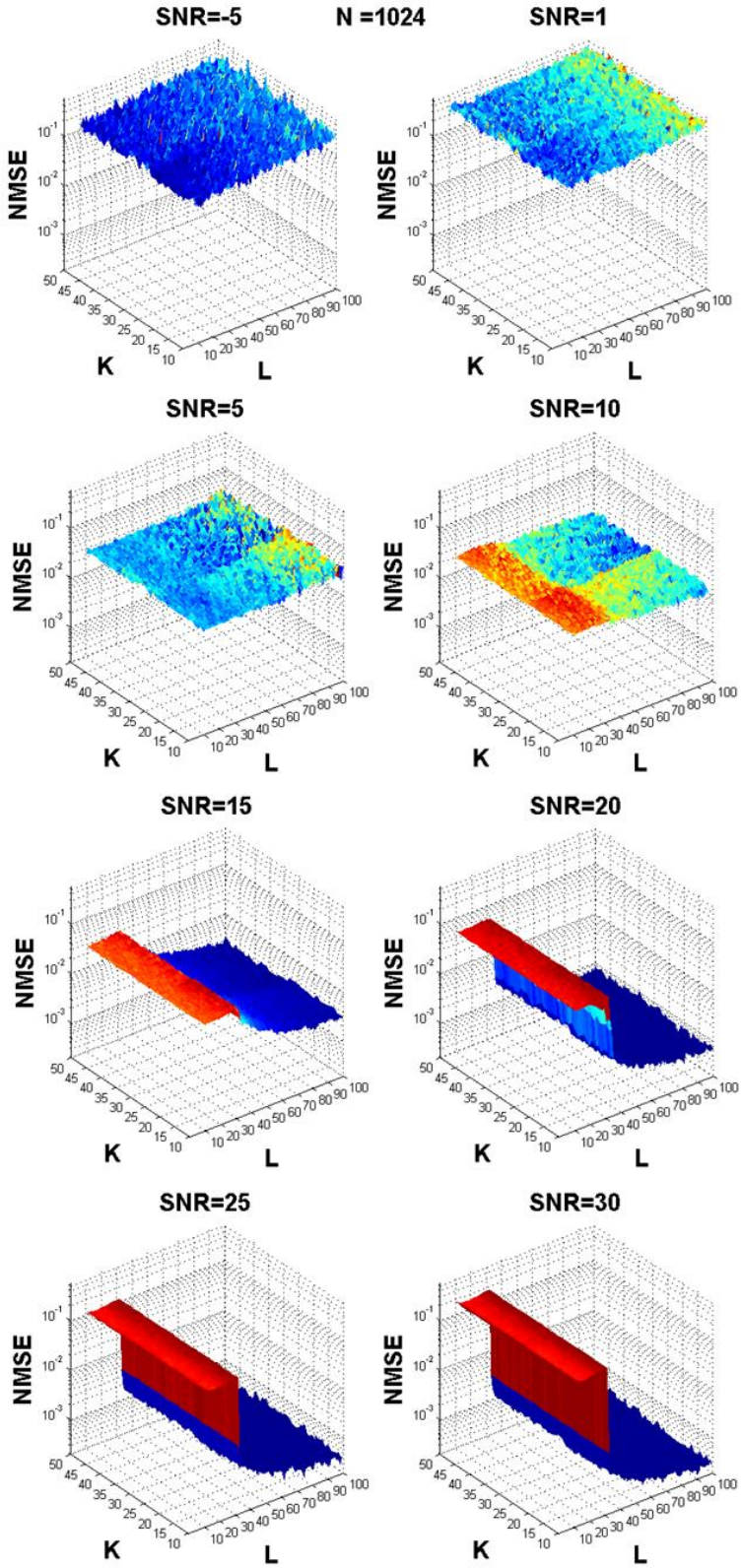

Figure 20. Variation of the normalized mean square error with respect to the values of K and L (N=1024)

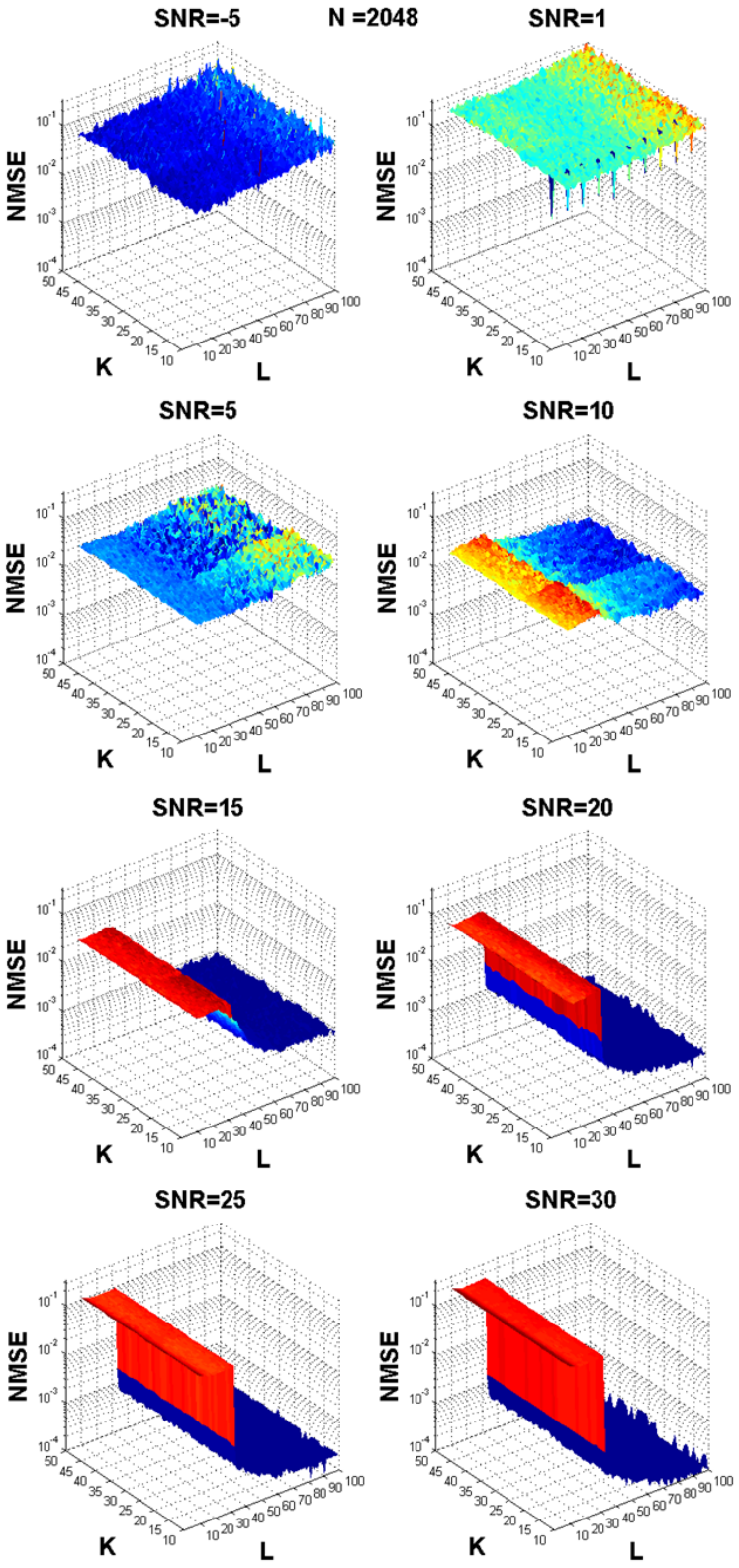

Figure 21. Variation of the normalized mean square error with respect to the values of K and L (N=2048)

After the analysis of the variables K and L with constant N, we shall now study the impact of the variables L and N to the NMSE, wherein the value of N was increased from 1024 to 7168 with a step of 1024, L was varied from 10 to 100 with a step of 1, and K was constant at 10. Examples of results of this simulation for an SNR of 15 dB are shown in Figure 22 and Figure 23, illustrating the variation of the NMSE with respect to L and N. Figure 22 illustrates the 3D-plot with N on the x-axis, L on the y-axis and NMSE on the z-axis and Figure 23 illustrates the 2D-plot of the same with L on the x-axis and NMSE on the y-axis. From these figures, it is evident that the NMSE decreases with increasing value of L as seen previously. As observed previously, the value of L where the NMSE begins to drop steeply is in the range of 30 to 40 and this evident from Figure 23. We also observe that the NMSE decreases to a very great extent of the order of 10^{-4} with the value of N increasing to 7168. The trade-off here is that with such a high number of samples being used, the SNR estimation time also increases reducing the overall performance of the system.

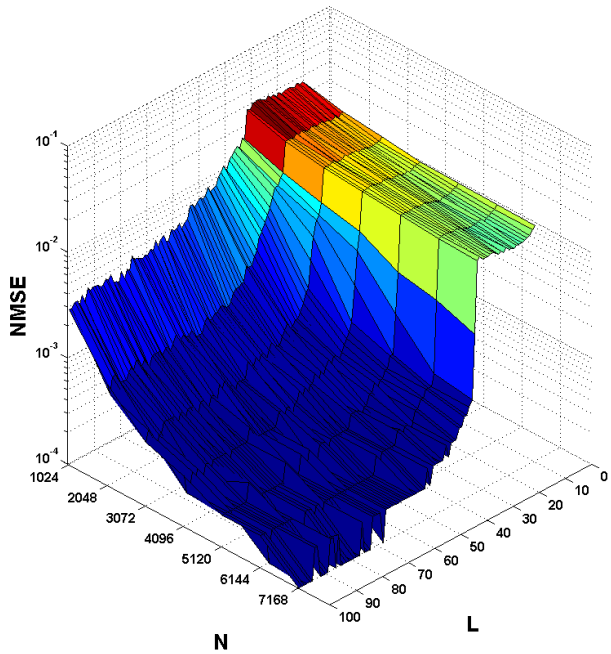

Figure 22. 3D plot of NMSE variation with respect to L and N

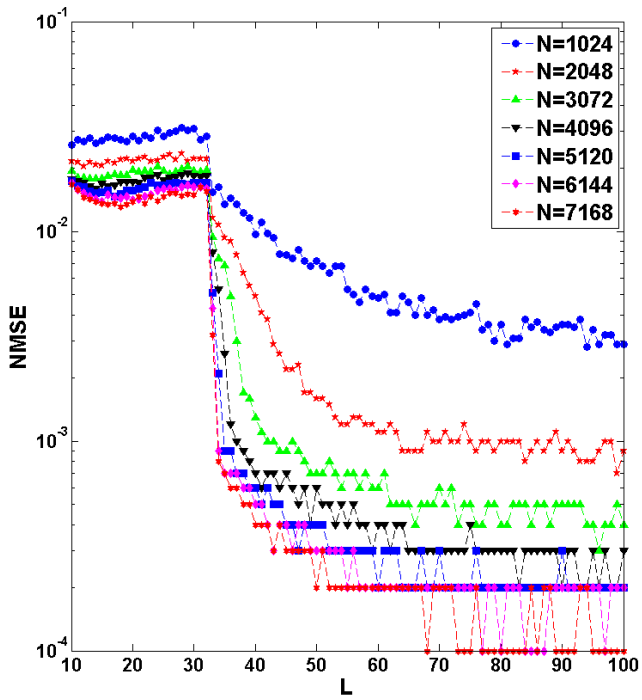

Figure 23. 2D plot of NMSE variation with respect to L and N

Performance Analysis: In order to select an optimum value for the variables L and N, we performed a timing performance analysis, wherein we computed the total processing time for estimating the SNR. In order to perform this analysis, we repeated the simulation trials with the value of N ranging from 1024 to 7168 with a step of 1024 and the value of L selected as 50, 75 and 100. These three values were chosen as we needed to choose any value of L greater than 40. The results of this simulation tests are shown in table 1. The frequency of the CPU used in these simulation tests is 3.16 GHz. Figure 24, illustrates the graph of the processing time with varying number of samples for the three different values of L.

From table 1 and Figure 24, it is evident that the processing time to estimate the SNR increases almost exponentially. We see that for the lowest value of L i.e. 50, the processing time varies from anywhere between 31.639 milliseconds for 1024 samples to

76.524 milliseconds for 7168 samples. The processing time varies from 46.8401 milliseconds to 145.225 milliseconds and 70.036 milliseconds to 262.381 milliseconds for L = 75 and L = 100 respectively with the number of samples ranging from 1024 to 7168. Relative to L = 50, it can be stated that the processing time for L=75 increases by almost double and that for L = 100 is approximately 3 to 4 times higher. Considering the NMSE variation from Figure 22 and Figure 23 and the processing time variations from Figure 14, we fixed the number of samples to an optimum value of 3072 and the value of L to 100 in order to achieve the SNR estimation with low error and low processing time.

Table 1. SNR estimation processing time for varying number of samples

N	**Processing time (milliseconds)**		
	L = 50	**L = 75**	**L = 100**
1024	31.6391	46.8401	70.0357
2048	38.4594	62.2195	94.1586
3072	43.9810	76.8402	122.8769
4096	52.3450	96.6398	153.2981
5120	59.2664	112.8243	181.7936
6144	63.3584	124.1219	226.6534
7168	76.5241	145.2247	262.3810

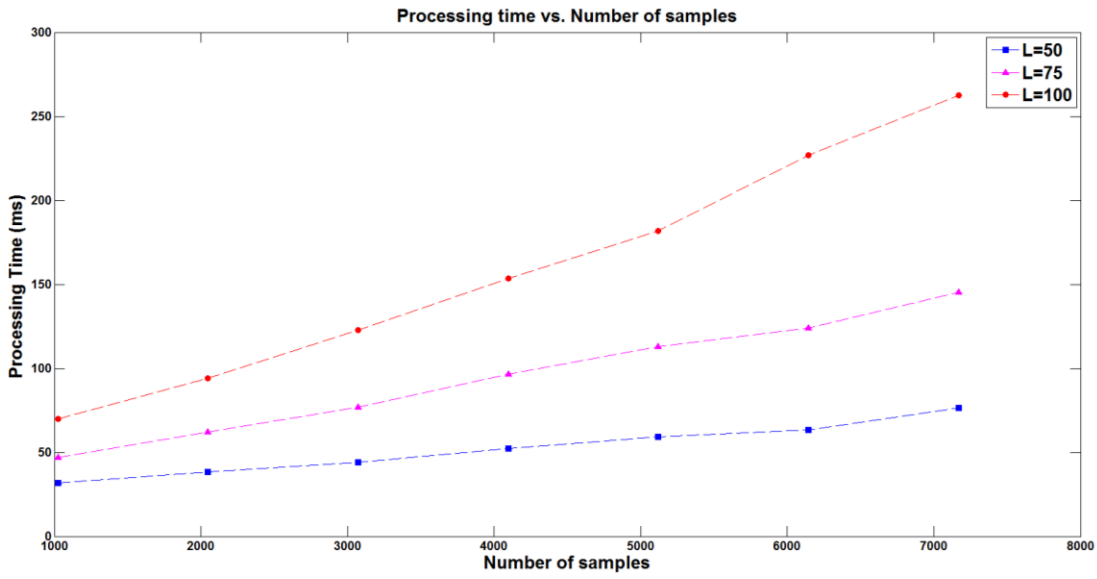

Figure 24. Graph of processing time with varying number of samples

After investigating the impact of various variables on the error and deciding upon the fixation of an optimal value for each, we performed real experiments using the USRP. In this experiment, a constant signal was generated from the signal generator that was fed to the USRP and fused with additive white Gaussian noise. The result of this experiment is illustrated in Figure 25, with both the simulation and the experimental plots performed under the same estimation conditions. It is observed that the error in simulation result and the experimental result do not differ much from each other at low values of SNR i.e. SNR less than -10 dB. With SNR values greater than -10 dB, the error in the simulation tends to be lesser than that of the experimental result and with increasing SNR this is clearly evident.

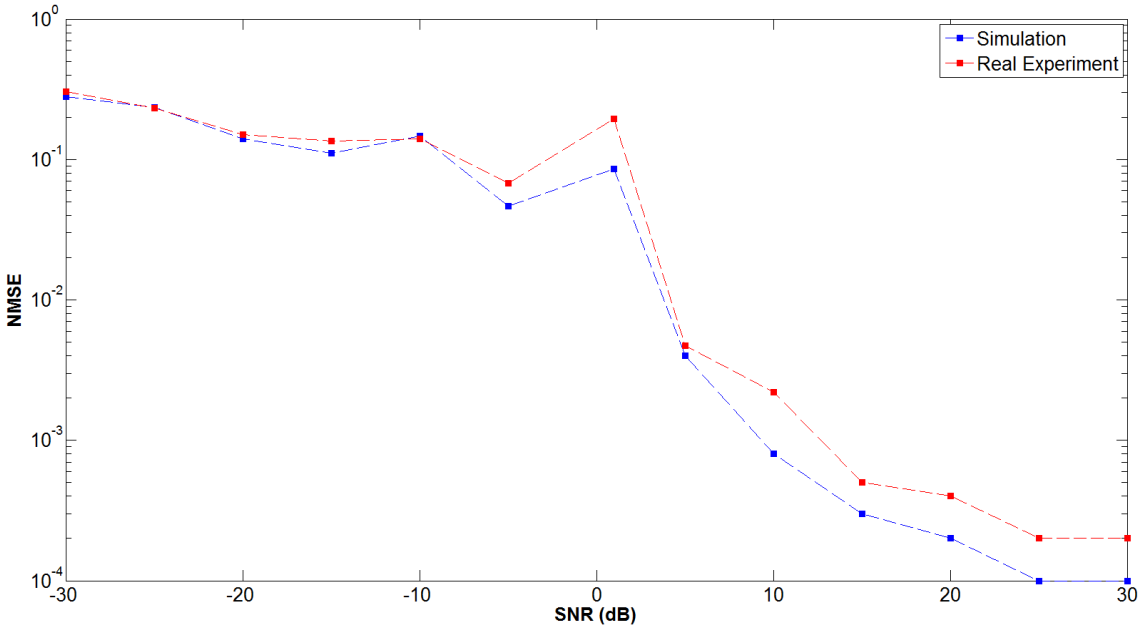

Figure 25. Simulation and Experimental result comparison for SNR estimation

From the above results we conclude that the implemented method of SNR estimation has shown simulation results that match with the experimental results. This technique is also suitable for the scenario of spectrum scanning as it does not require any knowledge of the transmitted signal.

Chapter 4

SPECTRUM SENSING

4.1. Background

Spectrum sensing is the process of obtaining awareness about the spectrum usage and existence of primary users in a determined area [4.1]. This falls in the domain of signal detection theory, in which we decide among some finite number of possible situations or "states of nature" [4.2]. The final decision made herein, ascertains the presence or absence of the primary user in the space and channel of interest for the secondary user. This essentially creates a situation of binary hypothesis where we are solely interested in the determination of presence or absence of a signal i.e. a transmission by the primary user or not.

$$H_0 : x(n) = w(n) \tag{1}$$

$$H_1 : x(n) = s(n) + w(n) \tag{2}$$

Equations 1 and 2, depict the binary hypothesis discussed above, where $x(n)$ in the above equations represents the received signal samples, $s(n)$ represents the transmitted signal and $w(n)$ is the noise of the additive white Gaussian noise (AWGN) channel. H_0 is the null hypothesis representing the situation of no transmission by the primary user and H_1 is the situation representing the primary user's signal transmitted with noise.

4.2. State of the Art

Various spectrum sensing techniques have been proposed in literature over the last decade [4.5-4.10] . As shown in Figure 26, these techniques can be classified in 4 categories:

1) Energy detection based techniques [4.5]

2) Cyclostationary feature based detection [4.6- 4.8]

3) Matched Filtering based detection [4.3,4.9]

4) Covariance based detection [4.10]

Figure 27 shows a comparison of the accuracy and the complexity of some of the most popular spectrum sensing techniques.

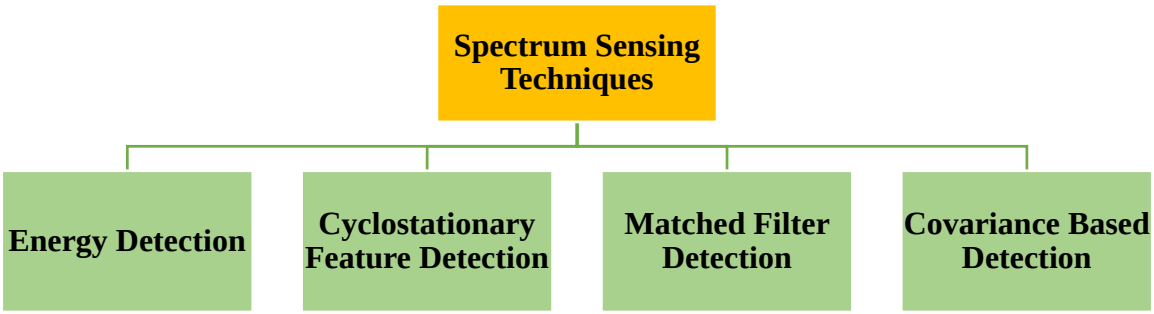

Figure 26. Spectrum sensing techniques classification

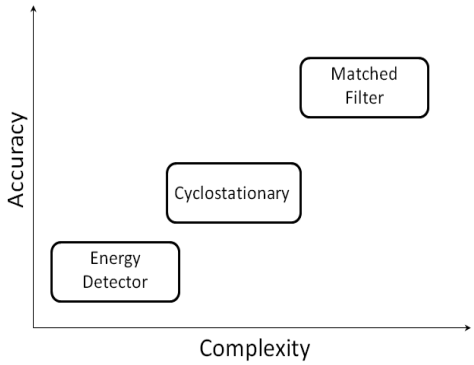

Figure 27. Comparison of spectrum sensing techniques (Modified from [4.1])

4.2.1. Energy Detection

Energy detection is the most simplest spectrum sensing approach in cognitive radio [4.3]. This method does not require the any prior information about the transmitted signal. In order to attain better performance there is still a requirement for the knowledge of the noise power [4.4]. In this technique, the total energy of the incoming signal is computed, therefore no dependency over the type of modulation scheme involved is present. Figure 28 shows the implementation of the energy detection technique using Welch periodogram averaging with a continuous time signal as the input to the analog-to-digital converter of the detector. In Figure 28, the signal input to the A/D is converted from analog to digital and then the digital samples are subject to the N-Pt FFT block for computation of the fast Fourier transform. These FFT values are averaged over the total number of samples and compared with the threshold in the energy detect block. Based on the comparison made with the threshold a decision is made as to the signal is present or absent.

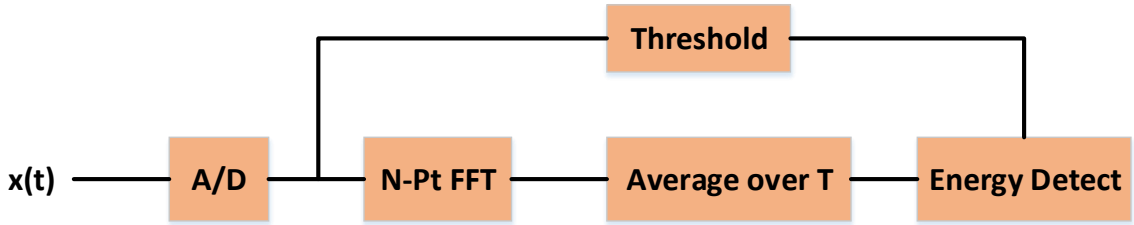

Figure 28. Implementation of an energy detector using Welch periodogram averaging [4.5]

The average energy of N samples of the incoming signal $x(n)$, is computed as given below,

$$T_{ED} = \frac{1}{N}\sum_{n=1}^{N}|x(n)|^2 \tag{3}$$

where, T_{ED} is the decision statistic of N number of samples in a detection cycle. The final decision of the detection is made by comparing the decision statistic against a pre-determined threshold, λ_{ED}, that depends on the noise floor [4.6]. Usually a fixed threshold

is used; however, the noise is uncertain, which degrades the sensing performance. A work-around to this issue would be to use a dynamic threshold instead of the fixed threshold. The major drawback of the energy detection is its inability to distinguish between the noise and the signal. There is a certain threshold known as SNR wall [4.7]. If the signal power is below this threshold then the energy detector fails to distinguish between this signal and a noise of even a slightly larger power. The conditions for energy detection with a threshold, λ_{ED}, is given as,

$$T_{ED} < \lambda_{ED} : Signal\ does\ not\ exist \rightarrow H_0 \tag{4}$$

$$T_{ED} > \lambda_{ED} : Signal\ exists \rightarrow H_1 \tag{5}$$

4.2.2. Cyclostationary Feature Detection

Cyclostationary Feature Detection relies on the features or the inherent properties of the incoming received signal [4.14]. Some statistics of the transmitted signal are periodic because of the inherent periodicities such as modulation rate and carrier frequency [4.8]. These features are perceived as cyclostationary features, whereas the noise is stationary. Therefore these periodicities enable these detectors to distinguish between primary user's signal and noise [4.9-4.12]. It also differentiates between different types of transmissions and primary systems [4.13]. An implementation of the cyclostationary feature detector is shown in Figure 29. In this figure the received analog signal was digitized by the A/D block and its Fast Fourier Transform was computed in the N-Pt FFT block. These FFT values were correlated with itself in the Correlate block and then averaged. The averaged outcome was subject to feature detection. Unlike energy detection which performs the energy computation using the time-domain samples, a cyclostationary feature detector performs a transformation from the time domain into the frequency domain and then conducts a

hypothesis test in the new domain [4.8].

Figure 29. Implementation of a cyclostationary feature detector [4.5]

Cyclic-autocorrelation function of the received signal, $y(t)$ is given by,

$$R_y^{\alpha}(\tau) = E[y(t+\tau)y^*(t-\tau)e^{j2\pi\alpha t}] \tag{6}$$

Where *E[.]* is the expectation operator, * denotes the complex conjugates and α is the cyclic frequency. The cyclic spectrum density is calculated as the Fourier series expansion of the cyclic autocorrelation function, which is given by,

$$S(f,\alpha) = \sum_{\tau=-\infty}^{\infty} R_y^{\alpha}(\tau)e^{-j2\pi f\tau} \tag{7}$$

The CSD function has peaks when the cyclic frequency, α is equal to the fundamental frequnecy of the transmitted signal. For any other frequencies no peaks are observed signifying the presence of noise which is hypothesis H_0. Furthermore a peak detector [4.15] or a generalized likelihood ratio test [4.11, 4.13] can be used to differentiate between the two hypothesis [4.8]. The ability of the cyclostationary detector to distinguish between noise and signal allows it to be less susceptible to noise uncertainty and hence has a lesser probability of false alarm.

4.2.3. Matched Filtering Detection

In the event of the secondary user being aware about the primary user's signal a priori, the matched filtering detection technique serves as the best option for signal detection as it maximizes the received signal-to-noise ratio [4.5]. To detect the presence of the primary user the matched filter technique correlates the already known primary user

signal with the incoming received signal. The merit of the matched filtering technique is that it requires less processing time as it needs very few samples to achieve a specific detection performance such as low probabilities of misdetection and false alarm. This merit is a conditional merit, in the sense, that the number of samples required is small only when the signal-to-noise ratio is high. But with the signal-to-noise ratio decreasing, the number of samples required by the matched filter also grows. Another drawback of the matched filter is that it needs to have a complete knowledge of the primary user's signal such as the bandwidth, frequency, modulation type, packet format in order to perform a precise matched filtering. If any of the information provided is incorrect then this would lead to an incorrect correlation in the matched filter, in turn leading to a degradation of the performance of the detector. In the event of unavailability of the perfect information of the primary user's signal, if a close-match pattern is known from the received signals then coherent detection or waveform-based sensing can be implemented to detect the presence of the primary user's signals [4.16], where the information about the waveform patterns is a pre-requisite. Similar to matched filter detection, more the accuracy of the information available, better is the sensing performance of the detector.

$$H_0: y(t) = n(t) \tag{8}$$

$$H_1: y(t) = \sqrt{\epsilon} x_p(t) + \sqrt{1-\epsilon} x(t) + n(t) \tag{9}$$

Equations 8 and 9 depict the hypothesis for the coherent detection case as in [4.8]. In coherent detection, a pilot tone, $x_p(t)$, with ϵ, the fraction of energy allocated to it, is orthogonal to $x(t)$, the desired signal and $n(t)$ is the additive white noise. The test statistic is given as the projected received signal in the pilot direction:

$$T = \frac{1}{N}\sum_{t=1}^{N} y(t)\hat{x}_p(t) \tag{10}$$

With increasing N, the test statistic under H_1 is greater than that of H_0. Comparing the value of T with a pre-determined threshold the presence of the primary user can be decided. The merits of the coherent detection are attributed to its robustness to noise uncertainty and it not being limited to the SNR wall unlike the matched filter detection. It is also seen to perform better than the energy detection in terms of the sensing convergence time [4.17, 4.18] as the sensing time of energy detection is observed to increase quadratically with reduction of SNR, unlike the coherent detector which increases linearly.

4.2.4. Covariance Based Detection

From the aforementioned sensing techniques, a conclusion can be drawn that the matched filtering detection and the cyclostationary features detection techniques require prior knowledge of the signal, whereas the energy detection technique requires the knowledge of the noise power if not the signal. A technique in spectrum sensing that can overcome the above mentioned problems is the covariance-based detection. This method capitalizes on the fact that the covariance matrix of the noise only samples behave differently from that of the covariance matrix of the signal samples. Therefore, the covariance matrix of the receiver obtained samples contains information which can be exploited for spectrum sensing. This technique is superior to the previously mentioned techniques because it does not require any signal or noise power to perform spectrum sensing [4.19]. Zeng and Liang in [4.19] and [4.20] have proposed two methods that utilize the covariance matrix to extract information required to detect the presence of a primary user's transmission. In [4.19], two statistics are introduced. The first one deals with the sum of the matrix elements that are

not in the main diagonal whereas the second one deals with the sum of the matrix elements that are in the main diagonal. The ratio of these two statistics is computed and then compared with a threshold which signifies either the presence of signal plus noise or only that of noise. In [4.20], the authors have proposed two metrics: the Minimum-to-Maximum Eigenvalue (MME) and the average received power to the minimum eigenvalue ratio also known as Energy with Minimum Eigenvalue (EME). Similar to the ratio of the two statistics in [4.19], the ratio of the MME to the EME is compared with a threshold to differentiate between noise and signal. In [4.19], the authors presented the received samples under the hypothesis,

$$H_0 \ : x(n) = \eta(n) \tag{11}$$

$$H_1 : x(n) = s(n) + \eta(n) \tag{12}$$

where, $s(n)$ is the transmitted signal samples passed through a wireless channel consisting of path loss, multipath fading and time dispersion effects; $\eta(n)$ is an i.i.d white noise having a zero mean and variance σ_z^2. The signal, $s(n)$ was assumed to be a superposition of received signal from multiple primary users. Hence no synchronization was needed [4.19]. L consecutive samples were considered defining the following vectors:

$$\mathrm{x}(n) = [x(n) \quad x(n-1) \quad \ldots \quad x(n-L+1)]^T \tag{13}$$

$$\mathrm{s}(n) = [s(n) \quad s(n-1) \quad \ldots \quad s(n-L+1)]^T \tag{14}$$

$$\eta(n) = [\eta(n) \quad \eta(n-1) \quad \ldots \quad \eta(n-L+1)]^T \tag{15}$$

where L is the smoothing factor. The statistical covariance matrices of the signal and noise are defined as,

$$R_x = E[\mathrm{x}(n)\mathrm{x}^T(n)] \tag{16}$$

$$R_s = E[s(n)\mathrm{s}^T(n)] \tag{17}$$

It can be verified that,

$$R_x = R_s + \sigma_\eta^2 I_L \tag{18}$$

Therefore, if there was no signal then $R_s = 0$ and the off diagonal elements of R_x are all zeros. In case a signal is said to be present and was correlated then the matrix $R_s \neq 0$ and therefore some off-diagonal elements of R_x are non-zero. Denoting r_{nm} as the element of the matrix R_x at the *m*th row and *n*th column, the two statistics are defined as,

$$T_1 = \left(\frac{1}{L}\right) \sum_{n=1}^{L} \sum_{m=1}^{L} |r_{nm}| \tag{19}$$

$$T_2 = \left(\frac{1}{L}\right) \sum_{n=1}^{L} |r_{nn}| \tag{20}$$

The ratio of $\frac{T_1}{T_2} = 1$ if there is no signal and $\frac{T_1}{T_2} > 1$, in the presence of a signal. Therefore this ratio can be used to detect the presence of the signal. In practice the ratio of T_1 and T_2 is compared with a threshold γ_1 which is chosen to meet the requirements of the probability of false alarm. Since in practice we only have limited number of samples we cannot obtain the statistical covariane matrix and hence obtain the sample covariance matrix. The autocorrelation of N_s number received signal, $x(m)$, is given by

$$\lambda(l) = \left(\frac{1}{N_s}\right) \sum_{m=0}^{N_s-1} x(m)x(m-l), \qquad l = 0,1,\dots,L-1 \tag{21}$$

Using the sample covariance matrix, the statistical covariance matrix R_x can be approximated. The sample covariance matrix is defined as,

$$\widehat{R_x}(N_s) = \begin{bmatrix} \lambda(0) & \lambda(1) & \dots & \lambda(L-1) \\ \lambda(1) & \lambda(0) & \dots & \lambda(L-2) \\ \vdots & \vdots & \ddots & \vdots \\ \lambda(L-1) & \lambda(L-2) & \dots & \lambda(0) \end{bmatrix} \tag{22}$$

Therefore to perform signal detection, firstly the received signal samples are auto correlated, with L as the chosen smoothing factor, to form the sample covariance matrix as defined above. Using this sample covariance matrix, the two statistics $T_1(N_s)$ and $T_2(N_s)$ are calculated. A threshold γ_1 is chosen to meet the requirements of the probability of false alarm. The ratio of the statistics is compared with this threshold and a signal is present if $\frac{T_1}{T_2} > \gamma_1$.

In [4.20], the authors propose two detection methods which again derives itself from the sample covariance matrix. The authors here, again, consider the received signal $x(n)$ as a combination of $s(n)$, the transmitted signal samples passed through a wireless channel consisting of path loss, multipath fading, and time dispersion effects; and $\eta(n)$, an independent and identically distributed white noise having a zero mean and variance σ_z^2.

In the Maximum minimum eigenvalue (MME) detection, the sample covariance matrix of the received signal is given as,

$$R_x(N_s) \stackrel{\text{def}}{=} \left(\frac{1}{N_s}\right) \sum_{n=L-1}^{L-2+N_s} \hat{\mathrm{x}}(n)\hat{\mathrm{x}}^+(n) \tag{23}$$

where $\hat{\mathrm{x}}(n)$ is defined as,

$$\hat{\mathrm{x}}(n) \stackrel{\text{def}}{=} [\mathrm{x}^T(n), \mathrm{x}^T(n-1), \dots, \mathrm{x}^T(n-L+1)]^T \tag{24}$$

$$\mathrm{x}(n) \stackrel{\text{def}}{=} [x_1(n), x_2(n), \dots, x_M(n)]^T \tag{25}$$

$x(n)$ is the received signal sample, L is the smoothing factor, M is the factor by which the received signal is over-sampled and N_s is the number of samples collected. Using the sample covariance matrix, $R_x(N_s)$, its maximum and minimum eigenvalues are computed as $\lambda_{\max}$ and λ_{min}. The ratio of $\lambda_{\max}$ and λ_{min} if greater than the chosen threshold γ_1, a

signal is said to be present, otherwise no signal is present.

In another method proposed in [20], the energy with minimum eigenvalue is considered for detection. This method is similar to the previous method as it also computes the sample covariance matrix as in equation 23. In the next step, the average power of the received signal is computed as,

$$T(N_s) = \left(\frac{1}{MN_s}\right)\sum_{i=1}^{M}\sum_{n=0}^{N_s-1}|x_i(n)|^2 \tag{26}$$

This is similar to the energy detection, with $T(N_s)$ being the decision statistic, M is over-sampling factor and N_s is the number of received signal samples. The minimum eigenvalue of the covariance matrix $R_x(N_s)$, is computed as λ_{min}. The ratio, $T(N_s)/\lambda_{min}$ is compared with a chosen threshold, γ_2. If $\frac{T(N_s)}{\lambda_{min}} > \gamma_2$, then a signal exists, else no signal exists.

The merit of the EME technique over that of the energy detection is that, the energy detection technique compares the energy of the signal to that of the noise power whose knowledge is to be known in advance, whereas in the case of the EME, the energy of the signal is compared with that of the minimum eigenvalue of the covariance matrix which is obtainable from the received signal only. Since these techniques like energy detection use only the received samples to perform detection without the aid of information about the transmitted signal and channel, they can be termed as blind detection methods [4.20].

4.2.5. Summary

A literature study of the different spectrum sensing techniques employed in detecting the presence of the primary users is performed. The aforementioned sections began by taking a short glimpse over the principle of spectrum sensing prior to the

understanding of the aforementioned spectrum sensing techniques. Different types of spectrum sensing techniques were reviewed such as energy detection, cyclostationary detection, matched filter detection, and covariance based detection. Unable to handle the noise uncertainty turned out to be the drawback of energy detection, which leads to the research of other types of spectrum sensing techniques that dealt with the properties of the received signals and were able to distinguish between the signal plus noise and noise only components of the received signal. Although the issue of noise uncertainty was taken care off, but each technique possessed a drawback in terms of design complexity or detection accuracy or the requirement of the knowledge of the transmitted signal prior to its reception. The covariance based detection has been simulated and tested by several authors in order to evaluate the performance of their methods. Mate *et al.* [4.21] performed experiments with GNU Radio software and Universal Software Radio Peripheral ™ (USRP ™) devices to evaluate the covariance and MME detection methods proposed in [4.19, 4.20]. Their results of the simulation tests implied that these methods performed poorly in practice because the autocorrelation of the noise samples were not delta correlated as assumed in [4.19, 4.20]. An in-depth analysis over the covariance based sensing technique has been performed in this survey as it is chosen as the foundation for the development of a new spectrum sensing technique which shall be looked upon in the upcoming section.

4.3. Methodology

4.3.1. Energy Detection

The energy detection technique, as discussed previously is one of the easily implementable spectrum sensing techniques. The decision statistic which is calculated

from the received signal samples is computed as the sum of the squared magnitude FFT of the received signal samples averaged over N samples. Mathematically it is given by

$$T_{ED} = \frac{1}{N}\sum_{n=1}^{N}|x(n)|^2 \tag{27}$$

N number of received signal samples from the USRP are stored in a Python-Numpy array whose FFT is computed using the Numpy library based numpy.fft.fft function. The resulting array of FFT elements is then squared, summed and averaged over N samples to obtain the decision statistic. This decision statistic is then compared with a threshold λ and a decision is made as to the channel is busy or available based on the below mentioned condition

$$\begin{gathered} T_{ED} < \lambda_{ED} : \text{Signal does not exist / available} \rightarrow H_0 \\ T_{ED} > \lambda_{ED} : \text{Signal exists / busy} \rightarrow H_1 \end{gathered} \tag{28}$$

4.3.2. Autocorrelation at lag 1

The authors in [4.19] assume that the noise η is such that

$$E\big(\eta(n)\eta(n+\tau)\big) = 0 \text{ for any } \tau \neq 0 \tag{29}$$

and

$$E\big(\eta(n)\eta(n+\tau)\big) \neq 0 \text{ for any } \tau = 0 \tag{30}$$

where, E represents the expectation operator and τ is a discrete time shift. This implies that the autocorrelation of the noise is a delta-dirac function and therefore the noise is regarded as delta-correlated. This holds well if the noise is Gaussian. In practice it is observed that the noise is not Gaussian as non-Gaussian noise components are also present, hence, the

autocorrelation of noise a non-delta-dirac function. The autocorrelation of N_s number of received samples, $x(n)$ is given by,

$$\lambda(l) = \sum_{n=0}^{N_s} x(n)x^*(n-l) \tag{31}$$

where, $\lambda(l)$ is the autocorrelation at lag l and * denotes the complex conjugation operator. To compute the autocorrelation at lag 1, equation 31 is evaluated at $l = 1$ and the resulting value i.e. $\lambda(1)$ is compared with a threshold. This threshold was determined experimentally analyzing the performance metrics probability of detection and false alarms.

Similar to energy detection, the number of received signal samples from the USRP are stored in a Python-Numpy array and auto correlated using the numpy library based numpy.correlate() function. Numpy.correlate() function has three different modes of operation: full, valid, and same. Each of these modes varies by the number of points involved in the autocorrelation process. In our works, we have chosen the full mode, in order to ensure all the signal samples overlap in the process of auto correlation and therefore the resulting, the resulting array of auto correlated values is an array of L elements, where $L = 2N_s$. This L-element array is symmetric about its midpoint as shown in Figure 30 and Figure 31. Therefore only the second-half of the L/2 elements are considered for analysis. Of the L/2 elements, the $L/2^{\text{th}}$ element denotes the auto correlation value at $l = 0$ and the Lth element denotes the auto correlation value at $l = N_s$. For the auto correlation at lag 1 method, only the $(\frac{L}{2} + 1)^{\text{th}}$ element at which $l = 1$ is of interest here. This value is then compared with a pre-determined threshold γ based on the rule given below,

$$\lambda(1) < \gamma : \text{Signal does not exist / available} \rightarrow H_0$$
$$T_{ED} > \gamma : \text{Signal exists / busy} \rightarrow H_1 \tag{32}$$

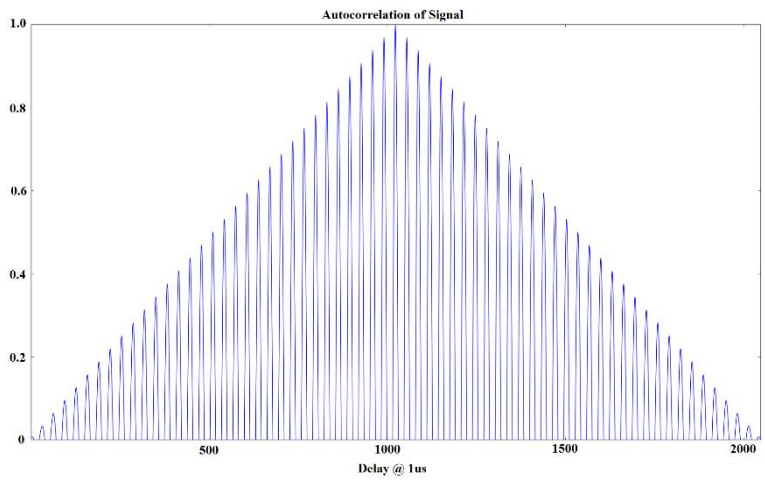

Figure 30. Autocorrelation of signal

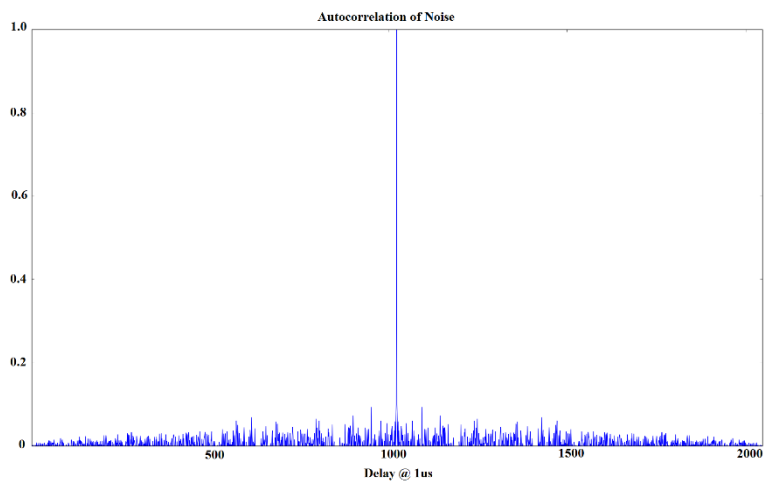

Figure 31. Autocorrelation of Noise

4.3.3. Correlation Distance

In [4.22], Hector, Reyes et al. proposed and developed a new technique based on the principle of autocorrelation. Since the additive white Gaussian noise is random, its autocorrelation is highly uncorrelated. However, the autocorrelation of the signal is

correlated as shown in Figure 30 and the degree of correlation defines the strength of the signal; higher the degree of correlation, the greater the signal strength. The autocorrelation of noise is uncorrelated and is illustrated in Figure 31.

N_s number of samples are received from the USRP receiver and stored in a Python-Numpy array. The autocorrelation of these N_s received signal samples is computed using equation 31 and stored in an M-element Python-Numpy array. As mentioned previously in auto correlation at lag 1, the M-element array is a symmetric one representing both the positive and negative values. Therefore this M-element array is reduced to an L-element array where $L = \frac{M}{2}$ and consisting of only the positive-half of the autocorrelation values. A reference line R, is another Python-Numpy array consisting of values that satisfy the equation given below:

$$R = \left(-\frac{1}{L}\right)t + 1\,; \quad 0 \le t \le L \tag{33}$$

The Euclidean distance between the reference line vector, R and the autocorrelation vector, $\lambda(l)$ is the metric that is used to determine the sensing result. It is denoted as $D_{Correlation}$ and is given by,

$$D_{Correlation} = \sqrt{\sum\left(R - \lambda(l)\right)^2} \tag{34}$$

This metric was further compared with an experimentally determined, fixed threshold, γ to arrive at the consensus of the spectrum sensing decision based on the following conditions:

$$\begin{aligned} D_{Correlation} > \gamma \;\; ; \quad Decision: H_0 \\ D_{Correlation} < \gamma \;\; ; \quad Decision: H_1 \end{aligned} \tag{35}$$

This newly developed spectrum sensing technique was coined the term “Correlation Distance”.

As discussed above the autocorrelation of noise is supposed to be a delta-dirac function, but this was not that was observed when the samples received from the USRP were auto correlated. This was due to the existence of non-Gaussian noise components and the same was observed in the autocorrelation at the first lag, $\lambda(1)$, proposed in [4.23]. The autocorrelation at the first lag, ideally states that, $\lambda(1) = 0$ in the absence of signal and $\lambda(1) \neq 0$ in the presence of signal. In an attempt to improvise the autocorrelation at the first lag technique and the correlation distance technique, an estimate of the non-Gaussian noise introduced by the USRP receiver was subtracted. This was performed, by creating a matrix consisting of several vectors containing N_s number of samples of the noise generated by the USRP. This matrix was then averaged into a single vector of N_s samples and was subtracted from every N_s number of received samples from the USRP.

The performance of the correlation distance technique was assessed by performing measurements of metrics such as probability of false alarm and probability of detection as a function of signal-to-noise ratio. Such metrics have been involved in the performance analysis of other spectrum sensing techniques. In this thesis, we also perform a comparative evaluation of the energy detection technique with fixed threshold, autocorrelation at lag 1, and the correlation distance technique in order to determine the most suitable sensing technique to enhance the process of radio spectrum scanning.

4.4. Results & Conclusion

Based on the aforementioned spectrum sensing techniques, several experiments were performed to validate and test the efficiency of the newly developed Correlation

distance technique. Furthermore the performance of this technique was evaluated and compared with that of the energy detection and autocorrelation at lag 1 using the metrics probability of detection and false alarm. In this section the results of the same have been discussed.

As mentioned before the autocorrelation of noise was a non-delta dirac function due to other non-Gaussian noise components. An estimate of the non-Gaussian noise introduced by the USRP receiver was subtracted from the received samples. Figure 32a demonstrates the result of the autocorrelation prior to subtraction of the non-Gaussian noise estimate. It is seen that the component with no signal has its first lag at 0.5 which signifies that the autocorrelation of noise is a non-delta dirac function. On the other hand, Figure 32b, illustrates the result of autocorrelation after subtraction of the non-Gaussian noise estimate. In this an overall shift is observed in each component when compared to its counterpart in Figure 32a. Also the no autocorrelation of the no signal component is a delta-dirac function, thereby signifying that the autocorrelation of noise is an uncorrelated one.

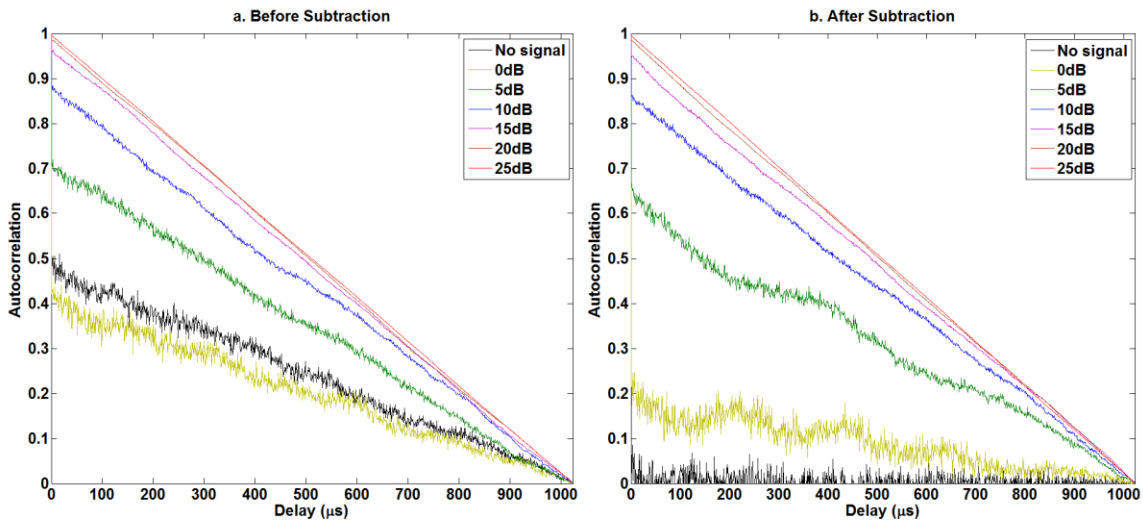

Figure 32. (a) Auto correlation of signal samples before subtraction of inherent USRP noise (b) Auto correlation of signal samples after subtraction of inherent USRP noise [4.22]

In order to evaluate the impact of threshold selection on the performance of the method, experiments were run for the correlation distance and auto correlation at lag 1 techniques with multiple threshold values. The probability of detection was the preferred metric to evaluate and select a specific threshold. The result of this experiment is illustrated in Figure 33a and 33b. Figure 33a illustrates the variation of the probability of detection with respect to SNR for different threshold values of the correlation distance technique. Among the four thresholds chosen for this technique 0.95, 0.9, 0.85 and 0.8; a higher probability of detection was observed for the threshold 0.95 as it began to detect the signal at a very low SNR of -18 dB and attained 100% detection by -9 dB. When compared with that of the autocorrelation at lag 1 technique in Figure 33b, among the four threshold values 0.1, 0.15, 0.2 and 0.25, the lowest threshold i.e. 0.1 had the higher probability of detection with initial detection at -16 dB and a 100% detection at -7 dB. Comparing the two techniques, we see that the correlation distance technique is more efficient as it attains a 100% detection probability at a lower SNR when than the autocorrelation at lag 1 method.

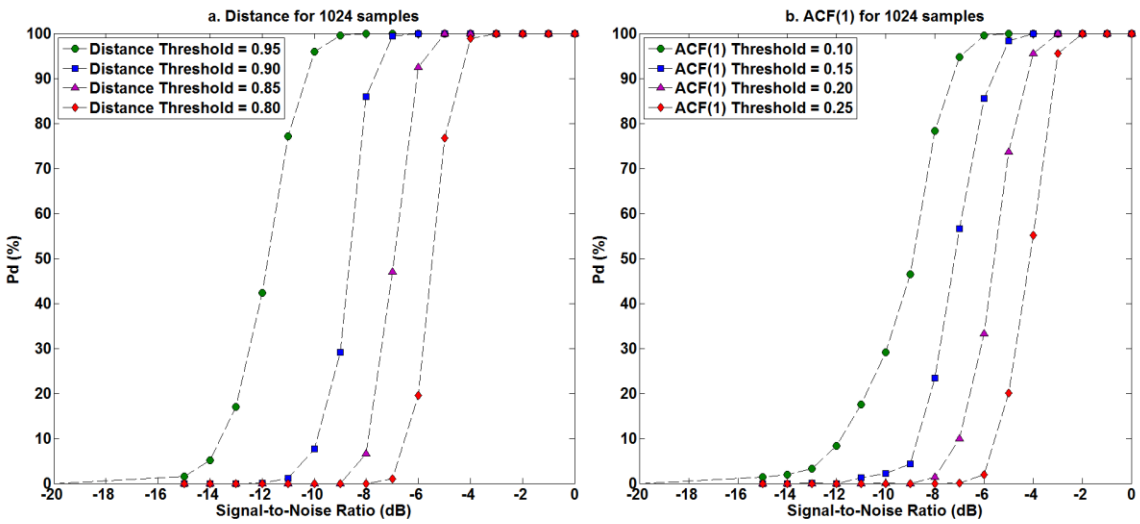

Figure 33. Variation of probability of detection with respect to signal-to-noise ratio for multiple thresholds – (a) Correlation distance technique (b) Autocorrelation at lag 1 technique [4.22]

With the selection of the thresholds for both the techniques, the evaluation of the above techniques with respect to different number of samples is performed. In the following experiment, the number of samples selected were 256, 512 and 1024. The reason for choosing lesser number of samples is that it will improve the overall processing time. But from the results of the experiment, as illustrated in Figure 34a and 34b, it is seen that with lesser number of samples the probability of detection is also lowered. In Figure 34a, it is observed that the initial detection of the signal with 256 samples occurs at an SNR lower than that of 512 and 1024 samples. But to attain a 100% probability of detection, the signal with 1024 samples is more efficient as it attains the same at an SNR of -9 dB whereas the signal with 256 samples attains the same at -8 dB. A similar pattern of result is seen for autocorrelation at lag 1 technique in Figure 9b where, the signal with 1024 samples at a 100% detection probability at an SNR of -7 dB, lower than that of the signal with 512 and 256 samples.

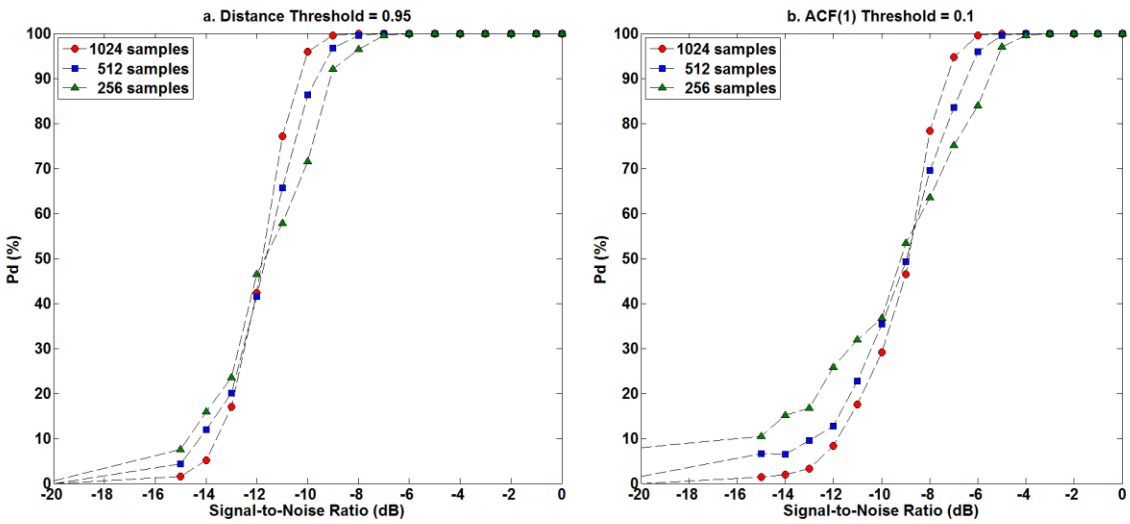

Figure 34. Variation of probability of detection with respect to signal-to-noise ratio for different number of samples – (a) Correlation distance technique (b) Autocorrelation at lag 1 technique [4.22]

Figure 35, illustrates a plot summarizing the results of Figure 33 and 34, by selecting the scenario of higher efficiency. In Figure 35, the variation of the probability of detection with respect to the signal-to-noise ratio is analyzed for the correlation distance technique with a threshold of 0.95 and for the autocorrelation at lag 1 technique with a threshold of 0.1. The number of samples used for this analysis is 1024. From this figure, we conclude that the correlation distance technique has a higher probability of detection when compared to the autocorrelation at lag 1 as it attains a 100% detection probability at an SNR of -9 dB, lower than that of the autocorrelation technique.

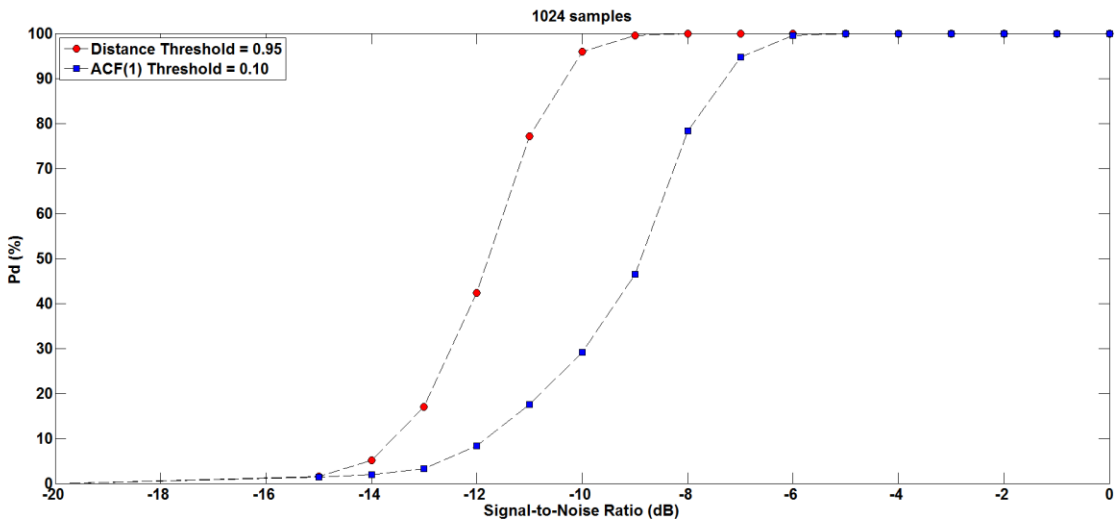

Figure 35. Variation of probability of detection with changing signal-to-noise ratio for 1024 samples and threshold level of 0.95 for correlation distance and 0.1 for ACF(1) [22]

In an attempt to compare the performance of the correlation distance technique with energy detection and the auto correlation at lag1 techniques with the varying number of samples used, experiments were performed to measure the probabilities of detection and false alarm. The number of samples used for these experiments varied from 1024 to 3072 and threshold values for each were chosen to analyze the worst-case scenarios in order to understand the variation of the probability of false alarm. Figure 36, illustrates the results of the same. From the plots of the probability of detection, it is observed that with increasing number of samples, the probability of detection increases. This increase is highly observable in the energy detection technique whereas the increase in the case of the autocorrelation at lag 1 is not very significant and this significance reduces even further for the correlation distance technique. Furthermore from the analysis of the probability of false alarm with increasing number of samples as illustrated in Figure 36, it is observed that the false alarm probability increases with higher number of samples in the case of energy detection technique. A probability of false alarm of 0% is attained at an SNR of -1 dB for

1024 samples whereas the same is attained at an SNR of 5 dB for 3072 samples. In the case of the autocorrelation at lag 1 technique, it is seen that with increasing number of samples the probability of false alarm decreases and for the correlation distance technique the false alarm tends to get closer to 0%. The false alarm probability almost remains a constant in the case of the autocorrelation at lag 1 technique and correlation distance technique for a given number of samples.

Experiments and simulations have shown that the Correlation Distance method developed herein is more efficient than the ACF(1) method in terms of probability of detection and false alarm, and more efficient than the energy detection method in terms of probability of false alarm.

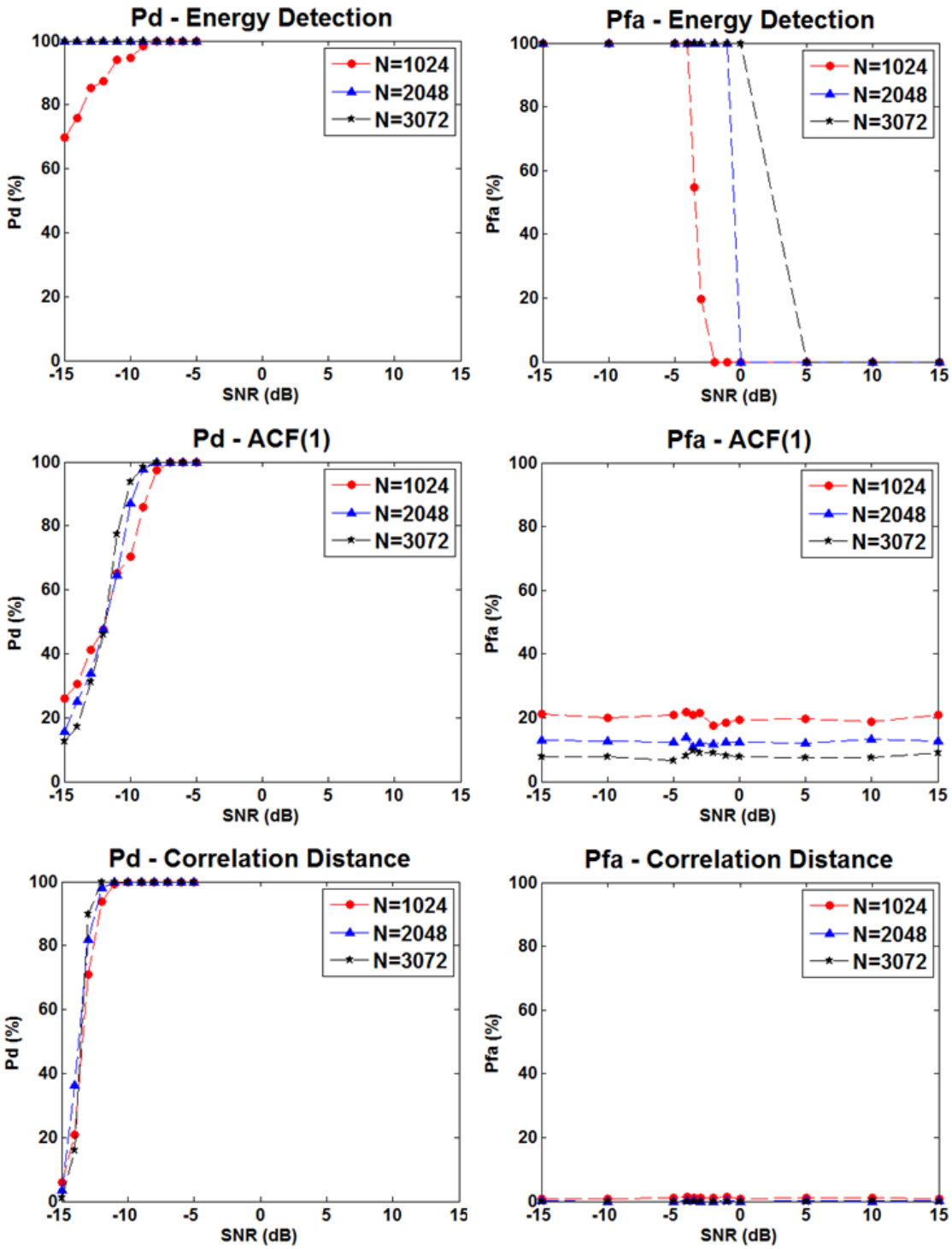

Figure 36. Performance analysis of energy detection, auto correlation at lag 1 and correlation distance technique for different number of samples.

Chapter 5

INFERENTIAL TECHNIQUE

5.1. Background

Statistics is the field of science that deals with the process of gathering data, performing analysis and interpreting results about the same in an organized and meaningful manner. These data are the foundation of modern science and are information used for reasoning, discussion or calculation [5.1]. The analysis of the data is usually performed using descriptive statistics or inferential statistics. In descriptive statistics the data known as population is collected, grouped and analyzed by assigning a proper descriptive model or a distribution family to it. Whereas on the other hand, inferential statistics is preferred when it is necessary to infer the behavior of the entire population from a subset of sample data [5.2]. The authors of [5.3] describe four paradigms of statistical inference: (i) Classical Statistics Paradigm (ii) Bayesian Paradigm (iii) Likelihood paradigm and (iv) Akaikean Paradigm. The paradigms of statistical inference that are of interest for this thesis are the Classical Statistics or Frequentist Inference and the Bayesian Inference as shown below.

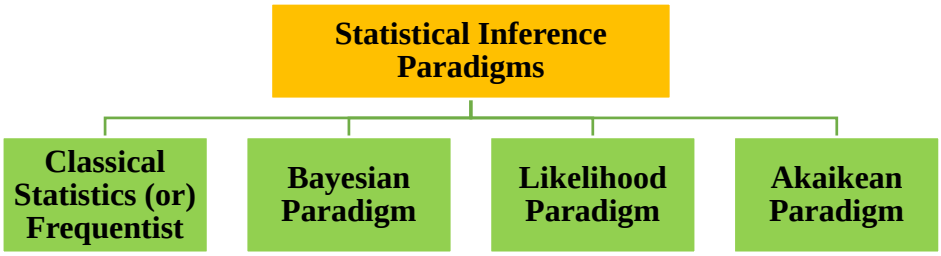

Figure 37. Statistical Inference Paradigms Classification

5.2. State-of-the-Art

There are two techniques that can be used for scanning the radio spectrum:

1. The frequentist inference infers the probability based on the frequency of observations.
2. The Bayesian inference infers the probability based on the previous knowledge and the current observation/evidence.

5.2.1. Frequentist Inference

The frequentist inference is a paradigm of statistical inference that is associated with the frequentist probability, wherein the probability of occurrence of the event is the limit of its frequency given a large number of trials. Therefore statisticians adapting the approach of frequentist inference assign probabilities to a repeatable event in which the uncertainty is due to randomness.

In the frequentist approach, the sample space is defined as the set of all possible outcomes of a random experiment, wherein an event, X, is a subset of the sample space under consideration. The frequency of occurrence of this event is a measure of its probability, $P(X)$ and is observed repeatedly in numerous iteration of the experiment. In a total of N_T trials, where N_X is the number of occurrences of the event, the probability or the frequency of occurrence is given by,

$$P(X) = N_X / N_T \tag{1}$$

It is seen that for a higher number of trials, the probability or frequency of occurrence tends to the true probability.

Hypothesis testing is a statistical method of making decisions given the data. In frequentist inference, it is seen that an alternate hypothesis is used to contrast the null hypothesis. Once both the null hypothesis and the alternate hypothesis are available, the data of the alternate hypothesis is used to calculate a test statistic which is then compared with the statistic that would occur when calculated with the data of the null hypothesis [5.4]. The comparison of these two values results in a p-value (probability value), which indicates if the null hypothesis must be accepted. In other words, the p-value is the probability of occurrence of the test statistic if the null hypothesis were to be true. This p-value has been misinterpreted at times as the probability of the null hypothesis to be true. A hypothesis cannot be assessed by probabilistic values as probability by frequentist interpretation considers long-run frequencies rather than available data. It is also to be noted that the p-value is the probability under null hypothesis of observing data at least as extreme as the data that were actually observed; meaning that the p-value is partly determined by data that were never observed [5.5]. Another point owing to the problem of the frequentist inference is that, since, the p-values were calculated over the sample space, any changes to this sample space could greatly affect the p-value [5.5].

Frequentist Inference, although possesses drawbacks as mentioned above, but still is a widespread approach in the calculation of probability of the long-run frequency of certain measurement or observation and hence its presence in multitude of applications. With the focus of this thesis being cognitive radios and radio spectrum scanning, it is worth mentioning that the frequentist inferential approach has been employed in the process of spectrum occupancy measurement surveys. A spectrum occupancy measurement and analysis was performed in Beijing, China in the year 2012 [5.6]. In this survey, a spectrum

analyzer in conjunction with a broadband antenna was used to record the data. With energy detection technique used for spectrum sensing, whenever the received samples' computed decision statistic exceeded a fixed threshold, the sensed channel was said to be occupied by a signal. Numerous scans were performed across different channels and then the channel occupancy was computed as,

$$\text{average\_spectrum\_occupancy} = \frac{N_o}{N} \tag{2}$$

where N_o, is the number of observations where the channel was said to be occupied and$N$, is the total number of observations. It can be seen here that with increasing the total number of observations, a true probability of the occupancy of a channel can be found.

5.2.2. Bayesian Inference

Bayesian inference is another statistical inference paradigm that is primarily associated with the Bayes' Rule. As discussed previously Bayesian networks consist of variables with causal relations that are graphically represented as a directed acyclic graph. Bayesian inferential learning is aimed at computing the Bayesian probabilistic inference. It is based on a hypothesis space H of possible causal models and given some observation data d, which describes the states of one or more variables in the causal system for different cases or situations. With the hypothesis and the observation data, the posterior probability distribution is computed and this distribution denotes the degree of belief that the causal model h corresponds to the true causal structure [5.7]. Mathematically to compute the posterior distribution, two quantities are needed; the first one is the prior probability and the second is the likelihood. The prior probability, $P(h)$ measures the plausibility of each causal hypothesis, h without taking into consideration the observation data, d.

Likelihood, $P(d|h)$ measures the likeliness of observing the data considering the hypothesis to be true. The posterior probability is dictated by the Bayes' Rule as the product of the prior probability and the likelihood and normalized by the sum of the same product over all alternate hypotheses. It is given by,

$$P(h|d) = \frac{P(d|h)P(h)}{\sum_{k'} P(d|h')P(h')} \tag{3}$$

The advantage of Bayesian inferential learning arises from its ability to use highly structured and informative priors and likelihoods that are drawn from its background knowledge. Another approach in defining the posterior as given in [5.8] considers a hypothesis (θ) whose prior probability is given by $P(\theta)$. The data observed is denoted as D. The posterior is then defined as,

$$posterior = \frac{likelihood \text{ x } prior}{marginal\ likelihood} \tag{4}$$

$$P(\theta|D) = \frac{P(D|\theta)P(\theta)}{P(D)} \tag{5}$$

where, $P(\theta|D)$ is the posterior probability, $P(D|\theta)$ is the likelihood which is the conditional probability of observing the data given the hypothesis to be true and $P(D)$ is the marginal likelihood or also known as the evidence. Comparing equation 1 and 3 and replacing θ and D by h and d respectively yields,

$$P(h) = \sum_{k'} P(d|h')P(h') \tag{6}$$

In general in equation 3, the marginal likelihood $P(D)$ can be ignored. In order to understand why it can be ignored, let us consider a hypothesis θ, to be a binary one which takes upon two values 0 and 1. The prior probability distribution is given by $P(\theta)$. The data observed, D, has a marginal likelihood $P(D)$ and the likelihood for this observed data

under both the hypothesis is given as $P(D = 0,1|\theta = 0)$ and $P(D = 0,1|\theta = 1)$. Therefore, the posterior distribution for hypothesis $\theta = 0$ and $\theta = 1$, is given as,

$$P(\theta = 0|D = 0,1) = \frac{P(D = 0,1|\theta = 0)P(\theta = 0)}{P(D = 0,1)} \tag{7}$$

$$P(\theta = 1|D = 0,1) = \frac{P(D = 0,1|\theta = 1)P(\theta = 1)}{P(D = 0,1)} \tag{8}$$

In both, equations 4 and 5, it is seen that any change in the marginal likelihood, $P(D)$, proportionally changes the value of the posterior under both conditions of $\theta = 0$ and $\theta = 1$. Hence this has no impact on the final posterior value that is computed, therefore it is ignored and equation 3 can be rewritten as,

$$P(\theta|D) = P(D|\theta)P(\theta) \tag{9}$$

Some of the applications of Bayesian inference in the field of Cognitive Radio are:

- Bayesian Sensing Scheduler
- Bayesian Channel Quality Prediction
- Bayesian Spectrum Sensing

Bayesian Sensing Scheduler

In cognitive radios, there are two types of users, primary user (PU) and secondary user (SU). Spectrum sensing is performed in order to find the best available channel for transmission by the SU. Multiple channels are sensed in a row and this can be performed periodically or on-demand. In [5.9], one-channel policy is considered wherein a single channel is used as long as that channel is idle and thereafter on becoming busy the spectrum sensing is performed to search for another channel. In [5.10], multiple-channel policy is considered wherein channels are sensed periodically for underutilization in order to support increased data rate. In both these policies the order of sensing the channels in order to be

aware of the PU status has a great impact on the total system efficiency. In [5.11] a Bayesian Sensing Scheduler is proposed which is based on statistical learning rather than rule-based learning. The scheduler has two phases: learning phase and the operation phase. A parameter known as the success rate is estimated through the Bayes' rule and from the law of large numbers theorem it is seen that after many sensing attempts this success rate is approximately close to the actual idle probability of the sensing channel. In the learning phase, each channel is sensed in an order at the beginning of its time slot and its success rate distribution is updated according to the Bayesian rule:

$$P(S|X) = \frac{P(X|S)P(S)}{P(X)} \tag{10}$$

Where X is the channel sensing random process and S is the success rate. Each channel has a utilization parameter apart from the success rate parameter and when the distance between these two parameters approaches a value that is smaller than a pre-determined threshold then the operation phase starts, wherein an eligibility vector is calculated based on the success rate, probability of detection, probability of false alarm and the channel quality of each channel.

Bayesian Channel Quality Prediction

In [5.12] a study of different spectrum prediction techniques in Cognitive Radio Networks has been studied. Some of the prediction based techniques are Hidden Markov Model-Based Prediction, Multilayer Perception Neural-Network-Based Prediction, Bayesian-Inference-Based Prediction, Moving-Average-Based Prediction, Autoregressive-Model-Based Prediction and Static-Neighbor-Graph-Based Prediction. From the aforementioned prediction techniques we shall now look into an application of Bayesian-inference-based prediction in cognitive radio networks applied in channel quality

prediction [5.13]. In this paper, the authors consider the cognitive radio network to be a time-slotted one wherein the secondary user performs spectrum sensing using one of the classical methods of spectrum sensing, energy detection at the beginning of a time slot. Once an idle channel is found the secondary user initiates transmission until the end of the time slot. It is assumed herein that the channel status is contained within a time slot i.e. the status of the channel does not change until the end of the time slot.

An illustration of this is shown in Figure 38.

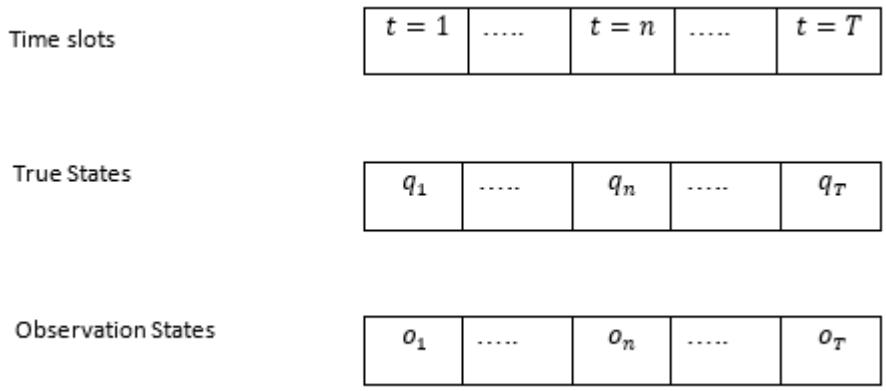

Figure 38. An illustration of the traditional spectrum sensing process [5.13]

The above spectrum sensing process can be modelled as a Hidden Markov Model. With the validation of the existence of a Markov chain in the channel utilization of a PU over time domain as in [5.14], the hidden channel occupancy states $Q = \{q_1, q_2, \dots, q_n, \dots, q_T\}$ is modelled as a Hidden Markov process. The SU on the other hand senses and generates the observations states $O = \{o_1, o_2, \dots, o_n, \dots, o_T\}$ which is a random Markov process dependant on the PU acitivty and sensing accuracy of the SU. Thus the complete spectrum sensing process can be modelled as a Hidden Markov Model. The authors of [5.13], model this HMM with transitional probabilities which are functions of time and hence non-static. The HMM with non-static transition probabilities are referred

as non-stationary hidden Markov models (NSHMMs). The priors for the NSHMM parameters are determined and are used in the process of the Bayesian Inference with Gibbs sampling as it is seen as a viable approach to reduce the computational complexity. The Gibbs sampling is an iterative process where the probability distribution obtained at iteration K-1 can be used as prior probability distribution for iteration K and the parameters obtained from iteration K-1 can be used as observations for iteration K. On deriving the posterior probability distribution for the kth iteration, the estimated parameters of the NSHMM are obtained and are used in a subsequent process to predict the channel quality which ranks the channels in a descending order of channel quality. Simulation results showed that the order of channels obtained here can be used for both spectrum sensing and spectrum decision to attain improved network performance.

Bayesian Spectrum Sensing

In [5.15], a Bayesian approach to signal detection in cognitive radios is proposed. The received samples, y, is represented as a vector of concatenated real and imaginary parts whose probability distribution function is in the form of standard multivariate normal distribution which is given by,

$$p(y|v) \propto v^{-N} e^{-\frac{Ns}{v}} \tag{11}$$

Where, y is the received samples vector, v is the variance, N is the number of samples, s is the sample energy. Considering θ as the parameter to indicate the presence or absence of a signal, the variance v is known when θ is perfectly known and its conditional distribution is is given by,

$$p(v|\theta) = \delta(v - v_\theta) \tag{12}$$

The prior of θ is denoted as $\pi_0 = \mathrm{P}(\theta = 0)$ and $\pi_1 = P(\theta = 1)$. The join posterior distribution of θ and v is given as

$$p(\theta, v|y) \propto p(y|v)p(v|\theta)p(\theta) \propto v^{-N} e^{-\frac{Ns}{v}} p(v|\theta)\pi_\theta \tag{13}$$

Marginalizing out v and substituting equation 12 we get,

$$p(\theta|y) \propto \pi_\theta \int v^{-N} e^{-\frac{Ns}{v}} p(v|\theta) dv \tag{14}$$

$$\propto \pi_\theta v_\theta^{-N} e^{-\frac{Ns}{v_\theta}}$$

A loss function or penalty function, $L(a, \theta)$ is introduced which is given by,

$$L(a, \theta) = \begin{cases} L_{FA} & a = 0, \theta = 1 \\ L_{MD} & a = 1, \theta = 0 \\ 0 & otherwise \end{cases} \tag{15}$$

Where L_{MD} is the penalty for misdetection and L_{FA} is the penalty for false alarm. The expected losses are given by

$$E[L(0, \theta|y) = L_{MD} p(\theta = 1|y) \tag{16}$$

$$E[L(1, \theta|y) = L_{FA} p(\theta = 0|y) \tag{17}$$

In order to perform the best decision of deciding $a = 1$, with the goal of minimizing the expected loss is, if $E[L(1, \theta|y)] < E[L(0, \theta|y)]$, which can be expressed in the form of odds ratio as,

$$\Phi = \frac{p(\theta = 1|y)}{p(\theta = 0|y)} = \frac{\pi_1}{\pi_0} (1 + \rho)^{\mathrm{N}\left(\frac{s}{\bar{v}} - 1\right)} > \frac{L_{FA}}{L_{MD}} \tag{18}$$

Where $\bar{v} = \frac{v_1 v_0 \ln\left(\frac{v_1}{v_0}\right)}{v_1 - v_0}$. After manipulations, the above equation is equivalent to,

$$s > \gamma_{BD} = \bar{v} + \left(\frac{1}{N}\right) . \frac{v_1 v_0}{v_1 - v_0} . \ln\left(L_\gamma \left(\frac{\pi_0}{\pi_1}\right)\right) \tag{19}$$

Where $L_\gamma = \frac{L_{FA}}{L_{MD}}$ is the loss ratio and γ_{BD} is the threshold of the Bayes Detector. Using the above ideology an Iterative Bayes Detector is designed. The convention followed in Energy Detection is that the threshold is set by setting a target P_{FA} and sample size N, but the detector is seen as unable to exploit the advantage of situations with good SNR where a sensing decision could have been made with a very small number of samples. But on the other hand a decision can be reached by a smart detector for sample size lesser than N for a high level of SNR denoted by the samples energy s and is given by,

$$s = \frac{1}{2N}\sum_{i=1}^{N}\left[(y_i^{re})^2 + \left(y_i^{im}\right)^2\right] \tag{20}$$

The Bayes detector unlike the Energy Detection, has an odds ratio as defined in equation 18 which provides a reliability value to the decision made by the detector based on the sample energy, s and the sample size. The author of [5.15] starts of by noting the P_{FA} and N for energy detection where the detection happens for $P_D = 0.99$. The SNR at this point is given by,

$$\rho_{0.99} = \frac{\gamma_{ED} - 1 - \frac{Q^{-1}(0.99)v_0}{\sqrt{N}}}{\frac{Q^{-1}(0.99)v_0}{\sqrt{N}} + v_0} \tag{21}$$

Where the energy detection threshold is given by,

$$\gamma_{ED} = \frac{Q^{-1}(P_{FA})v_0}{\sqrt{N}} + v_0 \tag{22}$$

Since the objective of the new algorithm is to attain a guaranteed detection with the same SNR for lesser number of samples and with a P_D not inferior to that of the ED, two rules are set. The first rule decides upon the presence of a signal or $\theta = 1$, by setting a high value for the target odd Φ_1^{tgt}, looping through a set of sample sizes, $n < N$, calculating the odds

for $\rho_{0.99}$ and comparing it with the value set initially checking. If higher then signal is detected else repeat for higher sample size until the sample size equals the maximum allowable for ED. The second rule also performs the same except for absence of the signal with a low value for target odd Φ_0^{tgt} and decides for absence when the value is lesser than the set value. At each and every iteration of the iterative Bayes detector, a new threshold is computed as the sample number varies for every iteration. This threshold is given by,

$$\gamma_{1,n} = \bar{v}_{0.99} + \left(\frac{1}{n}\right)\left(\frac{\bar{v}_{0.99}}{\log(1+\rho_{0.99})}\right)\log\left(\Phi^{tgt}\left(\frac{\pi_0}{\pi_1}\right)\right) \tag{23}$$

Where $\bar{v}_{0.99} = \frac{v_0(1+\rho_{0.99})\log(1+\rho_{0.99})}{\rho_{0.99}}$.

5.2.3. Summary

A study of the statistical inferential techniques enabled us to compare the frequentist and Bayesian inference techniques. As stated in [5.16], "A frequentist can calculate probabilities precisely, but often not the probabilities we want. A Bayesian can calculate the probabilities we want, but often cannot do it precisely." An observation made here is that the frequentist method is acclaimed to be more popular and frequently used in day-to-day life to perform inference based on the frequency of a large run of observations. On the other hand the Bayesian inference is more useful in situations requiring an inferential scheme that can provide the true probability of occurrence of an event at the instant of observing the evidence with a prior knowledge. Therefore we shall adopt the Bayesian inference in our works to enhance the process of scanning the radio spectrum.

5.3. Methodology

5.3.1. Bayesian Inference – Simplified Bayesian Model

The Bayesian approach is a probabilistic model that requires the prior knowledge in order to compute the posterior distribution. In the case of channel occupancy measurement, an array of linearly spaced values from 0 to 1 are considered to represent the set of occupancy probability values ranging from 0% to 100%. This set of probability values is denoted by P_{Occ}. The prior knowledge, denoted as $Prior_{Occ}$, is the prior occupancy values of the channels under consideration. In the event of not knowing the prior occupancy values of the radio spectrum, the prior distribution is characterized by a uniform distribution or binomial distribution. In the spectrum scanning process, we have considered the prior distribution as a uniform distribution; therefore all the channels initially have equal occupancies. Figure 39 demonstrates the Bayesian inference approach for the spectrum sensing scenario from a simulation performed in Python. The prior distribution chosen here is a uniform distribution. The subplots in these figures depict the variation of the posterior probability distribution with certain number of observations. The maximum value of the posterior probability distribution indicates the occupancy level of the particular channel under consideration. In subplots (a) and (b), we see that the detection remains consistently busy thereby inferring a 100% occupancy. In the subsequent subplots (c), (d), (e) and (f), the occupancy levels have varied from 75% to 56.3%. This variation in the occupancy levels is primarily attributed to those sensing attempts in which no signal was detected by the specific spectrum sensing technique. In subplot (e), the total number of detections is 10 out of a total number of 16 observations thereby resulting in a 62.5% occupancy. In the final subplot (f), the occupancy has further dropped down to 56.3%. With the availability of the prior distribution, N_s samples are sampled out of the USRP at a sampling frequency of F_s and is subject to spectrum sensing using energy detection,

autocorrelation at lag 1, and correlation distance technique. The resulting decision of each of the spectrum sensing technique is a binary value with 0 denoting absence of signal and 1 denoting the presence of signal. This decision is used to compute the likelihood, wherein, the decision value 0 signifies a signal presence probability, $SSProb$ of 0% and decision value 1 signifies a signal presence probability of 100%.

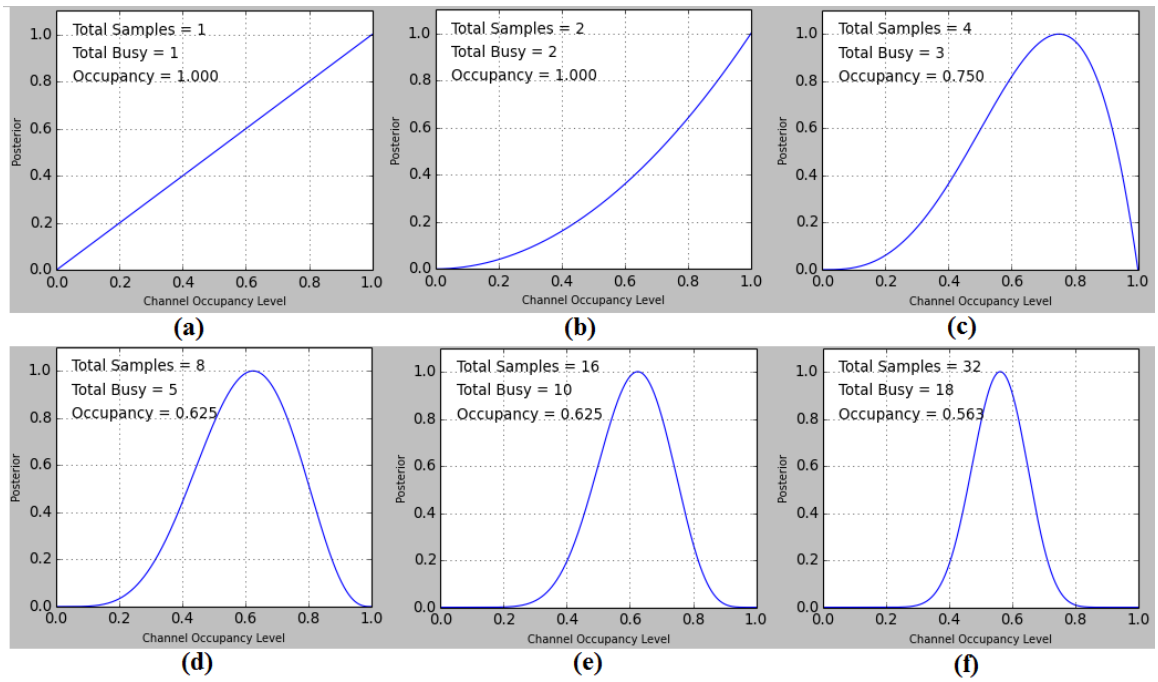

Figure 39. Variation of posterior using the Bayesian Inference Approach

The likelihood, Lik_{Occ} is given by,

$$Lik_{Occ} = (P_{Occ})^{SSProb} \text{ x } (1 - P_{Occ})^{1-SSProb} \tag{24}$$

where, Lik_{Occ} denotes the likelihood of observing a signal given the prior usage level, P_{Occ} denotes the set of probability values from 0 to 1 and $SSProb$ is the signal presence probability which is dependent on the decision of the spectrum sensing. With the computation of the likelihood, the posterior distribution, $Post_{Occ}$, can be computed as,

$$Post_{Occ} = Prior_{Occ} \text{ x } Lik_{Occ} \tag{25}$$

where, $Post_{Occ}$ is the posterior distribution, $Prior_{Occ}$ is the prior distribution of values (usage level) and Lik_{Occ} is the likelihood computed in equation 24. The index of the maximum value of the posterior distribution is obtained and the value of the P_{Occ} corresponding to this index gives the occupancy value of the channel at that instant. With this, the posterior distribution is assigned as the prior distribution for the next iteration of the spectrum sensing.

A flowchart describing the above methodology is provided in Figure 40. The first step would be to initialize the different variables such as end time of the spectrum survey, the array of probability values from 0 to 1 and the prior distribution. In our works the prior distribution is initialized with a uniform distribution as the current occupancy of the spectrum is unknown. The next step would be to check if the current time has exceeded the initialized end time. This check is in place to ensure the scanning process runs iteratively until the end time is reached. If the check passes then, the USRP is tuned to a particular frequency from a list of frequencies, the samples acquired by the USRP at that particular frequency are retrieved and stored in an array. This array of samples is now subject to spectrum sensing in the next step and the decision of the spectrum sensing is used to compute the likelihood. With the likelihood now available, the next step computes the posterior distribution and retrieves the probability value corresponding to the maximum value of the posterior distribution. Prior to proceeding to scan the next channel in the list, the array of prior distribution is replaced with the array of the newly computed posterior distribution. This complete process iterates over and over again till the conditional time check placed in the second step fails. Since three sensing techniques have been implemented for scanning, three different set of occupancy value calculations are

performed. Each technique has an individual prior, likelihood and posterior computation. Data is saved at regular intervals of every 15 minutes. In order to analyze the occupancy over different time frames as mentioned in table 1, the priors have been reset to a uniform distribution at the start of each time frame.

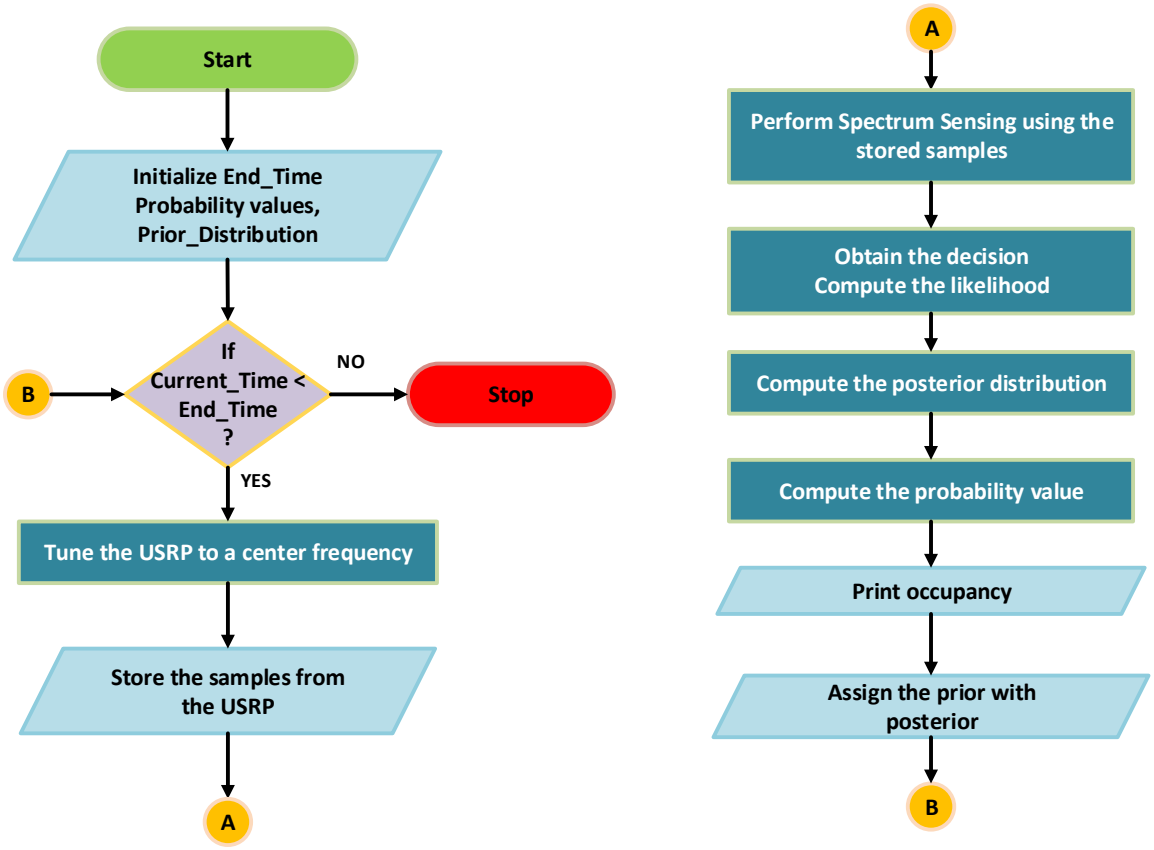

Figure 40. Experimental approach to spectrum scanning using Bayesian inference for the simplified Bayesian model

Table 2. Split-up of time frames

Time Frame	Time Duration
Midnight	00:00 – 06:00

Morning	06:00 – 12:00
Afternoon	12:00 – 16:00
Evening	16:00 – 20:00
Night	20:00 – 00:00

5.3.2. Bayesian Inference – Improved Bayesian Model

The Bayesian inference technique implementation discussed previously is for the simplified Bayesian model. Performing inference using the simplified model does not take into consideration the handling of uncertainties. In this section, the experimental approach to performing the Bayesian inference for the improved Bayesian model is detailed, which includes the handling of uncertainties.

With the improved Bayesian model, the Bayesian inference technique has been further improved to calculate the occupancy of the spectrum by including the detection and false alarm probabilities of the spectrum sensing methods. The detection and false alarm probabilities for each of the spectrum sensing technique was experimentally determined for a given SNR and was used in the occupancy calculation.

In the Bayesian Inference for the simplified model, the occupancy was calculated based on the decision made by the spectrum sensing techniques. In that, the decision was a binary variable, which took upon values 0, for signal absence and 1, for signal presence. The likelihood for a decision 0 was computed assuming that the signal presence probability, $SSProb$, is 0%, whereas for a decision 1, it was assumed that the signal

presence probability is 100%. Based on the likelihood computed and the prior usage level the posterior was computed which gave the updated usage level of the channel.

In the Bayesian this approach the SNR is estimated to obtain the probability of detection and false alarm values. A correction process is applied to obtain the closest true value of the SNR by applying the error of the estimation on the estimated value. The error value to be applied was experimentally determined using the SNR estimation technique. Based on the true value obtained, the corresponding detection and false alarm probabilities for each of the sensing techniques is obtained and this is used in the computation of the signal presence probability. The signal presence probability is a conditional probability which is conditioned on the decision of the spectrum sensing technique. Unlike the simplified Bayesian model inference, where a 0% and 100% signal presence probability was assumed for a decision of 0 and 1, here the signal presence probability is computed as given by,

$$SSProb = P(S_P = 1|S_D = 0,1) \tag{26}$$

$$= \frac{P\left(S_D = 0,1\ |S_P = 1\right) P(S_P = 1)}{P(S_D = 0,1|S_P = 1)\, P(S_P = 1) + P(S_D = 0,1|S_P = 0)\, P(S_P = 0)}$$

where, S_P denotes the signal presence, S_D denotes the decision of the spectrum sensing technique, $P(S_P = 1|S_D)$ is the signal presence probability and $P(S_P = 1)$ denotes the prior usage level of the channel. Since the end goal is to determine the occupancy of the channel which is the measure of the presence of the signal in the channel, we equate $S_P = 1$ in $P(S_P|S_D)$. The above equation depicts both the cases, when a decision is 0 and 1. Eqs. 27 and 28 examine the above equation in separate cases i.e. $S_D = 1$ and $S_D = 0$. In the case of a signal being detected, $S_D = 1$ and the signal presence conditional probability is given by,

$$SSProb = P(S_P = 1|S_D = 1) \tag{27}$$

$$= \frac{P(S_D = 1|S_P = 1)\, P(S_P = 1)}{P(S_D = 1|S_P = 1)\, P(S_P = 1) + P(S_D = 1|S_P = 0)\, P(S_P = 0)}$$

$$= \frac{P_D\, P(S_P = 1)}{P_D\, P(S_P = 1) + P_{FA} P(S_P = 0)}$$

where, $P(S_D = 1|S_P = 1)$ represents the detection probability, P_D and $P(S_D = 1|S_P = 0)$ represents the false alarm probability, P_{FA}. In the case of no signal detection, $S_D = 0$ and the signal presence conditional probability is given by,

$$SSProb = P(S_P = 1|S_D = 0) \tag{28}$$

$$= \frac{P(S_D = 0|S_P = 1)\, P(S_P = 1)}{P(S_D = 0|S_P = 1)\, P(S_P = 1) + P(S_D = 0|S_P = 0)\, P(S_P = 0)}$$

$$= \frac{P_{MD}\, P(S_P = 1)}{(P_{MD})\, P(S_P = 1) + (1 - P_{FA}) P(S_P = 0)}$$

where, $P(S_D = 0|S_P = 1)$ represents the misdetection probability, P_{MD} and P_{FA} is the false alarm probability. In the case of no signal detection, $S_D = 0$ and the signal presence conditional probability is given by,

With the calculation of the signal presence probability we would now calculate the occupancy level of the channel as done in the case of the simplified Bayesian model inference approach, by calculating the likelihood as in equation 24 and posterior as in equation 25. In the calculation of the likelihood, $SSProb$ would be equated with the value of the newly calculated signal presence probability. In order to analyze the occupancy over different time frames as mentioned in table 1, the priors have been reset to a uniform distribution at the start of each time frame.

A flowchart summarizing this complete process is as shown in Figure 41. The first step would be to initialize the different variables such as end time of the spectrum survey, the array of probability values from 0 to 1 and the prior distribution. In our works the prior distribution is initialized with a uniform distribution as the current occupancy of the spectrum is unknown. The next step would be to check if the current time has exceeded the initialized end time. This check is in place to ensure the scanning process runs iteratively until the end time is reached. If the check passes then, the USRP is tuned to a particular frequency from a list of frequencies, the samples acquired by the USRP at that particular frequency are retrieved and stored in an array. This array of samples is now subject to spectrum sensing in the next step after which the array of samples is subject to SNR estimation. Based on the estimated SNR value, the probability of detection and false alarm are obtained and applied with the binary decision of the spectrum sensing to compute the signal presence probability. With this the likelihood is computed followed by the computation of the posterior distribution to obtain the probability value corresponding to the maximum value of the posterior distribution. Prior to proceeding to scan the next channel in the list, the array of prior distribution is replaced with the array of the newly computed posterior distribution. This complete process iterates over and over again till the conditional time check placed in the second step fails. Rest of the aspects of the scanning are similar to the simplified Bayesian model inference.

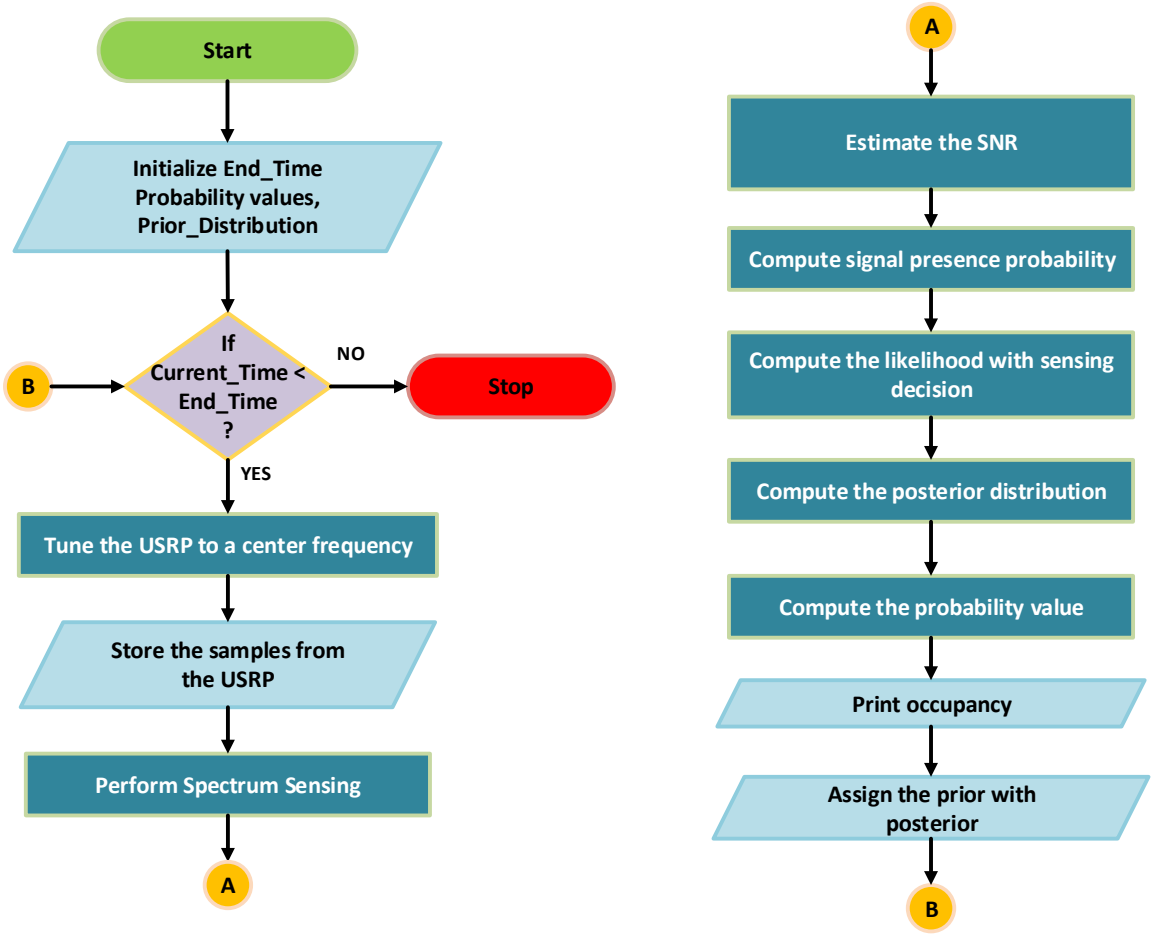

Figure 41. Experimental approach to spectrum scanning using Bayesian inference for the improved Bayesian model

5.3.3. Frequentist Inference

In the process of spectrum scanning, multiple channels are sensed in a sequential order and this complete process is iterated over and over for a specified number of times or for a desired period of time until which the channel occupancies are to be observed. The duration of the complete spectrum survey is of utmost importance in scanning the radio spectrum using the frequentist inferential technique as the total occupancy of the radio spectrum can be calculated only on the completion of the complete scanning process. This is because the frequentist inferential technique requires the knowledge of the total number

of observation cycles apart from the total number of cycles in which the spectrum was detected with a signal. The frequentist inference is computed as given by,

$$P_{Occupancy} = \frac{N_{Detected}}{N_{Observed}} \tag{29}$$

This equation defines the average spectrum occupancy of a given channel as the ratio of the number of sensing attempts where the channel was detected with a signal to that of the total number of sensing attempts performed or observed. An example of the spectrum sensing using the frequentist inferential method is shown in table 2. The table illustrates two columns; the sample number which defines the count of every sample that is observed; the sample state which is assigned a value 0 or 1 based upon the state of the channel being sensed, with 0 denoting the channel as empty and 1 denoting the channel as occupied.

Table 3. Spectrum Sensing with Frequentist Inferential Technique

Sample Number	Sample State
1	1
2	1
3	0
4	1
5	0
6	0
7	1
8	0
9	0
10	1

11	1
12	1
13	1
14	0
15	1
16	1

Based on the data from table 2 and using equation 29 we can compute the occupancy of the channel under consideration as:

$$N_{Observed} = 16$$

$$N_{Detected} = 10$$

$$P_{Occupancy} = \frac{N_{Detected}}{N_{Observed}} = \frac{10}{16} = 0.625$$

From the above calculations, we infer that the occupancy of the channel is approximately 62.5%.

The Universal Software Radio Peripheral (USRP) is tuned to a particular center frequency from a list of frequencies. N_s number of samples, sampled at a frequency F_s, is obtained from the USRP and stored in an array. The samples are processed based on the spectrum sensing technique that is applied. In this spectrum scanning procedure, we implemented the energy detection technique with a fixed threshold, autocorrelation function at lag 1 and the correlation distance technique. Each sensing technique performs a decision on the presence of the signal based on the preset threshold. The decision is a binary one resulting in a 1 for signal presence and a 0 for signal absence. This result is stored in an array and the next frequency from the list of center frequencies is chosen to

which the USRP is tuned and the complete process is repeated until the spectrum scanning end time is reached.

The analysis of the survey data was performed using R. R is a programming language and software environment for statistical computing and is widely used among statisticians and data miners. In the due process of scanning, a set of variables such as time of scan, scanned frequency, the decisions of each of the sensing technique and other variables of interest for future analysis are saved in a file. In order to avoid any intermittent crashes or data integrity issues, the data was saved after every fixed interval of time. The complete data of the spectrum survey is combined and then split into different files based on the days of the week of scanning, hence making it easier to analyze the occupancies on a daily basis. Each day is further divided into five time frames as shown in table 1, which allows us to analyze and understand the occupancy levels of a channel based in different times of the day. After splitting up the data based on different times of the day, the frequentist inference is applied on the respective decision columns of the sensing techniques.

A flowchart summarizing the complete process is as shown in Figure 42. The first step would be to declare the various variables and arrays required and initialize the same. With the initialization of the end time of the spectrum survey, a time check is performed if the current time has exceeded the initialized end time. This check is in place to ensure the scanning process runs iteratively until the end time is reached. On passing the check, the USRP is tuned to a particular frequency from a list of frequencies, the samples acquired by the USRP at that particular frequency are retrieved and stored in an array. This array of samples is now subject to spectrum sensing, whose binary decision results are stored in an

array which is saved in a file at regular intervals of 15 minutes. The USRP is tuned to the next frequency in the list and this process is iterative till the time check fails, upon which, the scanning process is terminated. After the termination, the stored binary decisions are averaged to compute the occupancy of the spectrum.

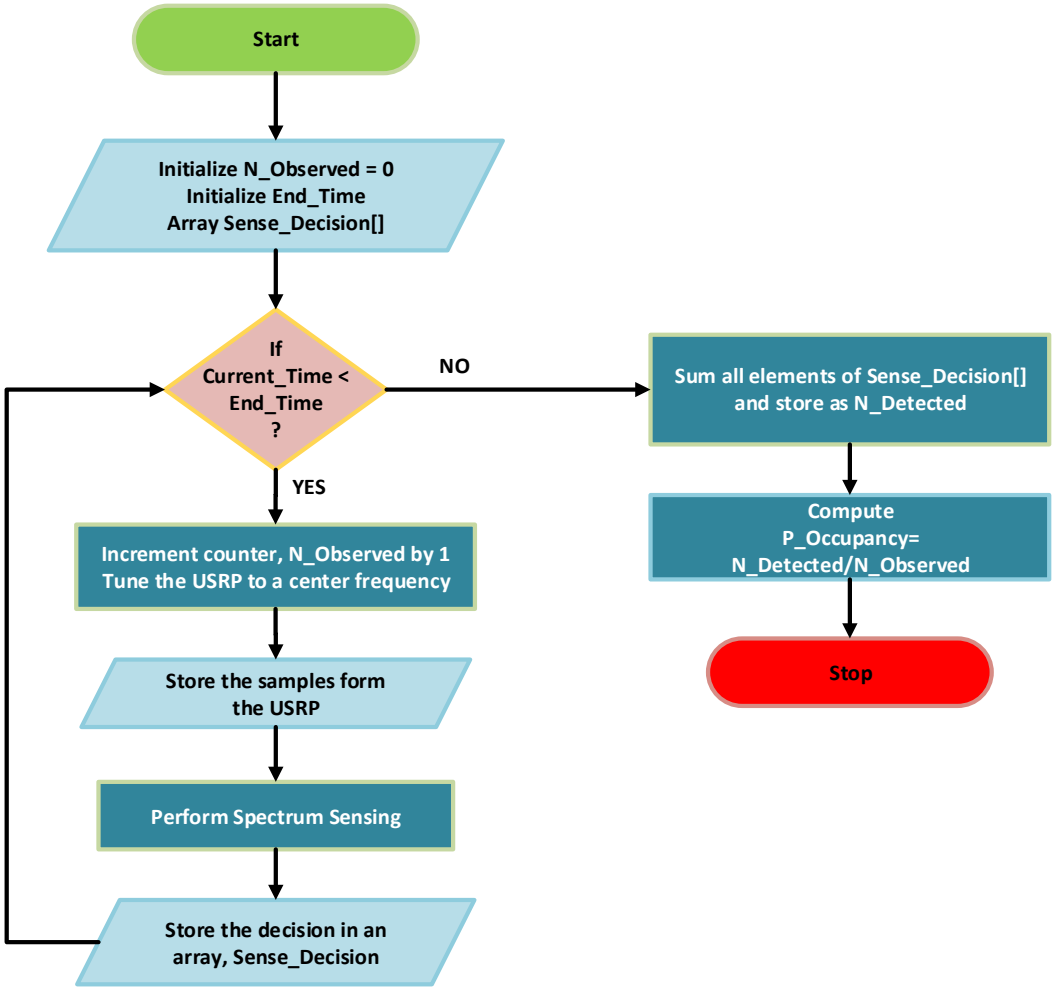

Figure 42.Experimental approach to spectrum scanning using frequentist inference

5.3.4. Experimental Setup

In this section, the experimental setup involved in scanning the radio spectrum is detailed. The setup description comprises of both the hardware elements used and the software programming techniques deployed to perform the scanning.

(a) Hardware Specifications

The hardware used in the scanning process is a Universal Software Radio Peripheral (USRP) Software Defined Radio (SDR) from Ettus Research as shown in Figure 43. The USRP consists of a daughterboard that is designed to work at a particular range of frequencies. The WBX USRP Daughterboard, is used in scanning the cellular bands GSM850 and GSM1900, while, the XCVR2450 USRP Daughterboard, is used in scanning the Wi-Fi bands 2.4 GHz and 5.8 GHz. The USRP is interfaced with the PC via a Gigabit Ethernet cable and on the software end the GNU Radio application is used.

Figure 43. Universal Software Radio Peripheral Software Defined Radio from Ettus Research

GNU Radio is a free and open-source software development toolkit that provides signal processing blocks to implement software radios. From a top-down view, GNU Radio executes what is known as a flowgraph, with each flowgraph consisting of signal processing blocks. A simple flowgraph is built in this scanning process that reads data from the USRP and prints out the sampled signal values. The flowgraph is as shown in Figure 44 and consists of a USRP Source block, complex to magnitude block and a printer_f block. The USRP Source block and the complex to magnitude block are GNU Radio built in blocks whereas the printer_f block is a user-defined block that was created as an interface to access the data samples read by the USRP Source block. The USRP Source block acts

as the software interfacing block of the USRP and the samples output from this block are complex by default, therefore, the complex to magnitude block is used to convert the complex samples to magnitude which is then input to the printer_f block. The printer_f block reads the data input to it from the complex to magnitude block and outputs it as an array of values whose length is based on the user input value to this block.

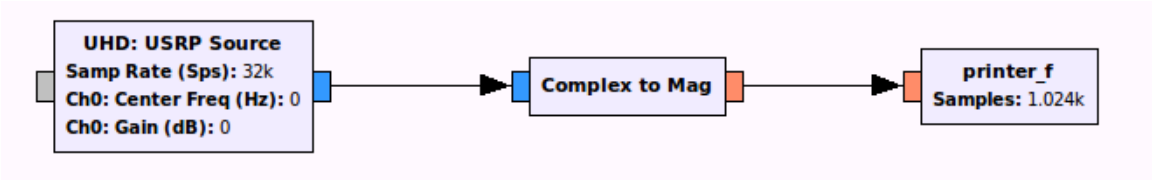

Figure 44. GNU Radio Flowgraph

The software development for the spectrum scanning was done in Python. Python is a general-purpose, high-level programming language that is shipped with the Ubuntu-Linux operating system. Since GNU Radio allows users to program in C++ and Python, python was chosen over other languages for this project. Python emphasizes code readability and its syntax allows programmers to express concepts in fewer lines of code than C++. R programming language is another language used in this project. R is suitable for statistical computing and graphical environments and has been used only in performing data analysis with respect to frequentist inference. R was chosen over python for performing data analysis as it has many built-in data manipulation functions that can be used to analyze large datasets.

(b) Software Specifications

The radio spectrum scanning was performed twice in the Memorial Union at the University of North Dakota. The first survey was started in the last week of December 2014 which spanned till the first week of January and included the frequentist and the Bayesian

Inference techniques. While the second survey included the frequentist, Bayesian and the Bayesian with detection and false alarm probabilities techniques and spanned from the 18th of July to the 24th of August 2015. The scanning/surveys were performed to measure the occupancy of the radio spectrum in the cellular bands, GSM850 and GSM1900, and the Wi-Fi bands, 2.4 GHz and 5.8 GHz.

A simple algorithm used in the initial survey to perform the scanning is as shown in Figure 45. Different channels in the aforementioned bands were scanned and each channel was sensed sequentially with the spectrum sensing techniques: Energy detection, Autocorrelation at lag 1 and Correlation distance to determine the occupancy status of that channel. The occupancy status was denoted by a 1 for signal presence and a 0 for signal absence. Table 4 summarizes the different channels scanned in the first survey and table 5 summarizes the channels scanned in the second survey. The second survey was improvised to collect data from channels in the GSM bands with a spacing of 200 KHz. The duration of the scan was decided prior to performing the scan and based on this duration the scan completion date and time were input to the program. This allowed the scan to progress uninterrupted till the specified completion date and time.

Table 4. List of scanned bands and channels in survey 1

Band	Start Frequency (MHz)	Stop Frequency (MHz)	Channel Spacing (MHz)	Number of Channels
GSM850 (U/L)	824	849	3, 2	11
GSM850 (D/L)	869	894	3, 2	11
GSM1900 (U/L)	1850	1910	3, 2	25

GSM1900 (D/L)	1930	1990	3, 2	25
2.4 GHz	2402	2497	5	20
5.8 GHz	5725	5875	5	31

Table 5. List of scanned bands and channels in survey 2

Band	Start Frequency (MHz)	Stop Frequency (MHz)	Channel Spacing (MHz)	Number of Channels
GSM850 (U/L)	824	849	0.2	126
GSM850 (D/L)	869	894	0.2	126
GSM1900 (U/L)	1850	1910	0.2	301
GSM1900 (D/L)	1930	1990	0.2	301
2.4 GHz	2402	2497	5	20
5.8 GHz	5725	5875	5	31

The USRP inherent noise was removed by subtracting an estimate of the non-Gaussian noise introduced by the USRP receiver. This was performed repeatedly with an interval of 15 minutes in order to ensure that no USRP inherent noise impacted the measurements of the spectrum scanning. All the channels to be scanned were stored in a python list. The USRP was tuned to a particular frequency, tun_freq from the list, using the function set_center_freq(self, tun_freq). Once the USRP successfully tuned to the frequency tun_freq, N_s number of samples were received from the USRP and stored in a

python-numpy array. This array of samples is subjected to spectrum sensing and the decision outcome of each of these techniques is stored for performing inference. These decision data need to be stored as the inference can be performed only post-scanning for frequentist inference, whereas, in the case of Bayesian inference and Bayesian inference with detection and false alarm probabilities, the occupancy of the scanned channel is inferred in real-time with the spectrum sensing decision making. After this, the USRP tunes to the next frequency in the list and repeats this process over and over. On reaching the last frequency in the list the scan still continued by tuning the USRP over to the frequency at the beginning of the list. This complete process iterated and lasted till the scan completion time was arrived.

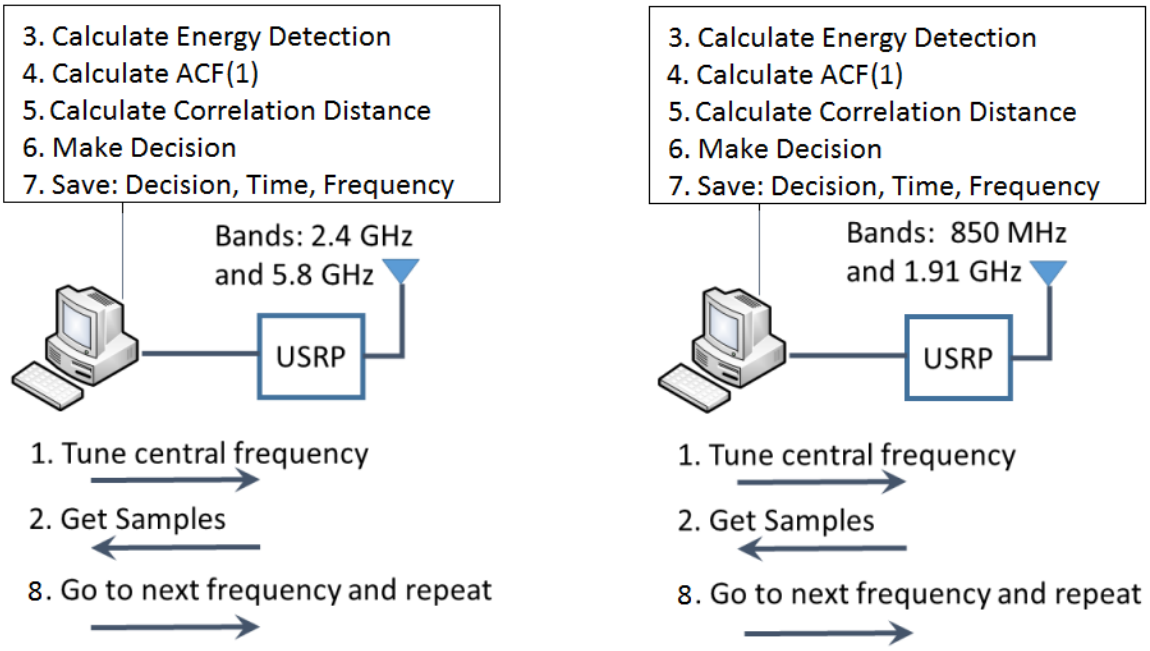

Figure 45.Spectrum scanning process illustration

5.4. Results & Conclusion

The analysis of the results is split into two sections. The first section will focus on the results of the first survey in which the occupancy values were calculated using the frequentist inference and simplified Bayesian model inference. The next section will follow up with the results of the second survey wherein the occupancy calculations were performed using the frequentist inference, simplified Bayesian and the improvised Bayesian inference.

5.4.1. Survey 1 results

(a) Frequentist Inference

Examples of results are shown in Figures 46 through 53 [5.17]. Each figure illustrates the occupancy of a particular channel in a selected band using the three aforementioned techniques (plots a, b, and c). Plots a illustrate the channel occupancy measurement performed using energy detection technique with fixed threshold; plots b illustrate the occupancy measurements performed using the ACF at lag 1 technique; and plots c illustrate the occupancy measurements performed using the correlation distance method.

Figures 46, 47, and 48 illustrate the occupancies of channel 1 (2.412 GHz), channel 6 (2.437 GHz), and channel 11 (2.462 GHz) of the 2.4 GHz band. Figure 46a shows the occupancy using the energy detection method. This figure shows that this channel is fully occupied (100%) at all times of the day, over the entire week. This high level of occupancy is attributed to the small value of the static threshold and the high false alarm rate of the energy detection method. Figure 46b illustrates the occupancy of the same channel (2.412 GHz) using ACF at lag 1, showing varying occupancy at different times of the day, which is an expected behavior. This method results in higher occupancy values than expected, as

it relies on only the first lag of the autocorrelation. Figure 46c shows the occupancy of the channel based on correlation distance. The occupancy values appear to be more realistic and expected as compared to those of the above two approaches, with high occupancy values during the peak usage hours of 12pm – 4pm (20% - 40%). This method owes its accuracy to the signal detection reliance on all the lags/points of the autocorrelation.

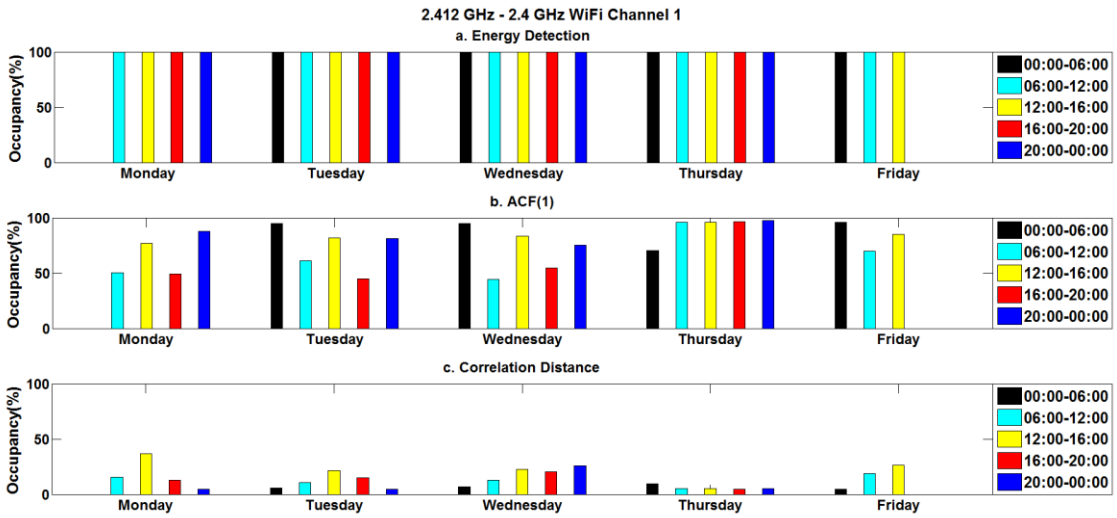

Figure 46. Average occupancy of channel 1 (2.412 GHz) of 2.4 GHz Wi-Fi band

Figure 47 illustrates the occupancy levels of channel 6 (2.437 GHz) of the 2.4 GHz band. The results of the occupancy levels measured with the energy detection method (Figure 47a) is similar to that of channel 1 (2.412 GHz) as shown in Figure 10a. With respect to the ACF at lag 1 (Figure 47b), we see that there is a slight variation in the occupancy levels as compared to the occupancy levels of channel 1. Comparing Figures 46c and 47c, a distinguishing result can be observed with the occupancy results of the correlation distance method of measurement. It is evident that the overall usage of channel 6 is less than that of channel 1.

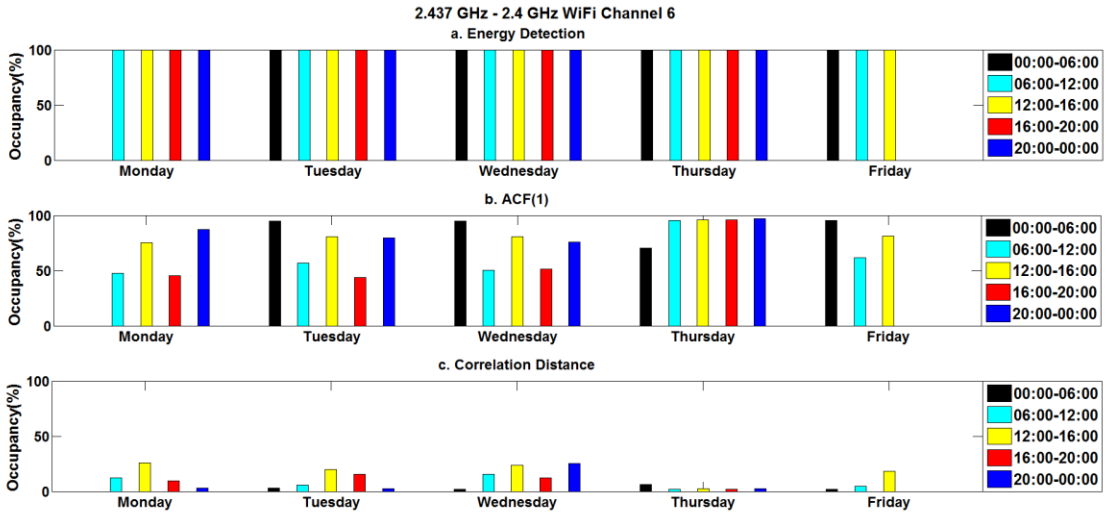

Figure 47. Average occupancy of channel 6 (2.437 GHz) of 2.4 GHz Wi-Fi band

The next highly occupied channel in the 2.4 GHz band is channel 11 (2.462 GHz). The results of the occupancy measurements with respect to the energy detection (Figure 48a) and ACF at lag 1 (Figure 48b) are similar to those of the previously mentioned channels 1 and 6, with slight variations in occupancy levels measured using ACF at lag 1 method. The distinguishing result is noticeable in the measurement performed using the correlation distance method as shown in Figure 48c, wherein a higher occupancy is noticed overall when compared to that of channel 6 (2.437 GHz). From the analysis of the results of the 2.4 GHz band, it is evident that channels 1, 6, and 11 are the most occupied channels of the 2.4 GHz band; channel 1 is the most occupied, followed by channel 11 and then by channel 6.

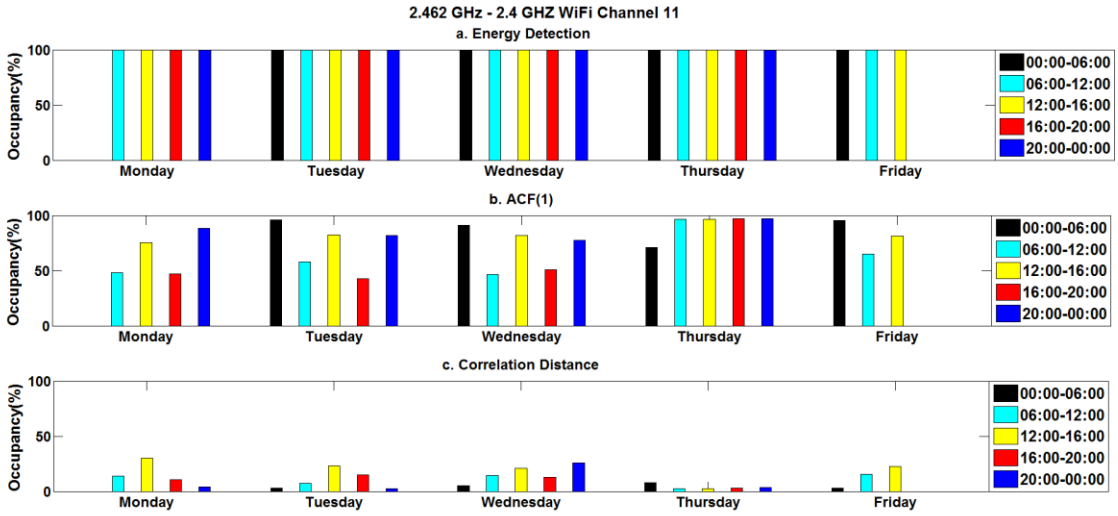

Figure 48. Average occupancy of channel 11 (2.462 GHz) of 2.4 GHz Wi-Fi band

In the next set of occupancy results, we will analyze the 5.8 GHz band and then the cellular bands such as GSM850 and GSM1900. Figure 49 illustrates the results of the occupancy measurements of channel 153 (5.765 GHz) of the 5.8 GHz band. As can be seen in Figure 49a, the results corresponding to energy detection show constant 100% occupancy while those corresponding to the autocorrelation at lag 1, shown in Figure 49b, are lower and vary with time. On the other hand, the measurement of the occupancy values corresponding to the correlation distance, as shown in Figure 49c, are more realistic and expected as compared to those of the above two approaches.

Owing to the public holiday on New Year's Day (January 1, 2015), the correlation distance method demonstrates low-to-no activity on that day, hence demonstrating a more precise and accurate technique of signal detection. We infer that occupancy is highest in the 12pm – 4pm interval over the week and is relatively low when compared to the 2.4 GHz band, which is expected behavior.

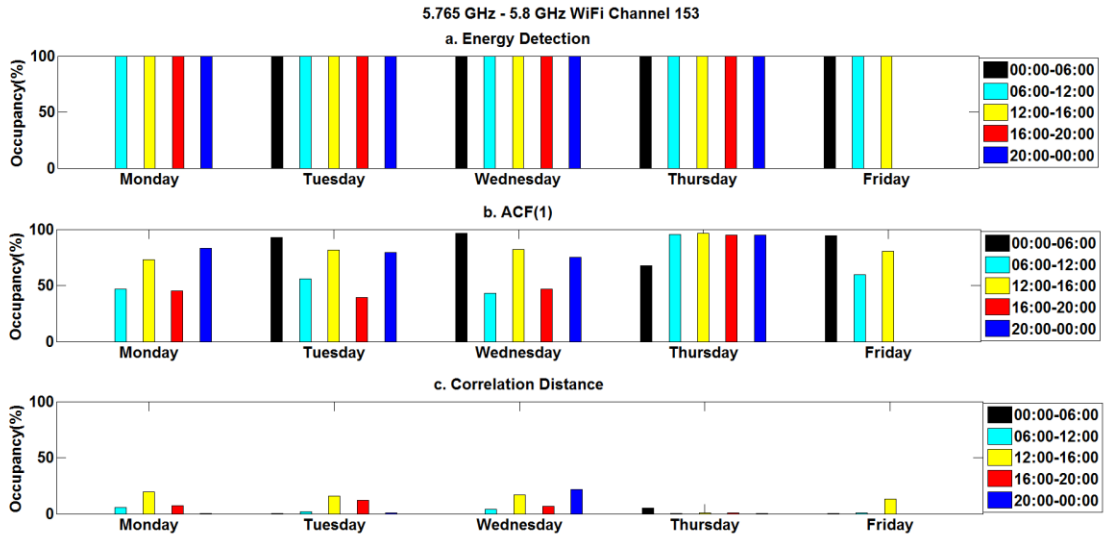

Figure 49. Average occupancy of channel 153 (5.765 GHz) of 5.8 GHz Wi-Fi band

Occupancies of the GSM850 and GSM1900 bands were also measured; their occupancy results are illustrated in figures 50 to 53. Figures 50 and 51 show the occupancies of the uplink (837 MHz) and downlink (882 MHz) channels, 192 of the GSM850 band. Both these channels (uplink and downlink) demonstrate 100% occupancy for all the three spectrum sensing techniques.

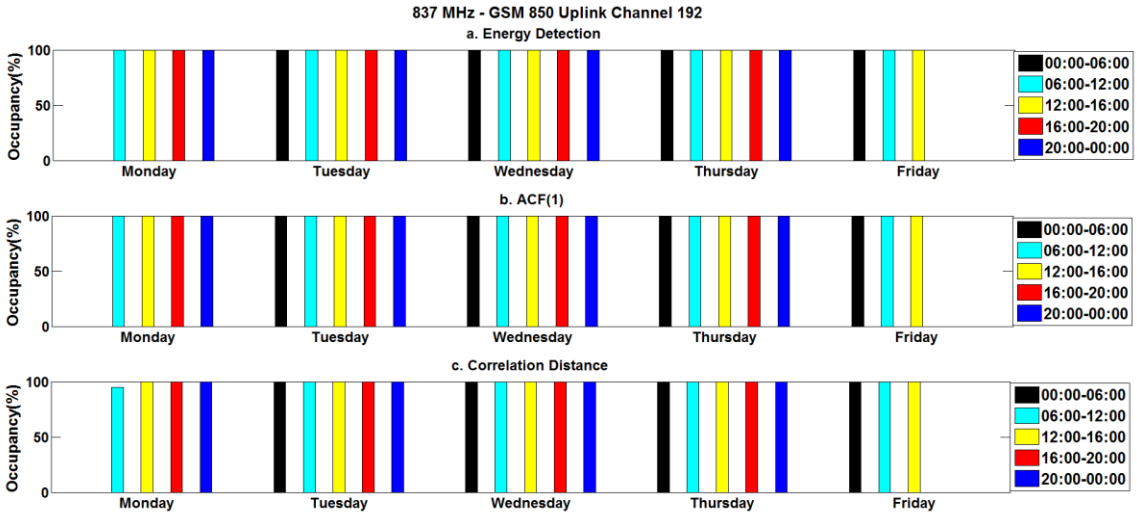

Figure 50. Average occupancy of channel 192 (837 MHz) of GSM-850 band

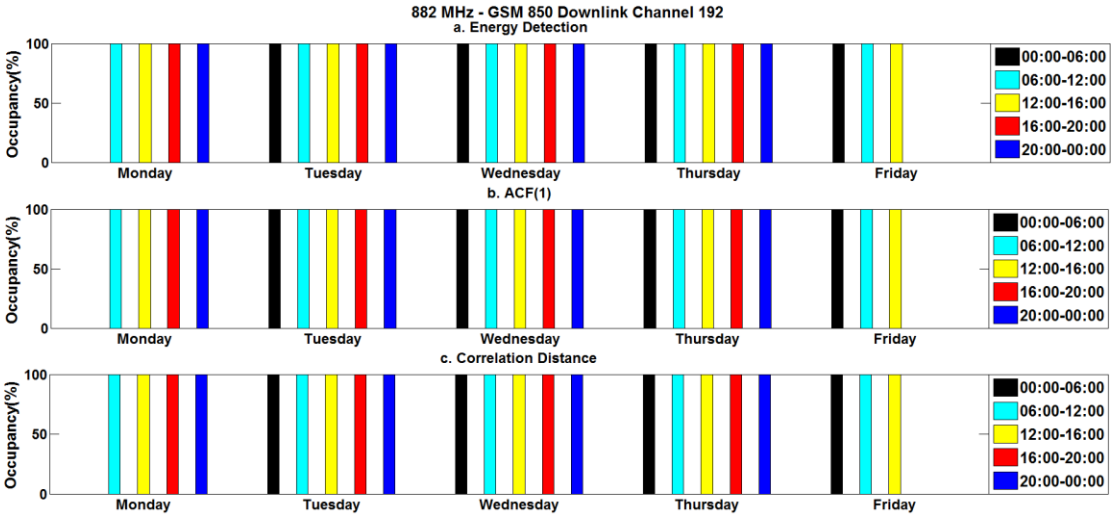

Figure 51.Average occupancy of channel 192 (882 MHz) of GSM-850 band

Figures 52 and 53 depict the occupancies of the uplink and downlink channel 661 of the GSM-1900 band. Due to broadcasting downlink, the downlink (1960 MHz) channel 661 of the GSM1900 band demonstrates a 100% usage for all the three techniques, while the uplink (1880 MHz) channel 661 of the GSM1900 demonstrates a low occupancy with the correlation distance technique and high occupancies with ACF(1) ($\geq$60%) and Energy Detection (100%).

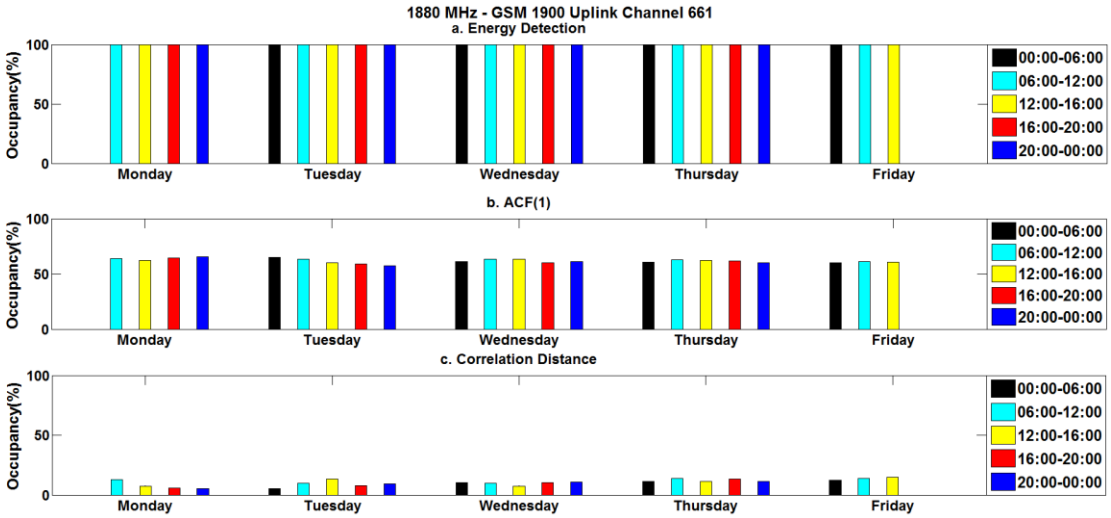

Figure 52. Average occupancy of channel 661 (1880 MHz) of GSM-1900 band

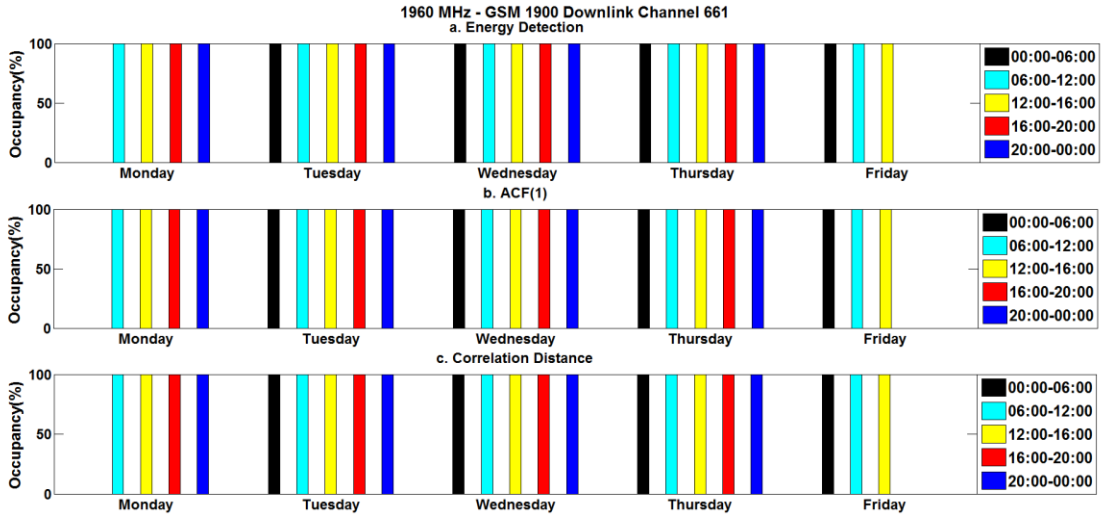

Figure 53. Average occupancy of channel 661 (1960 MHz) of GSM-1900 band

(b) Simplified Model Bayesian Inference

The examples of results shown in figures 54, 55 and 56 are the occupancy values of the 2.4 GHz WiFi band calculated using the simplified model Bayesian inference. Since this inferential technique does not take into account any uncertainties, the occupancy values would be similar to that of the frequentist inference. Since these measurements are performed in real time the occupancy values are measured at the specified instant of time in order to facilitate a method of comparison with the frequentist method. Similar to the plots in the frequentist inference, there are three subplots each depicting the occupancy outcome of a particular spectrum sensing technique.

Figure 54 depicts the occupancy of channel 1 of 2.4 GHz WiFi band i.e. 2.412 GHz. In energy detection technique, we see that the occupancy of the channel is 100%, whereas in the case of the ACF(1) the occupancy varies anywhere between 40% and 95%. The measurement performed using the Correlation distance technique results in occupancy values in the range of 3% to 40% over the week. When compared with Figure 46 (frequentist inference), the results of the two are similar as expected.

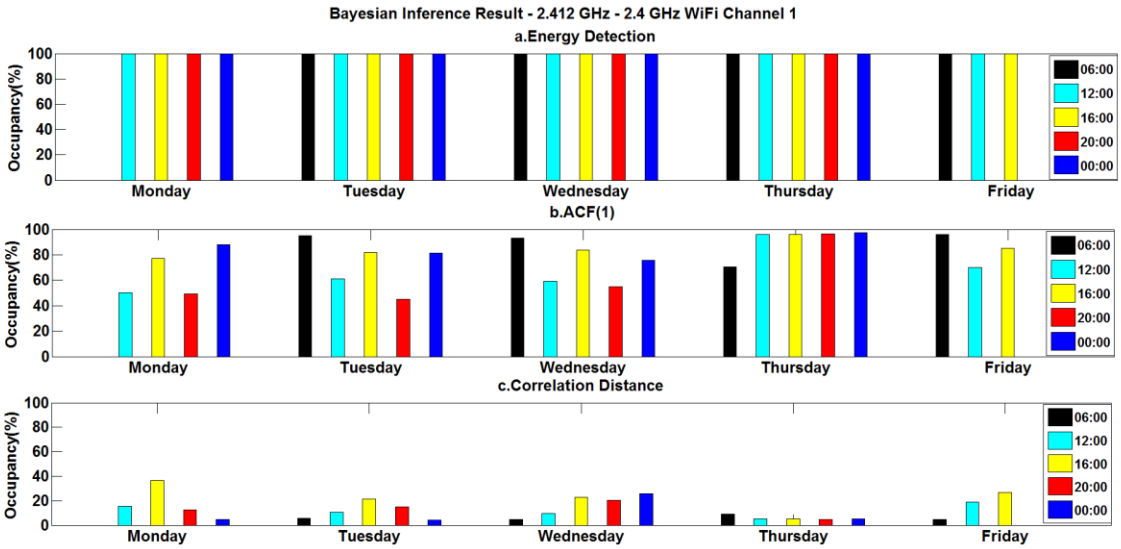

Figure 54. Occupancy of channel 1 (2.412 GHz) of the 2.4 GHz band

Figure 55 and 56 depict the occupancies of channels 6 and 11 of the 2.4 GHz WiFi band. The occupancy levels of both the channels measured using the energy detection technique depict a full occupancy. But, as seen previously, this is contradicted by the ACF(1) and the Correlation Distance techniques where the occupancy of both the channels is less than 100% and the occupancy values measured using the Correlation distance technique are more realistic. Similar to the frequentist inference results, once again it is shown that channel 1 (2.412 GHz) of the 2.4 GHz WiFi band is highly occupied when compared to that of channel 6 (2.437 GHz) and channel 11 (2.462 GHz).

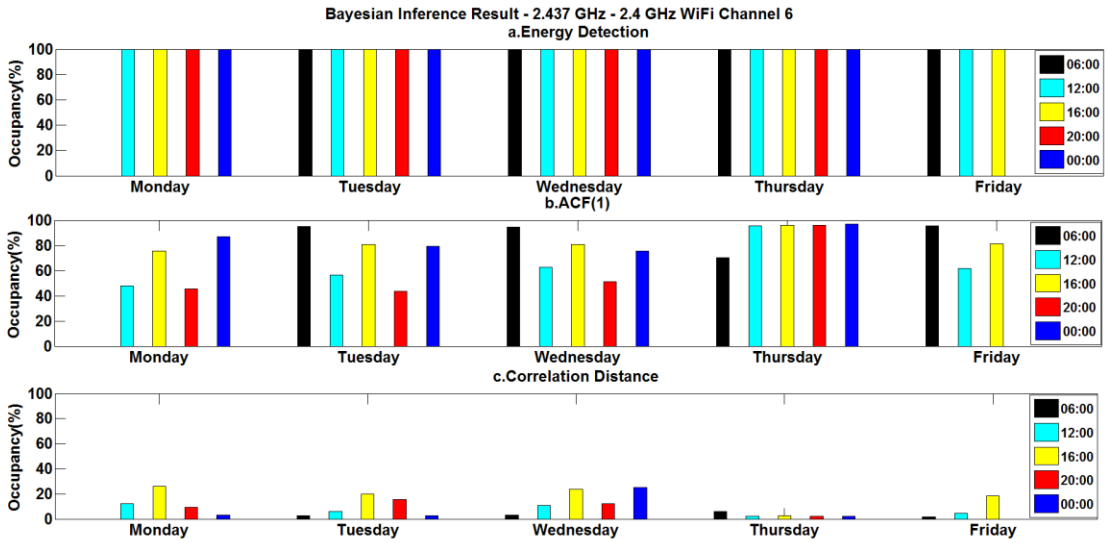

Figure 55. Occupancy of channel 6 (2.437 GHz) of the 2.4 GHz band

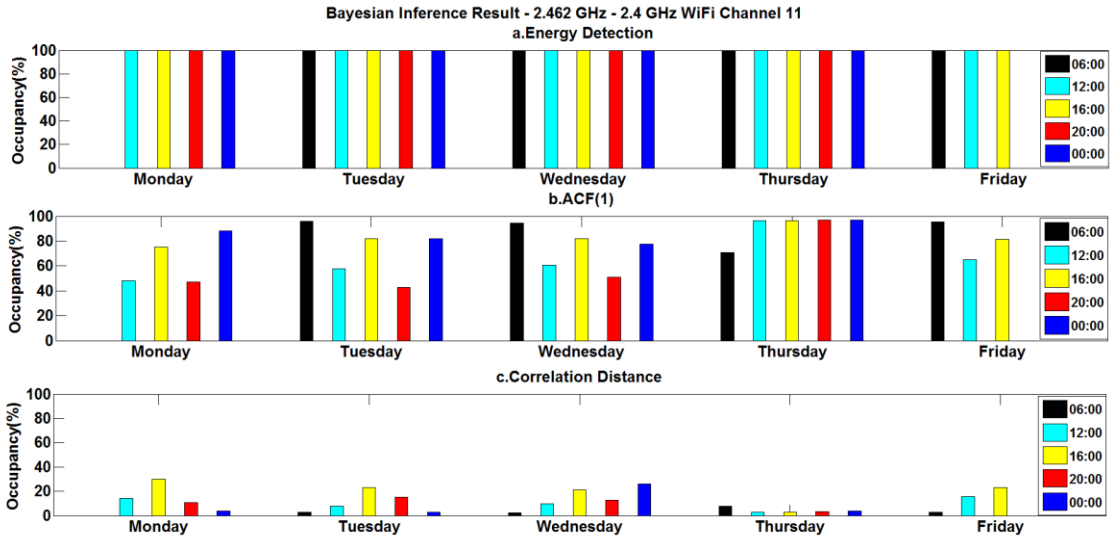

Figure 56. Occupancy of channel 11 (2.462 GHz) of the 2.4 GHz band

Figure 57 depicts a comparative evaluation of both the frequentist and Bayesian inference. In this comparison of channel 1 of 2.4 GHz WiFi band i.e. 2.412 GHz, the occupancy measurement values are almost equal for both the inferential techniques as expected.

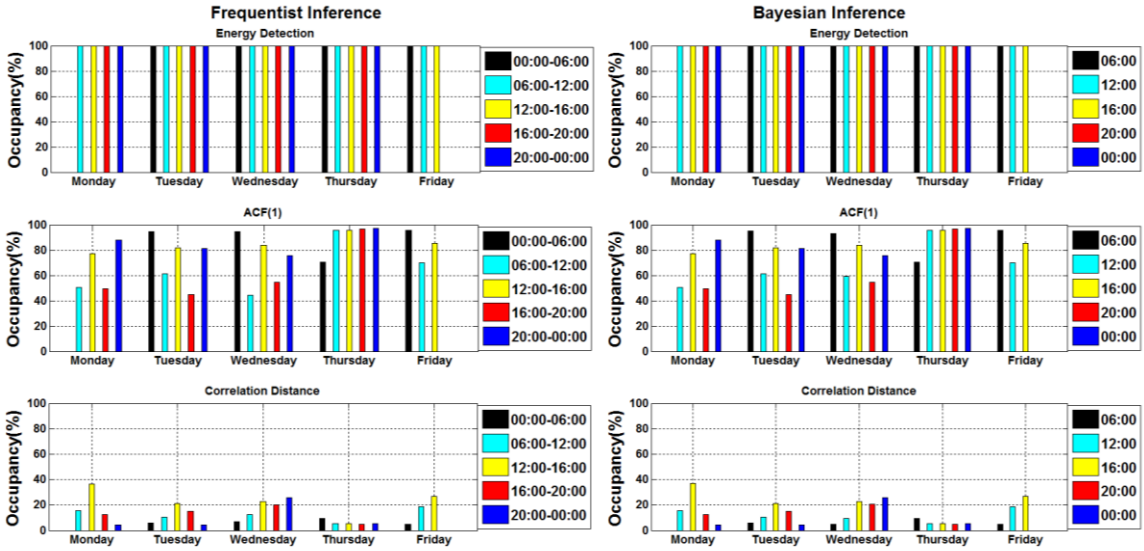

Figure 57. Comparative evaluation of Frequentist & Simplified Model Bayesian Inference: Occupancy of channel 1 (2.412 GHz) of the 2.4 GHz band

5.4.2. Survey 2 results

Examples of the results of the second survey are illustrated in figures 58 to 63, which are classified based on the inferential techniques. In this survey, besides the frequentist and the simplified model Bayesian inference, the improvised model Bayesian inference results have also been included. As mentioned previously, in the improvised model Bayesian inference, we performed a correction on the estimated value of the SNR with the addition and subtraction of the estimation error. Therefore for the improvised model, the occupancy values are depicted as bars with two different levels, wherein one level is presented in a lighter color shade compared to the other. The darker shade corresponds to occupancy values calculated by the subtraction of estimation error and the lighter shade corresponds to occupancy values calculated by the addition of estimation error.

(a) Frequentist Inference

Figures 58 and 59, illustrate the occupancy values of channel 1 of the 2.4 GHz band and channel 153 of the 5.8 GHz band, measured using the frequentist inference. Since this survey spanned over an entire week, the survey results can show a comparison in the occupancy values between the weekend and weekdays. In Figure 58, we see that with the correlation distance measurement the occupancy of channel 1 of 2.4 GHz is restricted to about 10% to 15% over the weekend, whereas during the weekdays the occupancy level of this channel ranges from anywhere between 10% to 40% with high occupancy levels being consistent during the noon to 4 pm time interval. Figure 59, on the other hand for the correlation distance technique represents the occupancy levels of channel 153 of the 5.8 GHz band (5.765 GHz), wherein the weekend shows no occupancy over the entire weekend except for the interval ranging from midnight to 6 am on Saturday where a 3.5% occupancy is observed.

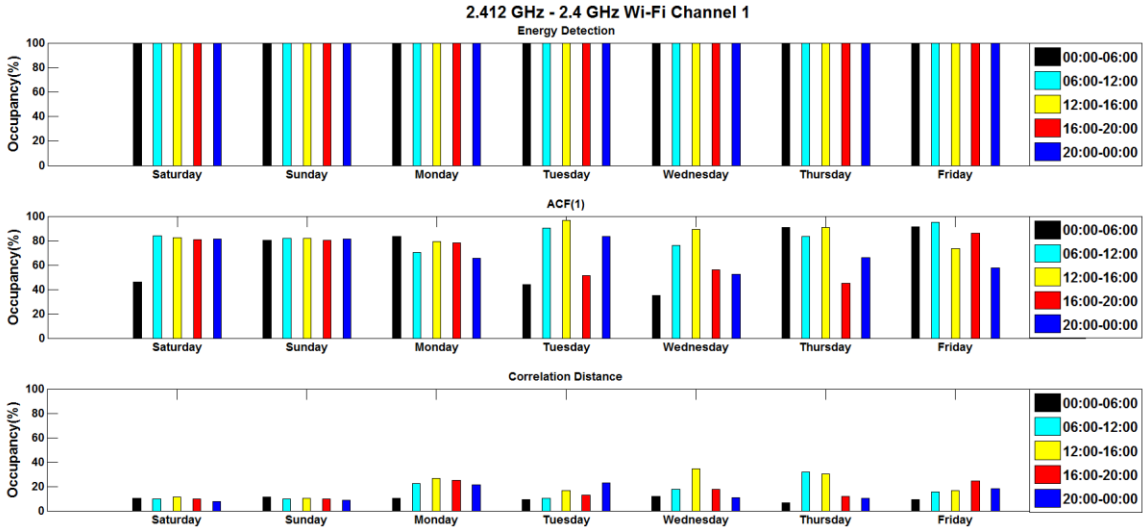

Figure 58. Average occupancy of channel 1 (2.412 GHz) of 2.4 GHz Wi-Fi band

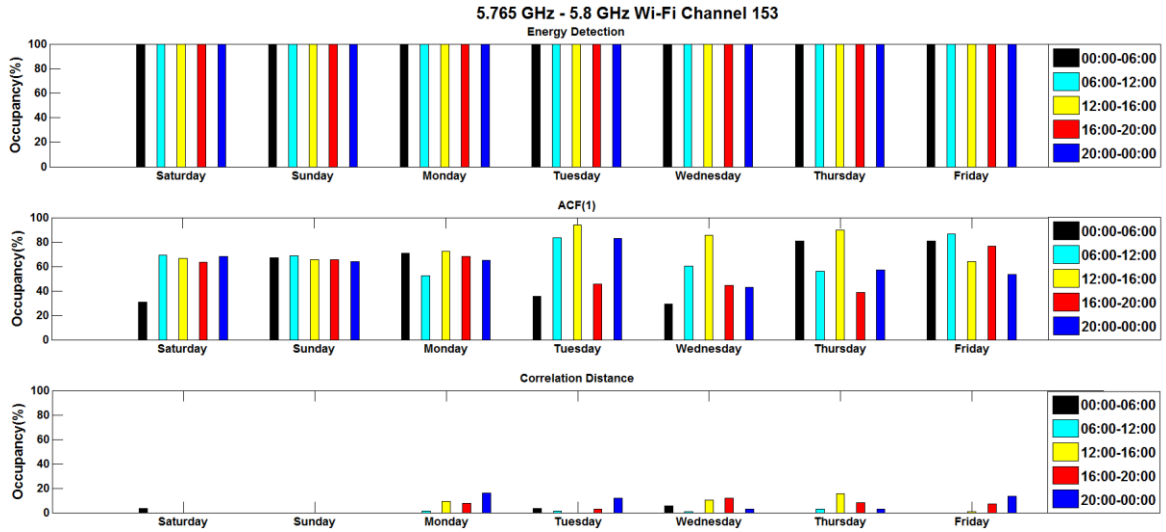

Figure 59.Average occupancy of channel 153 (5.765 GHz) of 5.8 GHz Wi-Fi band

(b) Simplified Model Bayesian Inference

Figures 60 and 61 illustrate the occupancy values of channel 1 of the 2.4 GHz band and channel 153 of the 5.8 GHz band, measured using the simplified model Bayesian inference. When both the figures 60 and 61 are compared with that of figures 58 and 59, we see that they are similar but the numerical values of the occupancy calculations in the Bayesian inference varies slightly from that of the frequentist inference. Once again it is evident from these figures that the usage level over the weekend has been low compared to that of the weekdays, which is as expected. Also it is observed that the usage in the middle of the week i.e. Wednesday is higher throughout the day when compared to any other day of the week.

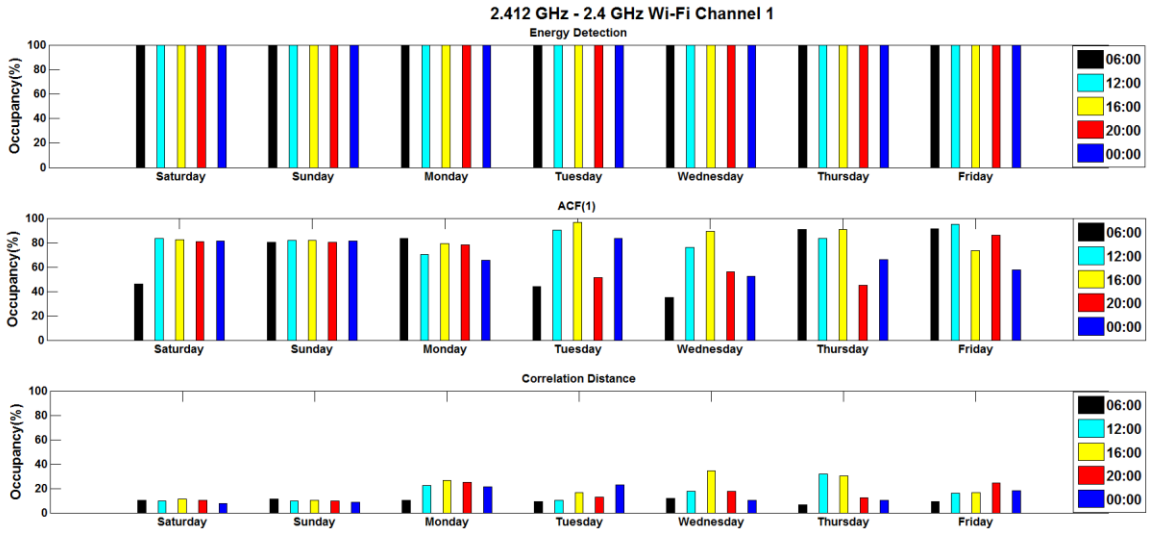

Figure 60. Occupancy of channel 1 (2.412 GHz) of 2.4 GHz Wi-Fi band

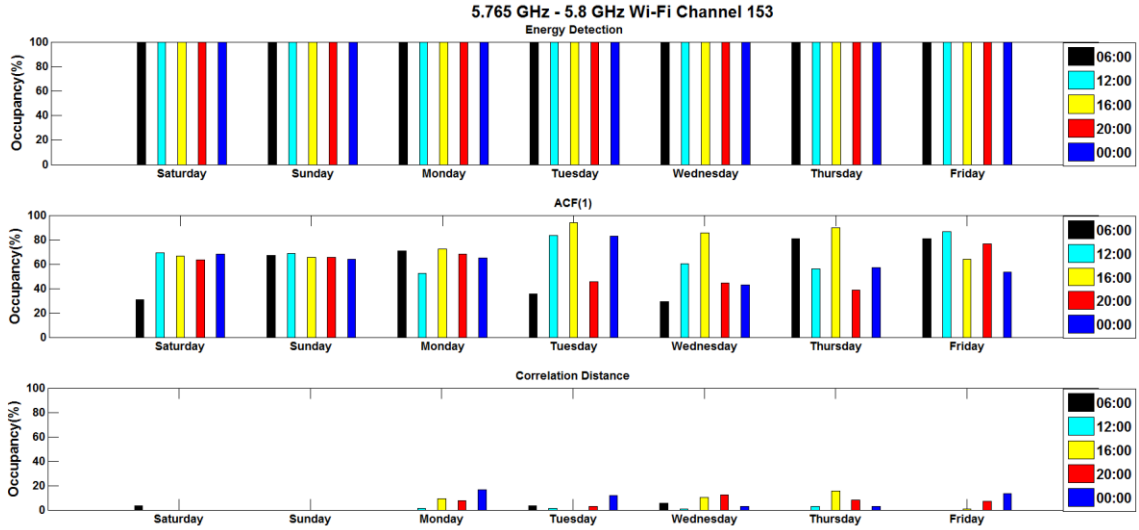

Figure 61. Occupancy of channel 153 (5.765 GHz) of 5.8 GHz Wi-Fi band

(c) Improved Model Bayesian Inference

Figures 62 and 63, illustrate examples of results of the improvised model Bayesian inference. With the improvised model we do see a significant change in the results of all the three spectrum sensing techniques when compared to the frequentist and the simplified model Bayesian inference. In figures 62 and 63, we see that the energy detection based occupancy values of channel 1 of 2.4 GHz band and channel 153 of 5.8 GHz band, do not

show a complete 100% occupancy as compared to figures 57 and 59. The occupancy levels herein range between 60% and 100% for both minimum and maximum values of the corrected SNR. This deflection from the previous results is attributed to the introduction of probability of detection and false alarm, which impacts the occupancy calculation process.

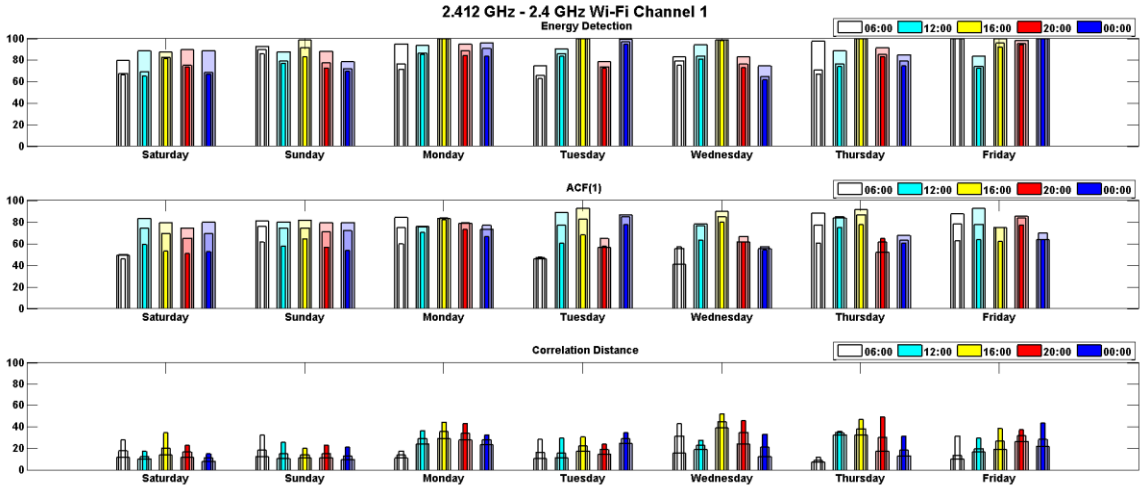

Figure 62. Occupancy of channel 1 (2.412 GHz) of 2.4 GHz Wi-Fi band

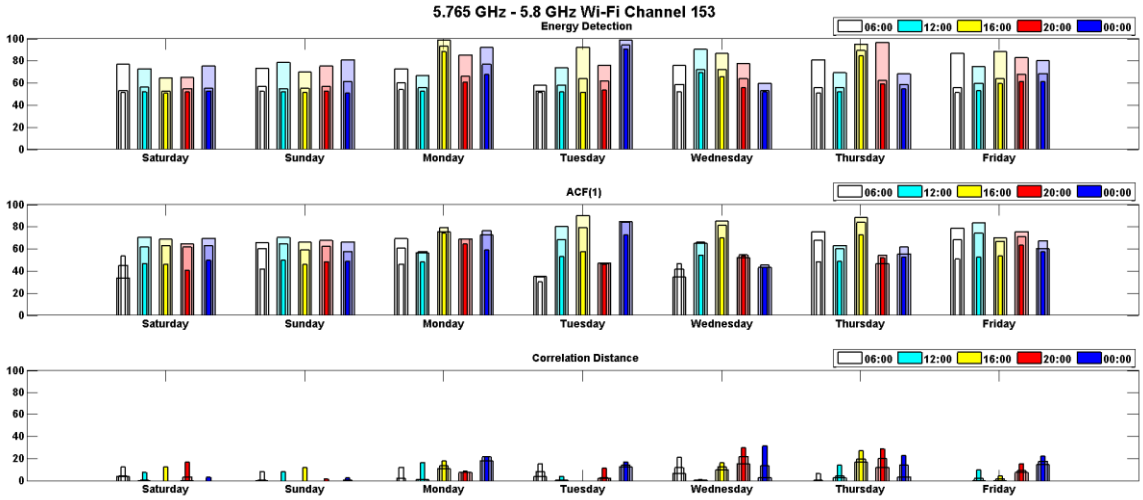

Figure 63.Occupancy of channel 153 (5.765 GHz) of 5.8 GHz Wi-Fi band

Finally we conclude that the various inferential techniques employed with the spectrum occupancy measurement technique have shown varying results. The results of the first

survey gave us an insight into the occupancy of the different channels measured in different bands and also showed the synchronization of results between the frequentist and the simplified model Bayesian inferential techniques. Furthermore the results of the second survey helped us in understanding how the improvised model could impact the results of the simplified model. The impact of introduction of various other variables into the model such as detection and false alarm probabilities have shown a significant impact on the occupancy results. Since the occupancy measurements were performed using the three different spectrum sensing techniques and the spectrum occupancy of certain channels were found to be less than 20% in certain bands of the radio spectrum, this has provided us with the opportunity to believe that the correlation distance technique seems to showcase results which are more realistic than the other techniques thereby signifying its efficiency in signal detection when compared to other techniques. The results also show that the occupancy changes depending on the time, day, and channel.

Chapter 6

CONCLUSION

In this thesis, a work aiming the improvement of the efficiency and reliability of the radio spectrum scanning has been performed. Initial studies indicated that an efficient spectrum sensing technique would provide better measurements in the occupancy measurements. Energy detection is an incumbent spectrum sensing technique that has been implemented in several spectrum surveys due to its implementation complexity being low. But, the major drawback of this technique is its inability to differentiate between signal and noise; therefore the results of the spectrum scans implementing this technique provided high occupancy measurements for certain bands although they were not expected to be. Further studies indicated that randomness or uncertainties existed in the wireless environment such as noise and interference that hampered the measurements. Therefore an uncertainty handling technique or model had to be developed.

The approach followed herein was to first develop a spectrum sensing technique that was more efficient than the existing ones. This was achieved by developing a technique that was able to differentiate between signal and noise using the principle of autocorrelation and Euclidean distance. Comparative evaluations were performed to study the efficiency of this technique with respect to the prevalent ones such as energy detection and autocorrelation at lag 1. The results of the comparative evaluation showed that the newly developed technique was more efficient than the aforementioned techniques.

With the development of the Correlation Distance spectrum sensing technique, a spectrum occupancy measurement was performed. The results of this survey yielded a significant change in the measurement of occupancy levels using the correlation distance technique when compared to the energy detection and auto correlation at lag 1 techniques. The occupancy measurement was performed using the frequentist inferential technique, wherein the result was computed after the completion of the survey.

With the achievement of the above outcome, the next task was to develop a Bayesian model to handle the uncertainty. In the initial phase, a simplified Bayesian model was developed, consisting of only deterministic variables and measured variables. The previous usage level and the spectrum sensing decision were regarded as the deterministic variables and the spectrum occupancy level was the measured variable. This Bayesian model in conjunction with the Bayesian inference technique were used to compute of the spectrum occupancy level. The adoption of the Bayesian inferential technique aided in real-time measurement of occupancy levels when implemented in a spectrum scanning experiment. It was seen that the results were similar to that of the frequentist inference as expected. Now, in order to implement uncertainty handling, random variables were added to the simplified Bayesian model. A random variable, received power, was added to the model from which the signal-to-noise ratio was estimated and values of probability of detection and false alarm for the estimated signal-to-noise ratio and the respective spectrum sensing technique were obtained. Bayesian inference was applied using the probabilities of detection and false alarm with the spectrum sensing decision and the previous usage level to infer the current spectrum occupancy level. Spectrum scanning experiment was performed once again using the

improved Bayesian model which yielded occupancy levels that were influenced by the newly included variables in the Bayesian model.

We therefore conclude that in order to increase the reliability of the radio spectrum scanning process we would have to investigate further to look for other parameters of uncertainty that affect the sensing channel and how they could be considered to be added in the Bayesian model. This thesis has laid the foundation for this type of work and presented itself with an implementation technique.

REFERENCES

1.1. N. Kaabouch, W.C.H., *Software-Defined and Cognitive Radio Technologies for Dynamic Spectrum Management.* IGI Global, 2014. I & II.

1.2. Akyildiz, I.F., et al., *NeXt generation/dynamic spectrum access/cognitive radio wireless networks: a survey.* Computer Networks, 2006. 50(13): p. 2127-2159.

1.3. Mitola, J. and G.Q. Maguire, Jr., *Cognitive radio: making software radios more personal.* IEEE Personal Communications, 1999. 6(4): p. 13-18.

1.4. Doyle, L., *Essentials of cognitive radio*. 2009: Cambridge University Press.

1.5. Yucek, T. and H. Arslan, *A survey of spectrum sensing algorithms for cognitive radio applications.* IEEE Communications Surveys & Tutorials, 2009. 11(1): p. 116-130.

1.6. Molisch, A.F., L.J. Greenstein, and M. Shafi, *Propagation issues for cognitive radio.* Proceedings of the IEEE, 2009. 97(5): p. 787-804.

1.7. Couillet, R. and M. Debbah, *Mathematical foundations of cognitive radios.* Journal of Telecommunications and Information Technology, 2009: p. 10 pages.

1.8. Tandra, R. and A. Sahai, *SNR walls for signal detection.* IEEE Journal of Selected Topics in Signal Processing, 2008. 2(1): p. 4-17.

2.1 Hora, S.C., *Aleatory and epistemic uncertainty in probability elicitation with an example from hazardous waste management.* Reliability Engineering & System Safety, 1996. 54(2): p. 217-223

2.2. Senge, R., et al., *Reliable classification: Learning classifiers that distinguish aleatoric and epistemic uncertainty*. Information Sciences, 2014. 255: p. 16-29.

2.3. Thunnissen, D.P. *Uncertainty classification for the design and development of complex systems*. in *3rd annual predictive methods conference*. 2003.

2.4. Laplace, P., *Analytic theory of probabilities.* Paris: Imprimerie Royale, 1810: p. 1-8.

2.5. Morgan, C.G. *Many valued probability theory*. in *34th IEEE International Symposium on Multiple-Valued Logic Proceedings*. 2004. IEEE.

2.6. Nielsen, T.D. and F.V. Jensen, *Bayesian networks and decision graphs*. 2009: Springer Science & Business Media.

2.7. Rabiner, L.R. and B.-H. Juang, *An introduction to hidden Markov models.* IEEE ASSP Magazine, 1986. 3(1): p. 4-16.

2.8. Sugiarto, I., P. Maier, and J. Conradt. *Reasoning with discrete factor graph*. in *IEEE International Conference on Robotics, Biomimetics, and Intelligent Computational Systems (ROBIONETICS)*. 2013. IEEE.

2.9. Barber, D., *Bayesian reasoning and machine learning*. 2012: Cambridge University Press.

2.10. Gopnik, A. and J.B. Tenenbaum, *Bayesian networks, Bayesian learning and cognitive development.* Developmental science, 2007. 10(3): p. 281-287.

2.11. Gu, T., et al., *A bayesian approach for dealing with uncertain contexts*. 2004.

2.12. Ben-Gal, I., *Bayesian networks.* Encyclopedia of statistics in quality and reliability, 2007.

2.13. Thirumuruganathan, S. and M. Huber. *Building Bayesian network based expert systems from rules*. in *IEEE International Conference on Systems, Man, and Cybernetics (SMC)*. 2011. IEEE.

3.1. Pauluzzi, D.R. and N.C. Beaulieu, *A comparison of SNR estimation techniques for the AWGN channel.* IEEE Transactions on Communications, 2000. 48(10): p. 1681-1691.

3.2. Simon, M. and A. Mileant, *SNR estimation for the baseband assembly.* Jet Propulsion Lab., Pasadena, CA, The Telecommunications and Data Acquisition Progress Report 42-85, 1986: p. 118-126.

3.3. Shah, B. and S. Hinedi, *The split symbol moments SNR estimator in narrow-band channels.* IEEE Transactions on Aerospace and Electronic Systems, 1990. 26(5): p. 737-747.

3.4. Shah, B. and J. Holmes, *Improving the Split-Symbol Moments SNR Estimator.* Jet Propulsion Lab., Pasadena, Calif. Inst. Technol. Tech. Rep. , 1997: p. 3338-90.

3.5. Van Trees, H.L., *Detection, Estimation and Modulation Theory*. Vol. 1. 1968, New York: Wiley.

3.6. Kerr, R.B., *On signal and noise level estimation in a coherent PCM channel.* IEEE Transactions on Aerospace and Electronic Systems, 1966(4): p. 450-454.

3.7. Gagliardi, R. and C. Thomas, *PCM data reliability monitoring through estimation of signal-to-noise ratio.* IEEE Transactions on Communication Technology, 1968. 16(3): p. 479-486.

3.8. Thomas, C., *Maximum Likelihood Estimation of Signal-to-Noise Ratio*. 1967, Univ. of Southern California: Los Angeles.

3.9. Gilchriest, C., *Signal-to-noise monitoring.* JPL Space Programs Summary, 1966. 4(37-27): p. 169-184.

3.10. Benedict, T. and T. Soong, *The joint estimation of signal and noise from the sum envelope.* IEEE Transactions on Information Theory, 1967. 13(3): p. 447-454.

3.11. Matzner, R., *An SNR estimation algorithm for complex baseband signals using higher order statistics.* Facta Universitatis (Nis), 1993. 6(1): p. 41-52.

3.12. Brandao, A., L.B. Lopes, and D.C. McLemon. *In-service monitoring of multipath delay and cochannel interference for indoor mobile communication systems*. in *IEEE International Conference on Serving Humanity Through Communications*. 1994. IEEE.

3.13. Li, B., R. DiFazio, and A. Zeira, *A low bias algorithm to estimate negative SNRs in an AWGN channel.* IEEE Communications Letters, 2002. 6(11): p. 469-471.

3.14. Quintana-Quiros, P. and T. Chit-Sang. *SNR estimation and jamming detection techniques using wavelets*. in *IEEE Green Energy and Systems Conference (IGESC)*. 2014.

3.15. Hamid, M., N. Bjorsell, and S. Ben Slimane. *Sample covariance matrix eigenvalues based blind SNR estimation*. in *IEEE International Instrumentation and Measurement Technology Conference Proceedings*. 2014. IEEE.

3.16. Yonghong, Z. and L. Ying-Chang, *Eigenvalue-based spectrum sensing algorithms for cognitive radio.* IEEE Transactions on Communications, 2009. 57(6): p. 1784-1793.

3.17. Hamid, M., et al., *Blind spectrum sensing for cognitive radios using discriminant analysis: A novel approach.* IEEE Transactions on Instrumentation and Measurement, 2013. 62(11): p. 2912-2921.

3.18. Hamid, M. and N. Bjorsell. *Maximum minimum eigenvalues based spectrum scanner for cognitive radios*. in *IEEE International Instrumentation and Measurement Technology Conference*. 2012. IEEE.

3.19. Hamid, M., et al. *Spectrum sensing through spectrum discriminator and maximum minimum eigenvalue detector: A comparative study*. in *IEEE International Instrumentation and Measurement Technology Conference*. 2012. IEEE.

3.20. Nadakuditi, R.R. and A. Edelman, *Sample eigenvalue based detection of high-dimensional signals in white noise using relatively few samples.* IEEE Transactions on Signal Processing, 2008. 56(7): p. 2625-2638.

3.21. López-Valcarce, R. and C. Mosquera, *Sixth-order statistics-based non-data-aided SNR estimation.* IEEE Communications Letters, 2007. 11(4): p. 351-353.

3.22. Gao, P. and C. Tepedelenlioğlu, *SNR estimation for nonconstant modulus constellations.* IEEE Transactions on Signal Processing, 2005. 53(3): p. 865-870.

3.23. Sharma, S.K., S. Chatzinotas, and B. Ottersten, *Eigenvalue-Based Sensing and SNR Estimation for Cognitive Radio in Presence of Noise Correlation.* IEEE Transactions on Vehicular Technology, 2013. 62(8): p. 3671-3684.

4.1. Yucek, T. and H. Arslan, *A survey of spectrum sensing algorithms for cognitive radio applications.* IEEE Communications Surveys & Tutorials, 2009. **11**(1): p. 116-130.

4.2. Poor, H.V., *An introduction to signal detection and estimation*. 2013: Springer Science & Business Media.

4.3. López-Benítez, M. and F. Casadevall, *Improved energy detection spectrum sensing for cognitive radio.* IET communications, 2012. **6**(8): p. 785-796.

4.4. Hoven, N., R. Tandra, and A. Sahai, *Some fundamental limits on cognitive radio.* Wireless Foundations EECS, Univ. of California, Berkeley, 2005.

4.5. Cabric, D., S.M. Mishra, and R.W. Brodersen. *Implementation issues in spectrum sensing for cognitive radios*. in *Asilomar conference on Signals, systems and computers*. 2004. IEEE.

4.6. Urkowitz, H., *Energy detection of unknown deterministic signals.* Proceedings of the IEEE, 1967. **55**(4): p. 523-531.

4.7. Tandra, R. and A. Sahai, *SNR walls for signal detection.* IEEE Journal of Selected Topics in Signal Processing, 2008. **2**(1): p. 4-17.

4.8. Wang, B. and K. Liu, *Advances in cognitive radio networks: A survey*. IEEE Journal of Selected Topics in Signal Processing, 2011. **5**(1): p. 5-23.

4.9. Zeng, Y., et al., *A review on spectrum sensing for cognitive radio: challenges and solutions.* EURASIP Journal on Advances in Signal Processing, 2010. **2010**: p. 2.

4.10. Čabrić, D. and R.W. Brodersen. *Physical layer design issues unique to cognitive radio systems*. in *IEEE International Symposium on Personal, Indoor and Mobile Radio Communications*. 2005. IEEE.

4.11. Öner, M. and F. Jondral. *Air interface recognition for a software radio system exploiting cyclostationarity*. in *IEEE International Symposium on Personal, Indoor and Mobile Radio Communications*. 2004. IEEE.

4.12. Sai Shankar, N., C. Cordeiro, and K. Challapali. *Spectrum agile radios: utilization and sensing architectures*. in *IEEE International Symposium on New Frontiers in Dynamic Spectrum Access Networks*. 2005. IEEE.

4.13. Lundén, J., et al. *Spectrum sensing in cognitive radios based on multiple cyclic frequencies*. in *International Conference on Cognitive Radio Oriented Wireless Networks and Communications*. 2007. IEEE.

4.14. Gardner, W., *Signal interception: a unifying theoretical framework for feature detection.* IEEE Transactions on Communications, 1988. **36**(8): p. 897-906.

4.15. Goh, L.P., Z. Lei, and F. Chin. *Feature detector for DVB-T signal in multipath fading channel*. in *International Conference on Cognitive Radio Oriented Wireless Networks and Communications*. 2007. IEEE.

4.16. Sahai, A., et al. *Fundamental design tradeoffs in cognitive radio systems*. in *Proceedings of the first international workshop on Technology and policy for accessing spectrum*. 2006. ACM.

4.17. Tang, H. *Some physical layer issues of wide-band cognitive radio systems*. in *IEEE international symposium on New frontiers in dynamic spectrum access networks*. 2005. IEEE.

4.18. Cabric, D., A. Tkachenko, and R.W. Brodersen. *Spectrum sensing measurements of pilot, energy, and collaborative detection*. in *IEEE Military communications conference*. 2006. IEEE.

4.19. Yonghong, Z. and L. Ying-Chang, *Spectrum-Sensing Algorithms for Cognitive Radio Based on Statistical Covariances.* IEEE Transactions on Vehicular Technology, 2009. **58**(4): p. 1804-1815.

4.20. Yonghong, Z. and L. Ying-Chang, *Eigenvalue-based spectrum sensing algorithms for cognitive radio.* IEEE Transactions on Communications, 2009. **57**(6): p. 1784-1793.

4.21. Mate, A., K.-H. Lee, and I.-T. Lu. *Spectrum sensing based on time covariance matrix using GNU radio and USRP for cognitive radio*. in *IEEE Long Island Systems Applications and Technology Conference*. 2011. IEEE.

4.22. Reyes, H., et al., *A spectrum sensing technique based on autocorrelation and Euclidean distance and its comparison with energy detection for cognitive radio networks.* Computers & Electrical Engineering, 2015.

4.23. Sharma, R.K. and J.W. Wallace. *Improved autocorrelation-based sensing using correlation distribution information*. in *International ITG Workshop on Smart Antennas*. 2010.

5.1. Larson, M.G., *Descriptive statistics and graphical displays.* Circulation, 2006. **114**(1): p. 76-81.

5.2. Vergura, S., et al., *Descriptive and inferential statistics for supervising and monitoring the operation of pv plants.* IEEE Transactions on Industrial Electronics, 2009. **56**(11): p. 4456-4464.

5.3. Bandyopadhyay, P.S. and M. Forster, *Philosophy of Statistics, Handbook of the Philosophy of Science*. 2010, Elsevier.

5.4. Schlotzhauer, S.D., *Elementary statistics using JMP*. 2007: SAS Institute.

5.5. Wagenmakers, E.-J., et al., *Bayesian versus frequentist inference*, in *Bayesian evaluation of informative hypotheses*. 2008, Springer. p. 181-207.

5.6. Xue, J., Z. Feng, and P. Zhang, *Spectrum Occupancy Measurements and Analysis in Beijing.* IERI Procedia, 2013. **4**(0): p. 295-302.

5.7. Gopnik, A. and J.B. Tenenbaum, *Bayesian networks, Bayesian learning and cognitive development.* Developmental science, 2007. **10**(3): p. 281-287.

5.8. Stone, J.V., *Bayes' Rule: A Tutorial Introduction to Bayesian Analysis*. 2013: JV Stone.

5.9. Niyato, D. and E. Hossain, *Medium access control protocols for dynamic spectrum access in cognitive radio networks: A survey.* Cognitive Radio Networks, 2008: p. 179-214.

5.10. Liang, Y.-C., et al., *Sensing-throughput tradeoff for cognitive radio networks.* IEEE Transactions on Wireless Communications, 2008. **7**(4): p. 1326-1337.

5.11. Mohamedou, A., et al., *Bayesian inference and fuzzy inference for spectrum sensing order in cognitive radio networks.* Transactions on Emerging Telecommunications Technologies, 2014.

5.12. Xing, X., et al., *Spectrum prediction in cognitive radio networks.* IEEE Wireless Communications, 2013. **20**(2): p. 90-96.

5.13. Xing, X., et al. *Channel quality prediction based on Bayesian inference in cognitive radio networks*. in *IEEE INFOCOM Proceedings*. 2013. IEEE.

5.14. Ghosh, C., et al. *Markov chain existence and hidden Markov models in spectrum sensing*. in *IEEE International Conference on Pervasive Computing and Communications*. 2009. IEEE.

5.15. Gokceoglu, A., R. Piche, and M. Valkama. *Bayesian approach to spectrum sensing for cognitive radio applications*. in *7th International ICST Conference on Cognitive*

Radio Oriented Wireless Networks and Communications (CROWNCOM). 2012. IEEE.

5.16. Ambaum, M.H., *Frequentist vs Bayesian statistics-a non-statisticians view*. arXiv preprint arXiv:1208.2141, 2012.

5.17 Subramaniam, S., H. Reyes, and N. Kaabouch. *Spectrum occupancy measurement: An autocorrelation based scanning technique using USRP* in *IEEE Wireless and Microwave Technology Conference (WAMICON)*, 2015. IEEE.